



BRNO UNIVERSITY OF TECHNOLOGY

FACULTY OF CIVIL ENGINEERING

AND

UNIVERSITY OF OVIEDO

***PILOT EVALUATION OF C50/60 FRACTURE
PROPERTIES BY BRAZILIAN DISC TEST***

BACHELOR THESIS

AUTHOR

D. Alejandro Parcero Alonso

SUPERVISOR

Assoc. Prof. Stanislav Seitzl, Ph.D.

SUPERVISOR SPECIALIST:

Ing. Petr Miarka

BRNO, CZECH REPUBLIC 2018

ABSTRACT

Along the years it has been so important for civil engineers to have acknowledgement about the durability of the materials in construction, especially about concrete. As it is known, most of the components of a structure are being requested to a mixed mode, which means that they are requested by forces in two different directions. It is very important to know about both stress intensity factors, in order to be able to predict how long the structure will endure until it collapses. This prediction can be done with the study of the Brazilian Disc, a concrete disc with a crack in the middle of it, requested by two symmetrical forces in different angles regarding the crack. The results for the stress intensity factors are calculate with ANSYS software.

KEYWORDS

Brazilian Disc, mixed mode, stress intensity factor, mechanic fracture, K_I/K_{II} , calibration curves, T – stress, crack growth.

RESUMEN

A lo largo de los años ha sido un tema de gran importancia para los ingenieros civiles el conocimiento acerca de la duración de los materiales en la construcción, especialmente el hormigón. Es sabido que la mayoría de los componentes que conforman grandes estructuras están solicitadas al modo mixto, o lo que es mismo, solicitadas por fuerzas en dos direcciones diferentes. Es muy importante conocer ambos factores de intensidad de tensión, con el objetivo de predecir la duración de la estructura sin que colapse. Ésta predicción se conoce con el estudio del Disco Brasileño, un disco de hormigón con una grieta en el medio, solicitado por dos fuerzas simétricas en diferentes ángulos con respecto a la grieta. Los resultados obtenidos para los factores de intensidad de tensión son calculados con el programa ANSYS.

PALABRAS CLAVE

Disco Brasileño, modo mixto, factor de intensidad de tensión, mecánica de la fractura, K_I/K_{II} , curvas de calibración, tensión T , crecimiento de grieta.

BIBLIOGRAPHIC CITATION

Alejandro Parcero Alonso, *Pilot Evaluation of C50/60 fracture properties by Brazilian Disc Test*. Brno, 2018. 56 p., 37 p. of attachments. Bachelor Thesis. Brno University of Technology, Faculty of Civil Engineering, Institute of Structural Mechanics. Supervisor: Assoc. Prof. Stanislav Seitzl, Ph. D. Supervisor Specialist: Ing. Petr Miarka.

ACKNOWLEDGEMENT

This thesis is the final part of my Bachelor's Degree of Mechanical Engineering in the University of Oviedo.

It has been prepared and elaborated in Brno, Czech Republic during the summer semester at my Erasmus+ agreement.

I would like to thank my tutors at the Faculty of Civil Engineering, Brno University of Technology because of their invaluable help to prepare this thesis. I would also like to thank all my professors in Oviedo and in Brno during all my university time that in a way or in another help me to achieve the necessary knowledge to be able to prepare this document.

Last, but the most important, I would like to thank my family to help me in every moment I need them. Also, to my girlfriend Helena, for helping me in the worst moments.

This paper has been written with financial support from the Czech Science Foundation: project **16 – 18702S (AMIRI)** and "National Sustainability Programme I" project "AdMaS UP – Advanced Materials, Structures and Technologies" (**No. LO1408**) supported by the Ministry of Education, Youth and Sport of the Czech Republic and Brno University of Technology.

TABLE OF CONTENT

1. INTRODUCTION	6
2. AIM.....	7
3. THEORETICAL BACKGROUND.....	8
3.1. CONCRETE CHARACTERISTICS	8
3.2. FRACTURE MECHANICS.....	10
3.3. BRAZILIAN DISC TEST.....	23
4. NUMERICAL MODELLING IN ANSYS.....	26
4.1. GEOMETRY.....	26
4.2. ELEMENT TYPE.....	26
4.3. MATERIAL PROPERTIES	28
4.4. MODELLING OF THE SPECIMEN.....	29
4.5. MESHING	33
4.6. BOUNDARY CONDITIONS.....	33
4.7. SOLUTION	36
5. RESULTS	38
5.1. SPECIMEN'S DATA.....	38
5.2. STRESS INTENSITY FACTORS.....	38
5.3. CALIBRATION CURVES	39
6. EXPERIMENTAL MEASUREMENT.....	41
6.1. MATERIAL	41
6.2. SPECIMEN'S GEOMETRY.....	41
6.3. EXPERIMENTAL PROCEDURE FOR BRAZILIAN DISC TEST	42
6.4. CALIBRATION CURVES FOR EXPERIMENT.....	42
6.5. EXPERIMENTALLY OBTAIN DATA	44
7. NUMERICAL DATA-COMPARISON	46
7.1. COMPARISON WITH MARIA VILLANUEVA'S THESIS.....	46
7.2. COMPARISON WITH EXPERIMENTAL RESULTS	48
7.3. COMPARISON WITH M. R. AYATOLLAHI AND M. R. M. ALIHA RESULTS.....	49
8. CONCLUSIONS.....	51
9. ANNEXES	52
9.1. ANNEX I. MACRO DOCUMENT.....	52
9.2. ANNEX II, TABLES AND RESULTS.....	63
9.3. ANNEX III. LIST OF ABBREVIATIONS.....	83
9.4. ANNEX IV. LIST OF SYMBOLS	84
9.5. ANNEX V. LIST OF FIGURES	85
9.6. ANNEX VI. LIST OF GRAPHS	87
9.7. ANNEX VII. LIST OF TABLES.....	89
10. REFERENCES	90
11. CURRICULUM VITAE.....	92

1. INTRODUCTION

The use of concrete as a construction material is due to the large number of advantages that their properties have. That is why it is a very useful material for constructions such as buildings and structures. As a composite material, concrete has many applications and uses. Some of these properties are the resistance to corrosion and aging.

Even so, although structures should be maintained with the aim of lasting so many time, some of the concrete structures built in the last decades are at the end of their serviceability [1,2].

Otherwise, concrete does not respond in a good way to tensile stresses. Because of this, the more used type of concrete is the prestressed concrete that along with steel bars allow to increase the tensile strength of this material. Prestressed concrete precast elements used in construction decreases time in comparison to the cast – in – place approach [3].

As important as the use and applications of concrete, is the crack analysis in structures. It is essential to know the stress state near the cracks present in a specimen in order to be able to know which way the crack will behave and in which directions it will grow. Some different tests can be used to carry out an investigation about this behaviour.

The structural behaviour of the structures previously mentioned should be studied for different conditions. These structures are not only subjected to uniaxial load, but to mixed mode I/II (biaxial) load, this means that they are requested to two different types of loads.

The Brazilian Disc test is usually used to obtain the stress intensity factors for different cases and conditions. It also allows engineers to know the tensile strength of concrete with ease. The test is a very simple test and the results are very approximate to the real value of the tensile strength calculated by a typical test. This kind of test is also known as indirect tensile test.

2. AIM

The aim of this document is to study the initiation mechanism and propagation of a crack situated in the middle of the Brazilian disc specimen.

The specimen will be requested by two symmetrical forces respect the diametrical axis until its failure. The results will be studied both cases by numerical simulation and by experimentally. The numerical simulation will be done by Finite Elements Method (FEM) in ANSYS software and it will be compared with the experimental results measured on the laboratory and with the results published by various researches. The crack study will be made based on the results obtained of the stress intensity factors for different sizes and different inclination angles of the relative crack length.

Then, the values of Stress intensity factor will be evaluated with the results obtained by application two ways, numerical simulation and experimentally on the laboratory. The calibration curves are prepared for a selected angle between notch and load points. A comparison between different models and approaches will be done to know how different the results can be.

3. THEORETICAL BACKGROUND

3.1. Concrete characteristics

3.1.1. COMPOSITE MATERIALS CHARACTERISTICS

Concrete is a composite material created from the union of various materials in which the main compound, called binder, is cement, a ceramic material. Because of this, concrete is also classified as a ceramic matrix composite material. It is created to improve the benefits of cement and has become one of the most used materials in construction. The properties that the concrete possesses are due to the fact that the matrix phase of the global compound is the ceramic material, and therefore acquires these properties. Concrete has some advantages such as the capacity of resistance to compressive forces or fire and durability. The compressive strength is a very important characteristic of concrete because enable to create long – life structures. In addition, it is possible to add various compounds to the concrete to further improve its properties.

Ceramic characteristics

Ceramics materials are characterised by its fragility and toughness. On one hand, the toughness is due to the atomic bonds which are a very hard opponent to the dislocations movement. Dislocations are the responsible of the deformation of the material because they let the movement to the atomic bonds and the plastic deformation [4]. However, in the ceramic materials, these atomic bonds are very hard, so this plastic deformation is almost equal to zero, which means very hard materials. Parallely, the deformation energy is very low in this family of materials, just the opposite respect to metallic materials.

On the other hand, fragility is also a characteristic due to the atomic bonds. Another reason is the existence of surface and inner imperfections, that can grow and introduce into the thickness of the structure and become a crack. These cracks can grow in the normal direction respect the load axis, developing in the failure of the structure. During the hardening of the cement, appears a contraction that make the inherent presence of cracks [4]. This situation produces the weakness of the structure and can be the origin of the most important problems on structural analysis. These cracks can grow due to the application of a tensile load and the material barely gets an elastic deformation which produces the failure of the specimen or structure. The crack growth is carried out because the cracks which are oriented in a normal plane respect the load axis grows in the normal direction inducing the fracture mechanism.

On the other hand, if a compression load is applied, then there is not a crack growth because the cracks change their orientation into the same as the compression and do not allow the growth [5].

3.1.2. MECHANIC CHARACTERISTICS

Tensile strength in ceramic materials is very low compared to metallic metals, this is due to the existence of cracks, so it depends on the fracture tenacity and on the crack length:

$$\sigma = \frac{K_{Ic}}{C\sqrt{\pi a}}, \quad (1)$$

where

σ is the applied pressure,

K_{Ic} is the fracture toughness,

C is a constant that depends on the geometry of the specimen,

a is the crack length,

The fracture intensity reaches the same value as the stress intensity factor when the crack is just going to grow, and the failure of the specimen occurs.

On the other hand, tensile strength is about 15 times less than compression strength, so ceramic materials are very suitable to work in compression situations rather than be requested to tensile loads.

3.1.3. TYPICAL TEST FOR COMPOSITE SPECIMENS

There are so many different tests to evaluate the mechanic properties of composite materials, and, specifically of concrete. These tests should be following European standards to obtain the material's compressive cube/cylindrical strength [6], flexural strength [7], Young's modulus [8] and indirect tensile strength. It is known that concrete and rock have similar behaviour, so it is useful to use it to test the tensile strength of concrete [9].

The compression test's aim is to know the compression strength of the specimen. It is very important for concrete structures because of its good behaviour to compression loads [10].

The bending test can be in three or four points. It is used because the stress – strain behaviour of fragile materials usually doesn't get described in the tensile stress because two reasons:

- It is very difficult prepare the specimens for the test.
- There is so much difference between the results get in the tensile test and in the compression one.

Because of that, the use of a specimen placed horizontally in a bending test allows the sample to experiment a compression state on the upper surface and a tensile state on the bottom surface.

Finally, the tensile test is a very difficult test for concrete specimens, due to the high cost of the preparation of the sample and because it is necessary to get a very good alignment between the load direction and the specimen's axis during the test. This is because if the alignment between both axes is not good; then can appears bending stresses and the results can be wrong.

This is reason why it is used to do an indirect tensile test called the Brazilian Test.

3.2. Fracture Mechanics

3.2.1. INTRODUCTION

Fracture and, in general, structures collapse and failure, has been a problem for years to the society [11]. Although it is usually thought that the problem was worse years ago, in fact this kind of failures are worse now because of the complexity of structures or components, so it means the necessity of study fracture mechanics. In an atomic view, the fracture in a material occurs when the stress applied at the atomic level is enough to break the bonds that hold atoms together.

The reason why the structures failure it generally turns into one of the following two categories:

- Carelessness during design, construction or performance of the structure. Which also can mean the neglect on the test period of the structure.
- Application of a new material or design: this means that if a structure is built with a new design different from the studied one, or if it is applied a new material which can change the general properties of the structure, it can get into failure. This is a more difficult type of failure to prevent because there are some factors that it is impossible to anticipate.

3.2.2. BRITTLE FRACTURE

There are two categories of fracture, depending on the solid type. It is possible to differentiate between ductile and fragile fracture. Because of the concrete properties, this kind of structures suffer fragile fracture.

The ductile fracture is characterized because of the existence of plastic deformation before the failure of the structure, which is localized in a very distorted zone [5].

On the other hand, the fragile fracture is just the opposite side respect from the ductile fracture. This means that there is not any plastic deformation before the failure. This is the kind of failure that it is necessary to avoid because it occurs without advice and can have catastrophic consequences.

3.2.3. GRIFFITH'S THEORY

In 1920, according to the first law of thermodynamics, when a system goes from non-equilibrium to equilibrium, there is a net decrease in energy, and so Griffith applied this idea to the formation a crack. The Griffith's Theory said that the low resistances in fragile solids are produced because of the crack's existence in the inner or outer surface [4]. These cracks are produced because of the manufacturing processes produced them.

As Inglis [12] published, the presence of a crack induces the concentration of stresses in the crack tips, which produces the actuation of a stress which can be higher than the one applied. The fracture is produced when this stress overcome the material's resistance.

The located stress on the crack tip (A) is:

$$\sigma_A = \sigma \left(1 + \frac{2a}{b}\right), \quad (2)$$

where

σ_A is the located stress at the crack tip A,
 σ is the applied stress,
 a and b are the two axes of the ellipse.

If the major axis, a , increases relative to b , the elliptical hole begins to take the appearance of a sharp crack and Inglis decide to express the previous equation in terms of the radius of the curvature ρ .

$$\sigma_a = \sigma \left(1 + 2\sqrt{\frac{a}{\rho}}\right), \quad (3)$$

where

σ_a , σ and a means the same as in the previous equation,
 ρ is the radius of curvature.

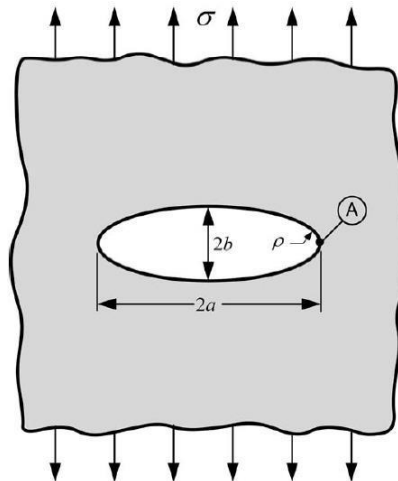


Figure 1: Elliptical hole in a flat hole.

But if it is assumed the following:

- $a \gg \gg b$, which means that the crack length is too much higher than the crack width
- $\rho = b^2/a$, being ρ the curvature's radius on the crack tip.

Then the located stress at the crack tip is:

$$\sigma_{loc} = 2\sigma \left(\frac{a}{\rho}\right)^{\frac{1}{2}}, \quad (4)$$

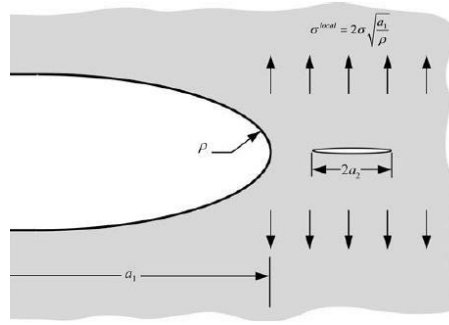


Figure 2: Sharp microcrack at the tip of a macroscopic crack.

The equation (4) predicts an infinite stress at the tip of an infinitely sharp crack ($\rho=0$). This caused some controversy because any material can support an infinite stress at the tip. This paradox motivated Griffith to develop his theory based on energy rather than local stress on the crack's tip.

When the located stress reaches the critical stress value, it results into the following equation:

$$\sigma_f = \left(\frac{E\gamma_s}{4a} \right)^{\frac{1}{2}}, \quad (5)$$

where

σ_f is the remote stress at failure,
 E is the Young's modulus,
 γ_s is the surface energy per unit area.

But this equation is not exactly because it cannot be applied to the atomic level. Due to this fact, Gehlen and Kanninen [13] developed the following equation in where discrete atoms were connected by nonlinear springs:

$$\sigma_R = \sigma_{max} = (\gamma_s E / a)^2, \quad (6)$$

where

a is the crack length,
 γ_s and E are the same terms as the previous equation.

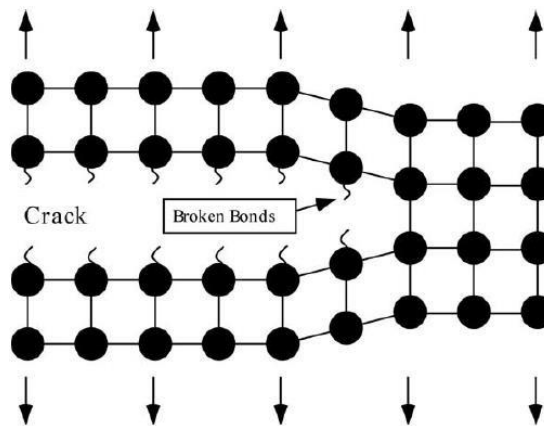


Figure 3: Crack propagation in an ideally brittle material.

Matching $\sigma_{loc} = \sigma_R$, then:

$$\sigma_R = \left[\left(\frac{\gamma E}{4a} \right) \left(\frac{\rho}{a} \right) \right]^{\frac{1}{2}}. \quad (7)$$

And if $\rho = a = 0.2 \text{ mm}$ and $\gamma = 10^{-2} Ea$, then:

$$\sigma_R = 10^{-3} E. \quad (8)$$

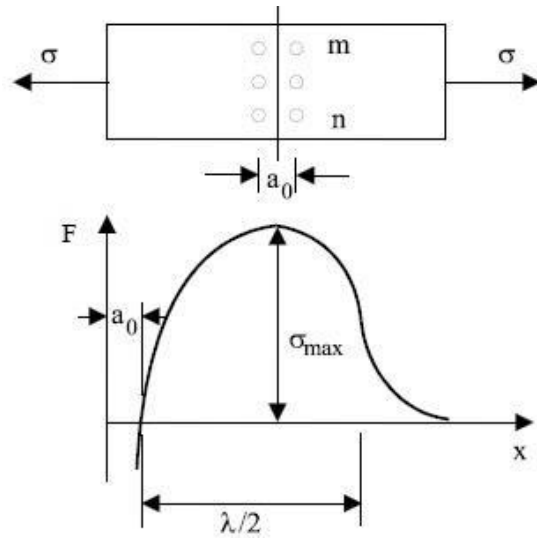


Figure 4: Necessary stress to overcome atomic bonds.

3.2.4. TENSIONAL STATE IN FRONT OF THE CRACK. STRESS ANALYSIS OF CRACKS

Applying the elasticity theory for a solid of any geometry with a crack subjected to external forces and assuming isotropic linear elastic material behaviour, it is possible to calculate the stress field expressions in the surroundings of the cracks. Defining a polar coordinate axis with the origin at the crack tip (see Figure 5), the stress field is given by the following expression [5]:

$$\sigma_{ij} = \left(\frac{K}{\sqrt{2\pi r}} \right) f_{ij}(\theta) + Cr^0 + Dr^{-\frac{1}{2}} + Er^{\frac{1}{2}} + \dots, \quad (9)$$

where:

- f_{ij} is a dimensionless function that depends on the θ angle,
- K is the stress intensity factor,
- σ_{ij} is the stress tensor,
- Both r and θ are defined in the Figure 5.

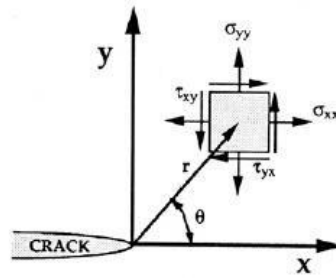


Figure 5: Definition of the coordinate axis and its stresses on the crack tip region.

The exact solution of the equation is a Taylor series in which only the leading term is important in the surroundings of the crack, in where it is possible to depreciate the rest of the terms. The higher – order terms depend on geometry, but the solution for any given configuration contains a leading term that is proportional to $1/\sqrt{r}$. Note that for $r = 0$, this equation describes a singularity. At this point, which is the crack tip, the stress tends to ∞ .

3.2.5. STRESS INTENSITY FACTOR

Each mode of loading produces the $1/\sqrt{r}$ [4] singularity at the crack tip, but the stress intensity factor K and the dimensionless factor f_{ij} depend on the mode. On the other hand, the stress intensity factor K is different for the three following modes, and each one differentiates between them as K_I , K_{II} , K_{III} .

The three possible modes that can be applied individually or combined in any cracked solid are:

- Mode I: the principal load is applied normal to the fracture plane (crack plane). It tends to open the crack.
- Mode II: there is a share load that slides one crack face with respect to the other face.
- Mode III: there is a share load that slides the crack in a parallel direction to the crack face.

A cracked body can be loaded in any one of these modes or a combination of two or three modes.

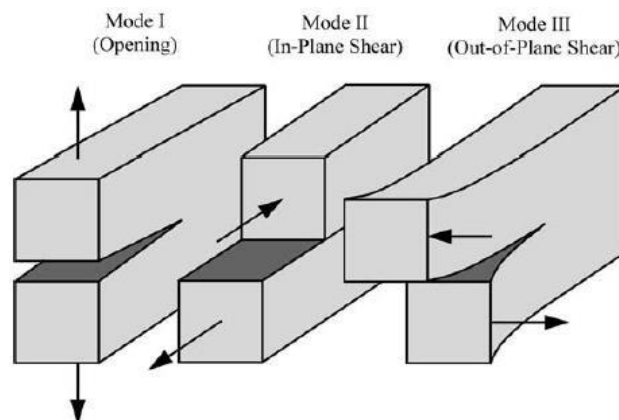


Figure 6: The three modes of loading that can be applied to a crack.

The stress fields ahead of a crack tip in an isotropic linear elastic material can be given by:

$$\lim_{r \rightarrow 0} \sigma_{ij}^{(I)} = \frac{K_I}{\sqrt{2\pi r}} f_{ij}^{(I)}(\theta) \text{ for Mode I,} \quad (10)$$

$$\lim_{r \rightarrow 0} \sigma_{ij}^{(II)} = \frac{K_{II}}{\sqrt{2\pi r}} f_{ij}^{(II)}(\theta) \text{ for Mode II,} \quad (11)$$

$$\lim_{r \rightarrow 0} \sigma_{ij}^{(III)} = \frac{K_{III}}{\sqrt{2\pi r}} f_{ij}^{(III)}(\theta) \text{ for Mode III.} \quad (12)$$

In a mixed – mode problem, in other words, more than one load mode is present, the individual contributions to a given stress component are additive:

$$\sigma_{ij}^{(total)} = \sigma_{ij}^{(I)} + \sigma_{ij}^{(II)} + \sigma_{ij}^{(III)}. \quad (13)$$

The following tables show detailed expressions for singular stress fields for Mode I and Mode II, displacement relationships for Mode I and Mode II and nonzero stress displacement components for Mode III.

	Mode I	Mode II
σ_{xx}	$\frac{K_I}{\sqrt{2\pi r}} \cos\left(\frac{\theta}{2}\right) \left[1 - \sin\left(\frac{\theta}{2}\right) \sin\left(\frac{3\theta}{2}\right)\right]$	$-\frac{K_{II}}{\sqrt{2\pi r}} \sin\left(\frac{\theta}{2}\right) \left[2 + \cos\left(\frac{\theta}{2}\right) \cos\left(\frac{3\theta}{2}\right)\right]$
σ_{yy}	$\frac{K_I}{\sqrt{2\pi r}} \cos\left(\frac{\theta}{2}\right) \left[1 + \sin\left(\frac{\theta}{2}\right) \sin\left(\frac{3\theta}{2}\right)\right]$	$\frac{K_{II}}{\sqrt{2\pi r}} \sin\left(\frac{\theta}{2}\right) \cos\left(\frac{\theta}{2}\right) \cos\left(\frac{3\theta}{2}\right)$
τ_{xy}	$\frac{K_I}{\sqrt{2\pi r}} \cos\left(\frac{\theta}{2}\right) \sin\left(\frac{\theta}{2}\right) \cos\left(\frac{3\theta}{2}\right)$	$\frac{K_{II}}{\sqrt{2\pi r}} \cos\left(\frac{\theta}{2}\right) \left[1 - \sin\left(\frac{\theta}{2}\right) \sin\left(\frac{3\theta}{2}\right)\right]$
σ_{zz}	0 (Plane stress) $\nu (\sigma_{xx} + \sigma_{yy})$ (Plane strain)	0 (Plane stress) $\nu (\sigma_{xx} + \sigma_{yy})$ (Plane strain)
τ_{xz}, τ_{yz}	0	0

Note: ν is Poisson's ratio.

Table 1: Stress Fields Ahead of a Crack Tip for Mode I and Mode II in a Linear Elastic, Isotropic Material.

	Mode I	Mode II
u_x	$\frac{K_I}{2\mu} \sqrt{\frac{r}{2\pi}} \cos\left(\frac{\theta}{2}\right) \left[\kappa - 1 + 2\sin^2\left(\frac{\theta}{2}\right)\right]$	$\frac{K_{II}}{2\mu} \sqrt{\frac{r}{2\pi}} \sin\left(\frac{\theta}{2}\right) \left[\kappa + 1 + 2\cos^2\left(\frac{\theta}{2}\right)\right]$
u_y	$\frac{K_I}{2\mu} \sqrt{\frac{r}{2\pi}} \sin\left(\frac{\theta}{2}\right) \left[\kappa + 1 - 2\cos^2\left(\frac{\theta}{2}\right)\right]$	$\frac{K_{II}}{2\mu} \sqrt{\frac{r}{2\pi}} \cos\left(\frac{\theta}{2}\right) \left[\kappa - 1 - 2\sin^2\left(\frac{\theta}{2}\right)\right]$

Note: μ is the shear modulus. $\kappa = 3 - 4\nu$ (plane strain) and $\kappa = \frac{3-\nu}{1+\nu}$ (plane stress).

Table 2: Crack – Tip Displacement Fields for Mode I and Mode II (Linear Elastic, Isotropic Material).

$\tau_{xz} = -\frac{K_{III}}{\sqrt{2\pi r}} \sin\left(\frac{\theta}{2}\right)$
$\tau_{yz} = \frac{K_{III}}{\sqrt{2\pi r}} \cos\left(\frac{\theta}{2}\right)$
$u_z = \frac{2K_{III}}{\mu} \sqrt{\frac{r}{2\pi}} \sin\left(\frac{\theta}{2}\right)$

Table 3: Nonzero Stress and Displacement Components in Mode III (Linear Elastic, Isotropic Material).

Considering load Mode I and $\theta = 0$, the shear stress τ_{xy} is also cancelled (the crack plane is a principal plane) and the stresses in the x and y directions are equal as following:

$$\sigma_{xx} = \sigma_{yy} = \frac{K_I}{\sqrt{2\pi r}}. \quad (14)$$

The next figure shows the variation of the σ_{yy} stress normal to the crack plane versus the distance r from the crack tip. The previous equation is only valid near the crack tip, where the $1/\sqrt{r}$ singularity dominates the stress field.

In this way, it is defined a singularity – dominated zone in the surroundings of the crack tip where all the present stresses in every point of the crack are directly proportional to the stress intensity factor K for each mode. this stress intensity factor defines the amplitude of the crack – tip singularity. Moreover, if K is known, then it is possible to solve for all components of stress, strain and displacement as a function of r and θ . This single – parameter description of the area placed in the proximities of the crack tip is the most important concept of the Fracture Mechanics.

On the other hand, the stress intensity factor K is an expression that only depends on the stress applied σ , the crack length a , and the specimen's geometry C , as following:

$$K = C\sigma\sqrt{\pi a}. \quad (15)$$

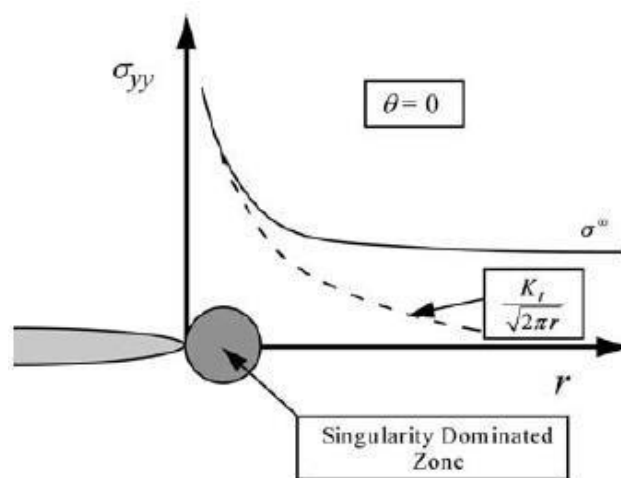


Figure 7: Variation of σ_{yy} on the crack tip area.

3.2.6. CRACK TIP PLASTICITY.

The expressions that defined the linear elastic stress state in the surroundings of the crack indicated that these equations tend to infinite at the crack tip ($r = 0$). However, in real materials stresses are always finite and in that part of the crack the yield strength of the material is overcome, it is plastically deformed and the material stops being elastic – linear.

In ceramic materials, as concrete o cement, this plastic deformation is very low, and the failure occurs almost immediately when the yield strength is overcome. It is possible to calculate the size of the plastic zone (assuming spherical zone) equalizing the y direction stress to the yield strength, and assuming crack plane ($\theta=0$), as follows:

$$\sigma_{yy} = \frac{K}{\sqrt{2\pi r}} = \sigma_{ys}, \quad (16)$$

where

- σ_{yy} is the normal stress in a linear elastic material,
- σ_{ys} is the yield strength.

Then, the size of the plastic zone will be:

$$r_y = \frac{1}{2\pi} \left(\frac{K_L}{\sigma_{ys}} \right)^2. \quad (17)$$

It can be demonstrated that the size of the plastic zone is twice higher, in other words, the value of r_y corresponds to the radius of this zone, because it has been supposed that this zone is spherical.

If we despise the strain hardening, then the stress distribution for $r = r_y$ can be represented by a horizontal line at $\sigma_{yy} = \sigma_{ys}$, and also the stress singularity is truncated by yielding at the crack tip. This is illustrated on the Figure 8:

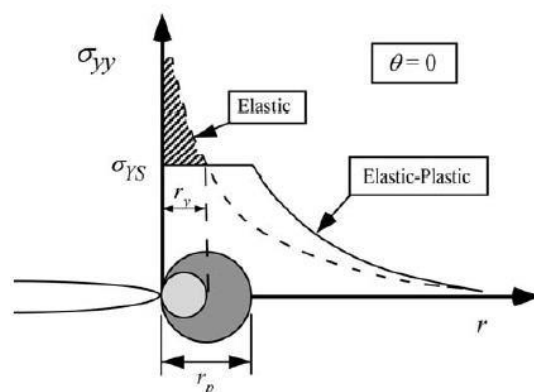


Figure 8: Plastic zone in the front of the crack.

3.2.7. PRINCIPLE OF SUPERPOSITION

As well as cannot be summed a normal stress with a shear stress, it is impossible to be summed the stress intensity factors as long as the mode of loading is consistent:

$$K^{(total)} = K_I^{(A)} + K_I^{(B)} + K_I^{(C)}, \quad (18)$$

but,

$$K_{(total)} \neq K_I + K_{II} + K_{III}. \quad (19)$$

3.2.8. MIXED – MODE FRACTURE

When two or the three modes of loading are present, the following equation indicates that the energy release rate contributions from each mode are additive:

$$G = \frac{K_I^2}{E'} + \frac{K_{II}^2}{E'} + \frac{K_{III}^2}{2\mu}, \quad (20)$$

where

$$E = E' \text{ Young's modulus for plane stress}, \quad (21)$$

and

$$E' = \frac{E}{1-\nu^2} \text{ Young's modulus for plane strain}. \quad (22)$$

That equation gives the energy release rate for planar crack growth at an angle $90^\circ - \beta$ from the applied stress.

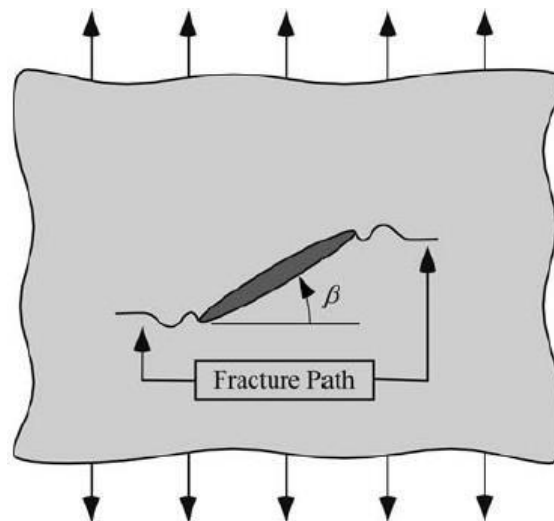


Figure 9: Propagation of a crack not orthogonal to the applied normal stress.

The last figure illustrates that when fracture occurs, the crack tends to propagate orthogonal to the applied normal stress, in other words, the mixed – mode crack becomes a Mode I crack.

PROPAGATION OF AN ANGLED CRACK.

For uniaxial loading, the stress intensity factor for Mode I and Mode II are given by:

$$K_I = K_{I(0)} \cos^2 \beta, \quad (23)$$

$$K_{II} = K_{I(0)} \cos \beta \sin \beta. \quad (24)$$

Where $K_{I(0)}$ is the Mode I stress intensity when $\beta = 0^\circ$. The crack – tip stress fields for the Mode I portion of the loading are given by:

$$\sigma_{rr} = \frac{K_I}{\sqrt{2\pi r}} \left[\frac{5}{4} \cos \left(\frac{\theta}{2} \right) - \frac{1}{4} \cos \left(\frac{3\theta}{2} \right) \right], \quad (25)$$

$$\sigma_{\theta\theta} = \frac{K_I}{\sqrt{2\pi r}} \left[\frac{3}{4} \cos \left(\frac{\theta}{2} \right) + \frac{1}{4} \cos \left(\frac{3\theta}{2} \right) \right], \quad (26)$$

$$\tau_{r\theta} = \frac{K_I}{\sqrt{2\pi r}} \left[\frac{1}{4} \sin \left(\frac{\theta}{2} \right) + \frac{1}{4} \sin \left(\frac{3\theta}{2} \right) \right]. \quad (27)$$

The singular stress fields for Mode II are given by:

$$\sigma_{rr} = \frac{K_{II}}{\sqrt{2\pi r}} \left[-\frac{5}{4} \sin \left(\frac{\theta}{2} \right) + \frac{3}{4} \sin \left(\frac{3\theta}{2} \right) \right], \quad (28)$$

$$\sigma_{\theta\theta} = \frac{K_{II}}{\sqrt{2\pi r}} \left[-\frac{3}{4} \sin \left(\frac{\theta}{2} \right) - \frac{3}{4} \sin \left(\frac{3\theta}{2} \right) \right], \quad (29)$$

$$\tau_{r\theta} = \frac{K_{II}}{\sqrt{2\pi r}} \left[\frac{1}{4} \cos \left(\frac{\theta}{2} \right) + \frac{3}{4} \cos \left(\frac{3\theta}{2} \right) \right]. \quad (30)$$

In the case that the crack forms an infinitesimal kink at an angle α from the plane of the crack, then the local stress intensity factors at the tip of this kink differ from the nominal K values of the main crack.

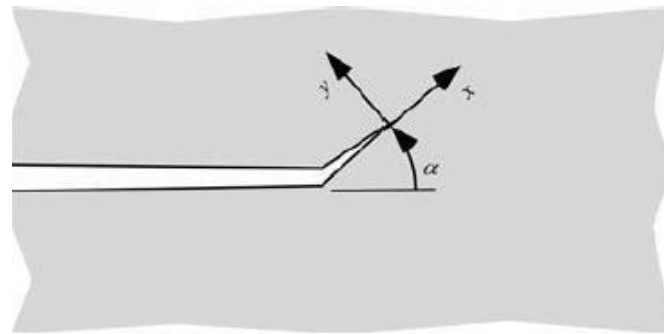


Figure 10: Infinitesimal kink at the crack tip and the $x - y$ coordinate system.

Defining a local $x - y$ coordinate system at the tip of the kink and considering the previous equations, if these equations define the local stress fields, the local Mode

I and Mode II stress intensity factors at the tip are obtained by summing the normal and shear stresses at α :

$$k_I(\alpha) = \sigma_{yy} \sqrt{2\pi r} = C_{11}K_I + C_{12}K_{II}, \quad (31)$$

$$k_{II}(\alpha) = \tau_{xy} \sqrt{2\pi r} = C_{21}K_I + C_{22}K_{II}, \quad (32)$$

Where k_I and k_{II} are the local stress intensity factors at the tip of the kink and K_I and K_{II} are the stress intensity factors for the main crack, given in the equations (23) and (24). The coefficients C_{ij} are given by:

$$C_{11} = \frac{3}{4} \cos\left(\frac{\alpha}{2}\right) + \frac{1}{4} \cos\left(\frac{3\alpha}{2}\right), \quad (33)$$

$$C_{12} = -\frac{3}{4} \left[\sin\left(\frac{\alpha}{2}\right) + \sin\left(\frac{3\alpha}{2}\right) \right], \quad (34)$$

$$C_{21} = \frac{1}{4} \left[\sin\left(\frac{\alpha}{2}\right) + \sin\left(\frac{3\alpha}{2}\right) \right], \quad (35)$$

$$C_{22} = \frac{1}{4} \cos\left(\frac{\alpha}{2}\right) + \frac{3}{4} \cos\left(\frac{3\alpha}{2}\right), \quad (36)$$

The energy release rate for the kinked crack is given by:

$$G(\alpha) = \frac{k_I^2(\alpha) + k_{II}^2(\alpha)}{E}. \quad (37)$$

The following figure illustrates a plot of $G(\alpha)$ normalized by $G(\alpha = 0)$.

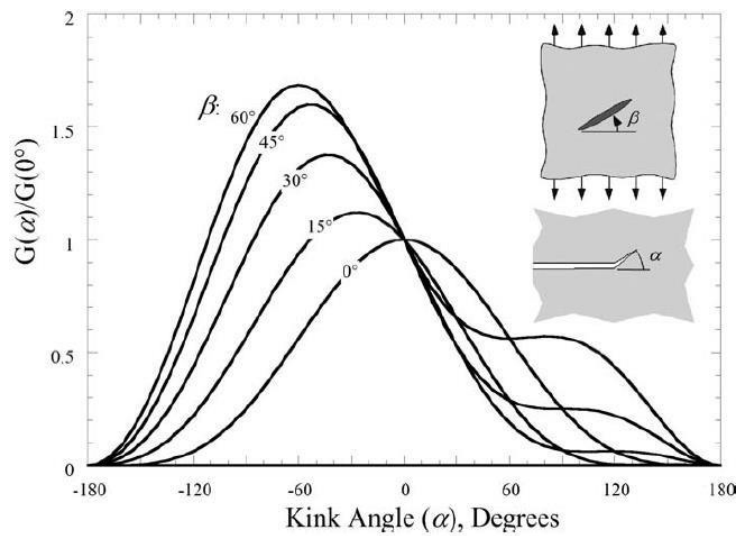


Figure 11: Local energy release rate at the tip of a kinked crack.

The peak in $G(\alpha)$ at each β corresponds to the point where k_I shows a maximum and $k_{II} = 0$. So, the maximum energy release rate is given by:

$$G(\alpha) = \frac{k_I^2(\alpha^*)}{E}. \quad (38)$$

Where α^* is the angle at which both G and k_I shows a maximum and $k_{II} = 0$. Crack growth in a homogeneous material should initiate along α^* .

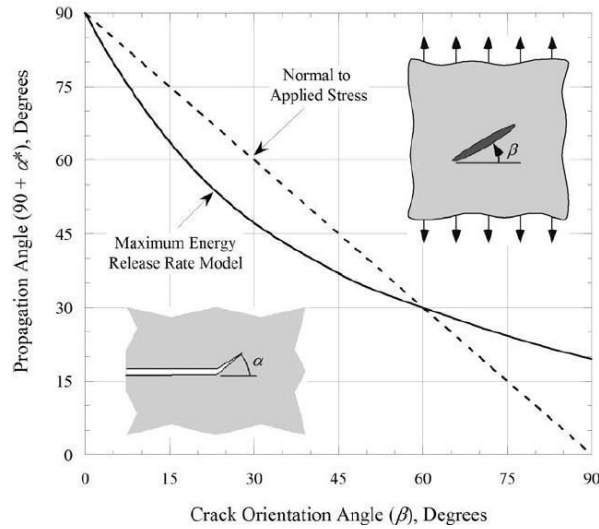


Figure 12: Optimum propagation angle for a crack oriented at an angle β from the stress axis.

This figure exhibits the effect of β on the optimum propagation angle. The dashed line corresponds to propagation perpendicular to the remote principal stress.

3.2.9. T – STRESS

The T – stress is a parameter that allows engineers to characterize the level of constraint and the fields of stresses and displacements around the crack tip [14]. This parameter represents the stress parallel to the crack line, only in plane conditions.

When the crack is inclined with respect to the action of the loads, as this thesis' case. Generally, the stress intensity factor is enough to characterize the stress state and the displacements, but there are some cases where the parameter T – stress can be large in comparison with the other parameters, reason why it is important to take it into [15].

There are many methods to calculate the T – stress [16]. As examples, different approaches stand out, as Fett [17,18] who proposed several solutions for the T – stress for a centrally cracked BD with different crack lengths and loading conditions or Ayatollahi et al. [19,20] who obtained the elastic T – stress directly by evaluating the stresses along the crack flanks and near the crack tip using the FEM.

However, apart from these methods, one of them can explain the T – stress parameter referring to the characterization of the crack tip by polar coordinates, as follows:

$$T = \lim_{r \rightarrow 0} (\sigma_{xx} - \sigma_{yy})_{\theta=0}, \quad (39)$$

where

- σ_{xx} and σ_{yy} represent the stress components along the axis x and y ,
- θ is the polar coordinate angle.

For θ equals to zero, then the T – stress can be calculated by the difference between σ_{xx} and σ_{yy} .

3.2.10. SINGLE – PARAMETER VERSUS MULTI – PARAMETER APPROACH

The linear elastic fracture mechanics (LEFM) describe the stress distribution state in cracked components in terms of the stress intensity factors. This approach is the most common for assessment of fracture behaviour of several structures and materials [21].

The LEFM is also called as single – parameter because the stress intensity factor is the only parameter which is taken into account in order to define the stress and displacements fields near the crack tip. However, the LEFM has several limitations. The most important is that the extent of the zone of non – linear behaviour that should be small enough in comparison to the typical structural dimensions.

For materials as composite (as concrete or ceramic, as cement) that are quasi – brittle materials, this restriction is too strong because there are many parameters which have to be considered in the process of their fracture such as heterogeneities, microcracks or other defects [11].

In general, the fracture process of ceramic materials is characterized by the existence of a large fracture zone. Thus, the principles of the conventional linear elastic fracture mechanics concept are not valid for this case.

On the other hand, the multi – parametric approach is used to the problems have been explain before. The use of more one or two parameters to approximate the stress and displacement states present a gear advantage for materials as ceramic. This multi – parametric approach is based on the Williams expansion.

3.2.11. WILLIAMS EXPANSION.

The Williams solution of the crack-tip stress and displacement field distribution in a cracked specimen provides a reasonable approximation. It is expressed in a form of a series expansion, particularly as a power series. This solution was originally delivered for a homogeneous elastic isotropic cracked material with an arbitrary remote loading.

The stress series expansion is the following:

$$\sigma_{ij} = \sum_{n=1}^{\infty} r^{\frac{n}{2}-1} A_n f_n^{\sigma}(\theta, n) + \sum_{m=1}^{\infty} r^{\frac{m}{2}-1} B_m g_m^{\sigma}(\theta, m) \quad i, j \in \{x, y\}, \quad (40)$$

$$u_i = \sum_{n=0}^{\infty} r^{\frac{n}{2}} A_n f_i^u(\theta, n, E, \nu) + \sum_{m=0}^{\infty} r^{\frac{m}{2}} B_m g_i^u(\theta, m, E, \nu) \quad i, j \in \{x, y\}. \quad (41)$$

3.3. BRAZILIAN DISC TEST

3.3.1. INTRODUCTION

The BD test is an indirect tensile test, representative and simple, that is useful to obtain the maximum load in a specimen before the collapse. Is a widely used test to evaluate the tensile strength and is specified in the standards [22].

This test is thought to be carried out on cylindrical specimens, although it is possible to carry out using prismatic or cubic specimens, but it is necessary the use of correction coefficients that the standard provides.

3.3.2. TEST DESCRIPTION

This essay consists in the application of a diametral compression load in a cylindrical specimen along two opposite generatrices until the failure. This load configuration induces a relatively uniform load tensile along the diameter of the plane of the vertical load, and this traction spend the specimen and produces the failure.

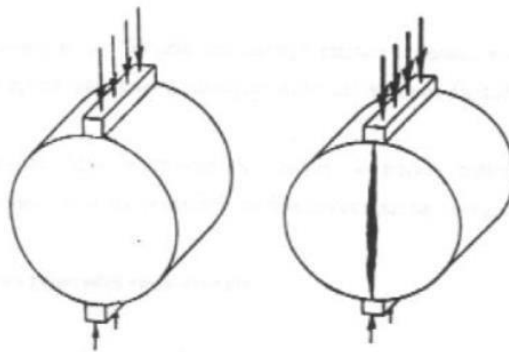


Figure 13: The specimen is loaded by compression loads along the vertical diametral plane.

In order to load the specimen, it is necessary to situate the example horizontally between the two plates of a press. As part of this mechanism there are two elements that oversee avoid the local failure of the specimen during the test. It will be necessary to consider the temperature of the test because the material behaviour will widely depend on this variable.

The following are some of the most important advantages of this test:

- Is a very simple test.
- The failure is not affected by the conditions of the specimen's surface.
- The applied load can be static or dynamic, modifying the press type in function of the type of study.

Aside from the tensile strength information, this test can inform about the elastic properties as static/dynamic elasticity module or the permanent deformation.

3.3.3. THEORETICAL STRESS DISTRIBUTION

The theoretical solution of the stress distribution inside a cylindrical specimen is based on the analysis of the elastic and linear behaviour of a material.

When a diametral compression load is applied to a cylindrical specimen, it develops a bi-dimensional stress state inside. The applied load along the two-diametrical opposite generatrices describes horizontal and vertical main stress planes. Particularly, on the vertical plane appears a variable compression stress and a theoretical uniform tensile stress.

If an analysis if the break is made, it is shown that the initial crack appears when the horizontal tensile stress developed on the vertical plane reaches the tensile strength value of the material.

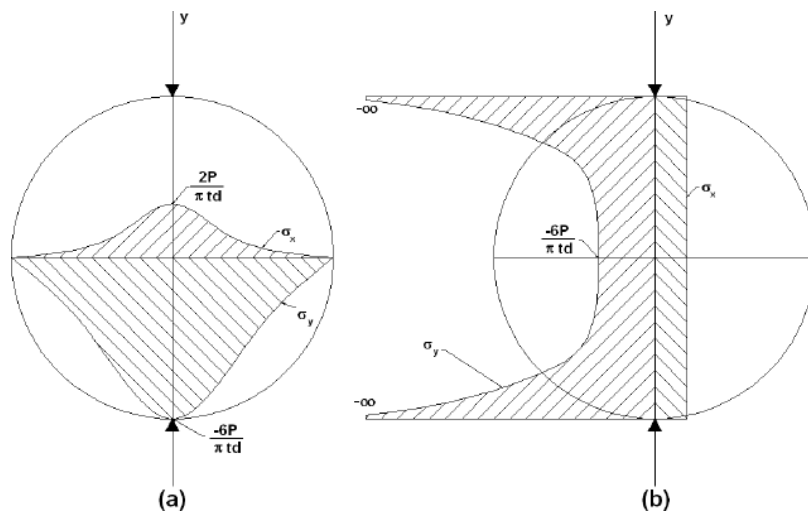


Figure 14: Theoretical stress distribution on horizontal and vertical axis.

3.3.4. TENSILE STRENGTH

The initial failure occurs by tensile break, therefore, the indirect tensile strength in the failure moment:

$$\sigma = \frac{2P_{max}}{\pi t d}, \quad (48)$$

where

- σ is the indirect tensile strength to the failure,
- P_{max} is the maximum load or failure load,
- t is the thickness of the specimen,
- d is the diameter of the specimen,
- x, y are the coordinates respect from the specimen's centre.

According to this linear load conditions, the specimen would collapse near the load points due to the compression stresses and not in the central area due to the tensile stresses.

However, this compression stresses are considerably reduced distributing the loading along the load plate. This plate reduces the vertical compression stresses and change the horizontal stresses along the vertical diameter from tensile to compression near the application points. The resulting stress distribution is illustrated on the following figure.

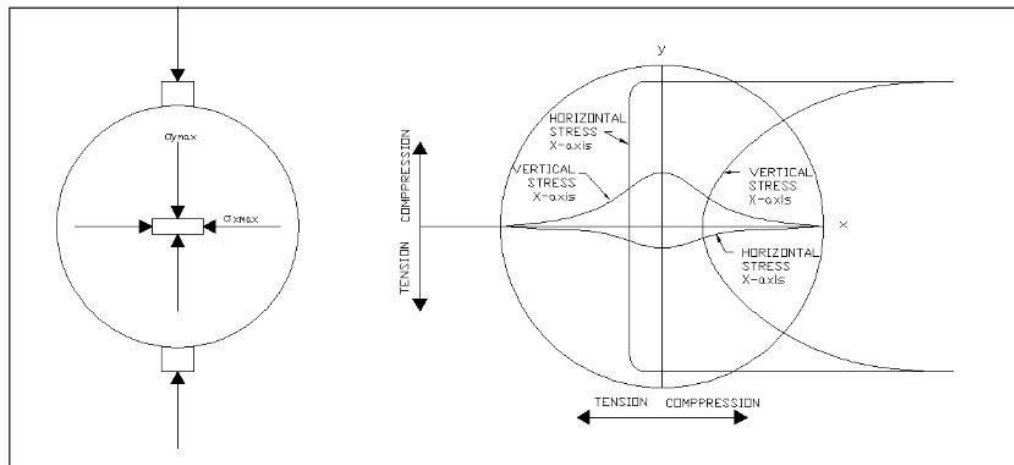


Figure 15: Stress distribution in a specimen subjected to a load applied on a curved support load plate. [23]

4. NUMERICAL MODELLING IN ANSYS

The numerical modelling of the test has been done in ANSYS software [24]. ANSYS is a software of engineering simulation which allows engineers to know how a product will work in a certain environment. This behaviour is studied under the ideas of the FEM to structures.

ANSYS is divided in three different tools, called modules, which are pre – processor, processor, post – processor. The pre – processor creates the geometry and the meshing. In this part is also defined the material properties. In the processor part is applied the forces and the boundary conditions and it is obtained the solution for the problem. Finally, in the post – processor is possible to have a visualization of the results as well as the deformed shape of the geometry. The visualization of the results included a list of the results in a table.

In this thesis, the geometry of the model has been modelled as a 2D model with plane strain conditions. As it has been said before, one of the aims of the thesis is obtain the calibration curves for each mode of stress intensity factors.

4.1. GEOMETRY

The modelled disc has the following dimensions diameter, $D = 100$ mm with relative crack length, $a/R = [0,1; 0,9]$ and notch angle $\alpha = 0^\circ, 90^\circ$.

The aim of this variety of the crack ratio and the notch angle is to study the stress intensity factors to different crack length.

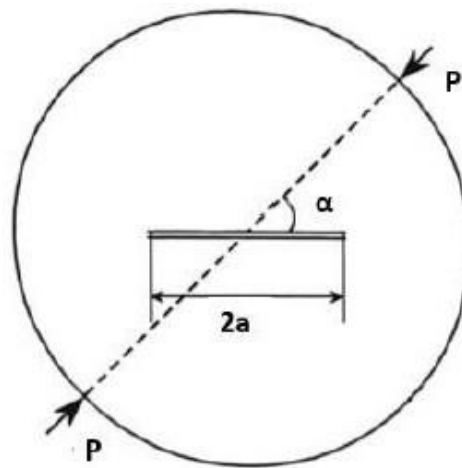


Figure 16: Scheme of geometry of a typical BD specimen with a load arbitrary position alongside crack.

4.2. ELEMENT TYPE

There so many element types available to use in analysis. These elements are identified by a name consisting of a group label and a unique identifying number.

Each element is identified by a maximum of eight characters. Depending upon the element type used it is possible to model solids in 2D or 3D. 2D models are defined in a XY plane, and at the time that a 3D element is included on the set, the model becomes 3D.

The command KEYOPT sets the element type, which are defined on the *ET* command. In this thesis the element type used is PLANE183. This element type is a higher order 2 -D, 8 – node or 6 – node element (see Figure 17). This element has two degrees of freedom at each node: translations in the nodal x and y directions. This element can be used as a plane element (plane stress, plane strain and generalized plane strain) or as an axisymmetric element [25]

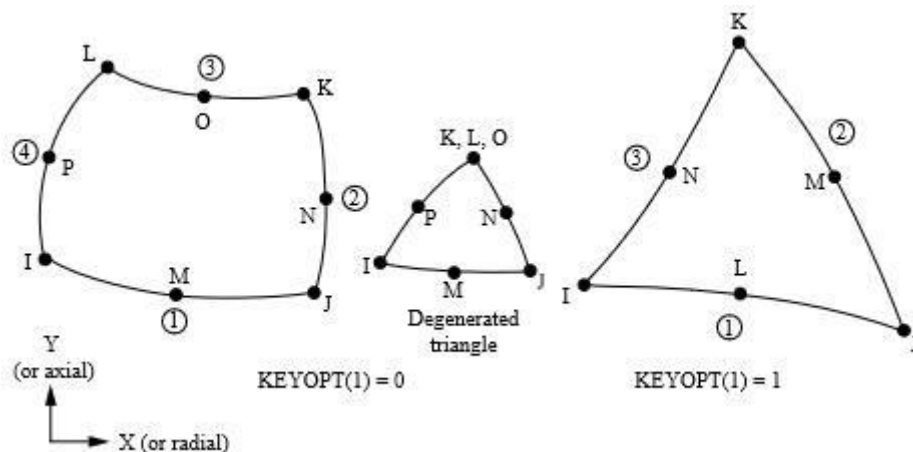


Figure 17: Element type PLANE183 2D 8 – node taken from [24].

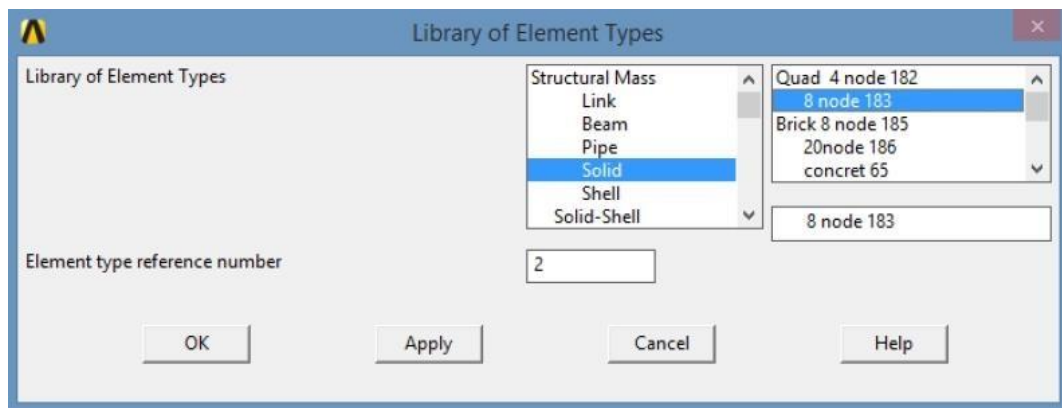


Figure 18: Element type PLANE183 used in ANSYS.

In general, four shapes of elements are possible to use: keypoints, lines, areas and volumes. However, in this thesis will be used only the first ones, in order to create a 2D solid.

KEYPOINTS

Keypoints refer to points that are created to define geometric entities. In other words, keypoints are necessary to model the specimen.

LINES

As well as keypoints are necessary to define geometric entities, lines also, because they join one keypoint with another, creating a complete 2D entity. It will be necessary to create both straight and arc lines.

AREAS

Areas define the space between three or more lines with the aim of creating a 2D solid. It is important to note that it is possible to create an area both joining lines between them or keypoints.

4.3. MATERIAL PROPERTIES

The material properties used in this model are the typical properties for concrete C50/60:

	YOUNG'S MODULUS	POISSON'S RATIO
CONCRETE C50/60	44 GPa	0.2

Table 4: Material Properties for concrete C50/60 used on the experiment.

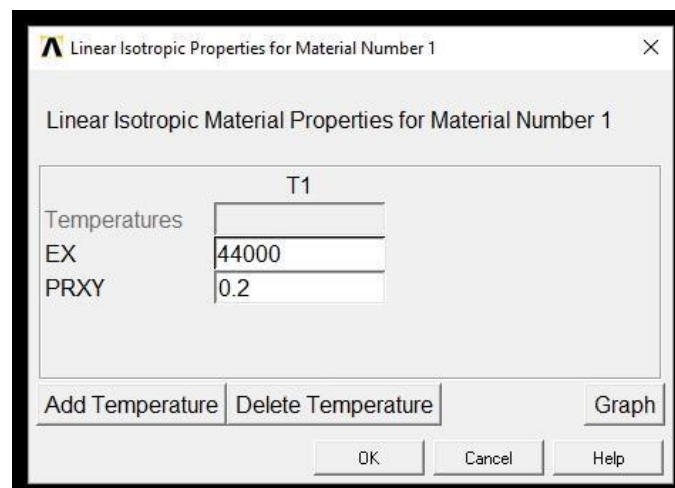


Figure 19: Material properties in ANSYS.

Note that the units used in ANSYS are Newtons (N) and millimetres (mm). That is the reason why EX is 44000 MPa (N/mm²) what it is 44 GPa = 44000 MPa.

4.4. MODELLING OF THE SPECIMEN

Once the element type and the material properties are defined it is necessary to follow the following steps in order to create the specimen model.

4.4.1. MODELLING OF THE KEYPOINTS

There is a total of 53 keypoints, but not all of them are modelled in the same way. This means that there are some keypoints in Cartesian coordinate system, and others that are modelled in cylindrical coordinate system.

First of all, it is necessary to model the first keypoint on the coordinate's origin (0,0) which will be the one that will be referenced by the rest of the keypoints.

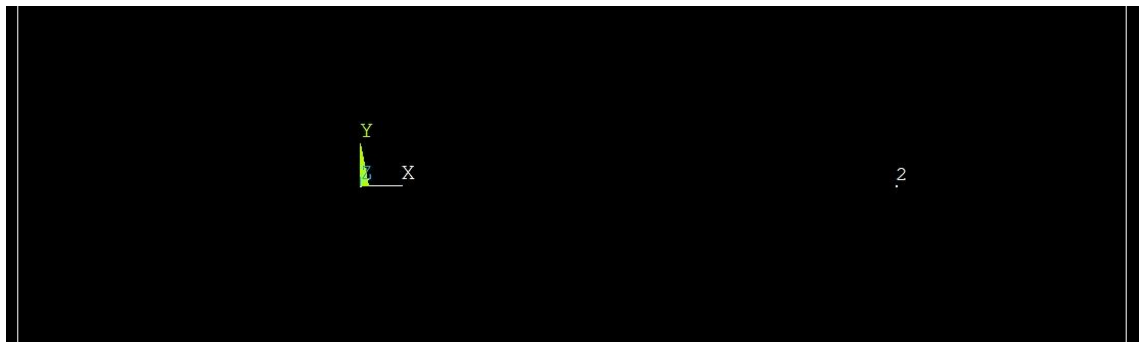


Figure 20: First and second keypoints. Keypoint number 2 at the coordinate (1,0) in relation with the first keypoint which is on the coordinate origin.

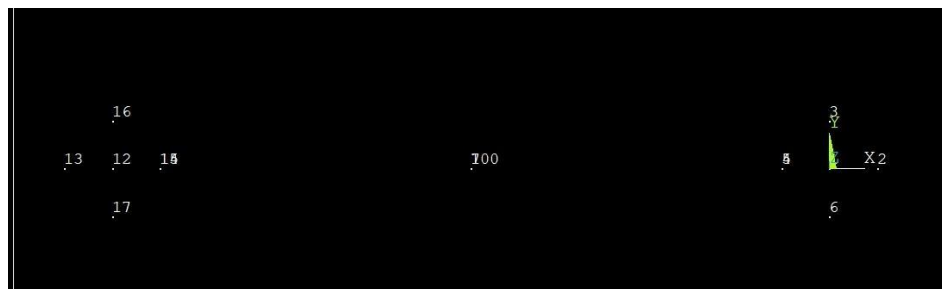


Figure 21: Crack tips of the specimen.

The keypoints modelled in the Figure 21 are in the Cartesian coordinate system. In that figure it is possible to appreciate the shape of the crack tip in both sides of the crack length.

Note also that there are two keypoints at the same three locations. This is because the crack length will tend to open once the loads are applied and it is necessary to study the situation for each part. This is illustrated in the next figures:

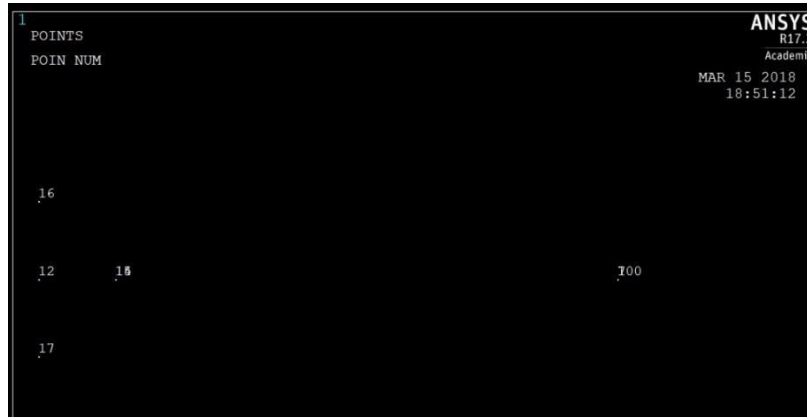


Figure 22: Crack tip left part.

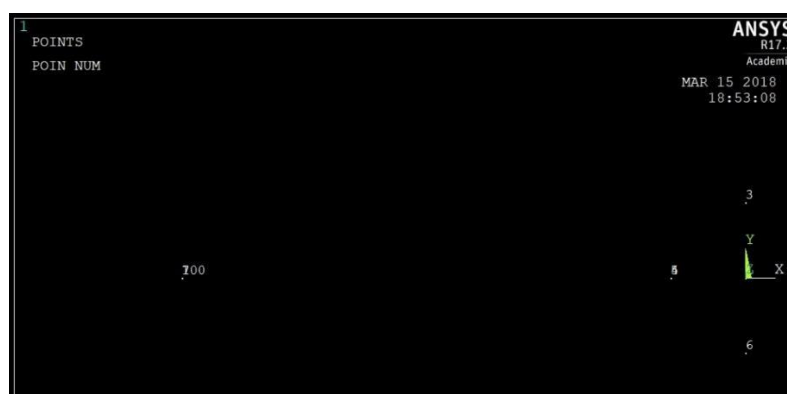


Figure 23: Crack tip right part.

The rest of the keypoints belong to the peripheral contour and it is necessary to use the cylindrical coordinate system.

In order to use this new coordinate system, is necessary to use the *LOCAL* command to use the cylindrical coordinate system instead of the Cartesian one.

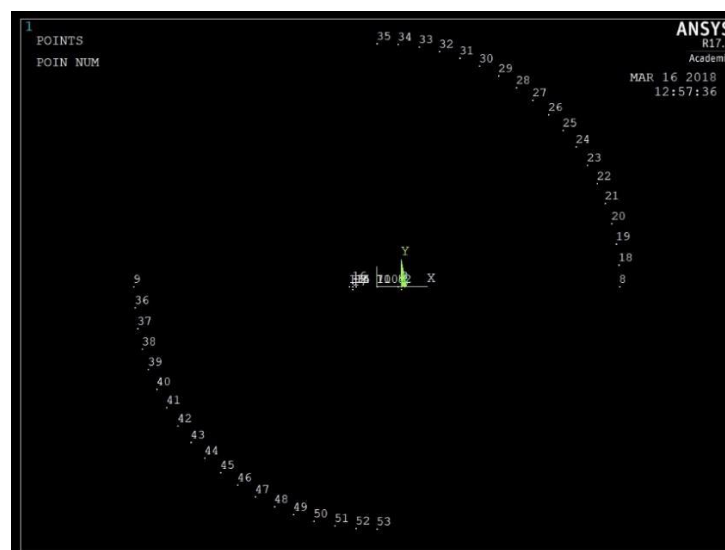


Figure 24: Periphery contour keypoints.

4.4.2. MODELLING OF THE LINES

There is a total of 72 lines. In the same way as the keypoints, not all the lines are modelled equally. This means that some lines will be modelled in the Cartesian coordinate system and others in the cylindrical coordinate system.

For the keypoints of the crack tip the modelled lines will be on the Cartesian coordinate system, but since the current coordinate system is cylindrical, it is necessary to use a new command to call the previous coordinate system and not use the *LOCAL* command again. This new command is *CSYS*.

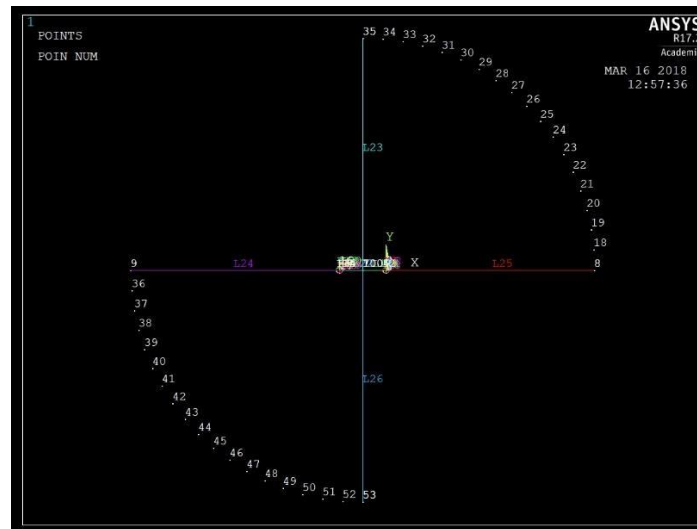


Figure 25: Lines in the surroundings of the crack.

For the lines in the periphery contour, it is necessary to call the cylindrical coordinate system, so it is necessary to use the *CSYS* command before modelling the lines.

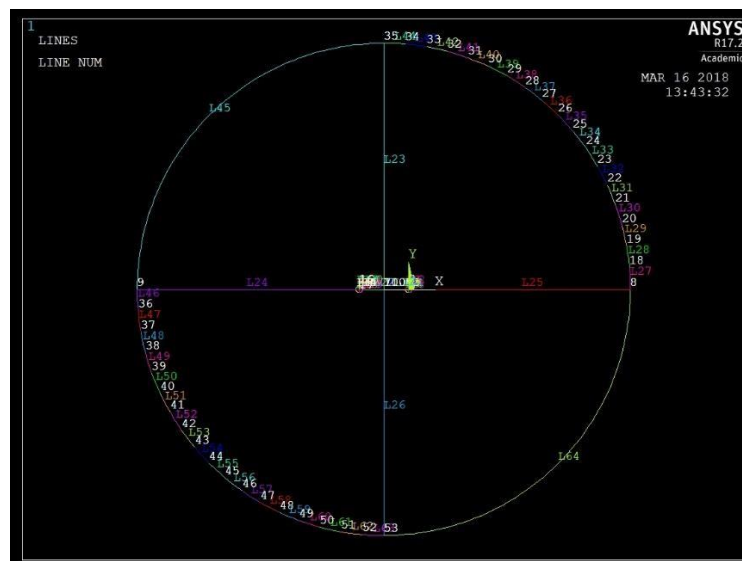


Figure 26: Lines in the periphery contour.

Once the lines are modelled, the next step is model the areas, but as it has been said before, areas modelled from lines have a maximum number of 10 lines. So, because of that, it is necessary to divide the first and the third quarters of the specimen into different geometries in order to model areas. These new lines will be in the Cartesian coordinate system.

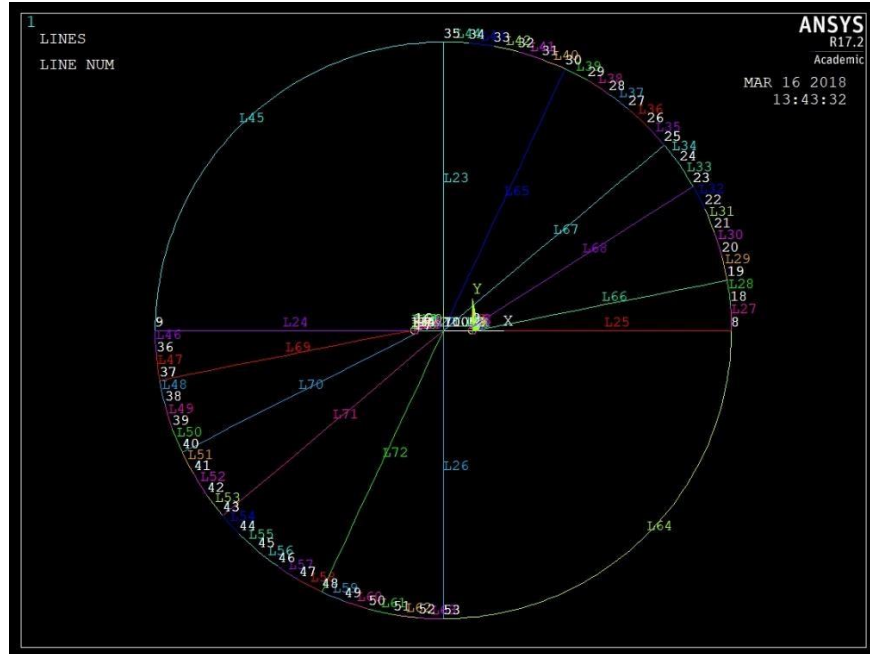


Figure 27: Lines dividing areas.

4.4.3. MODELLING AREAS

There is a total of 20 areas, all of them modelled in the Cartesian coordinate system.

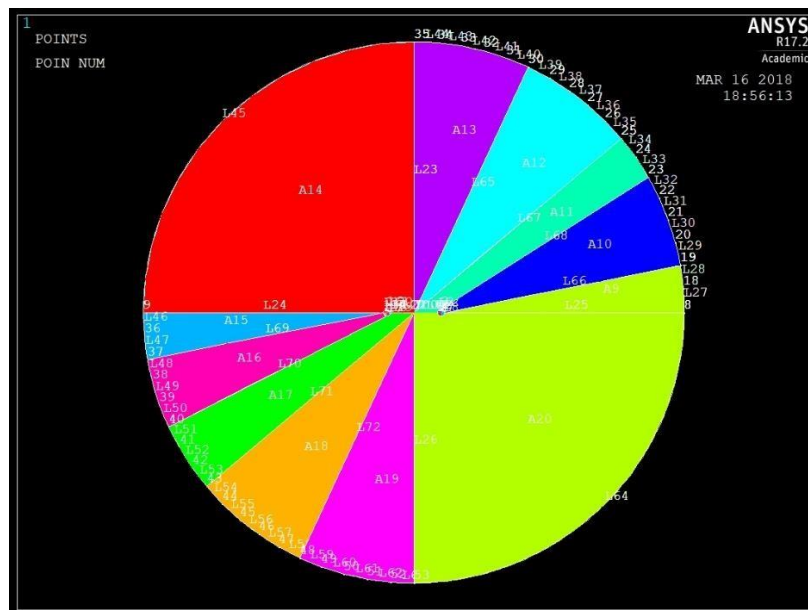


Figure 28: Areas modelling.

4.5. MESHING

Meshing is defined as the process of dividing the whole component into several elements so that whenever the load is applied on the component it distributes the load uniformly called as meshing. If the solid is not mesh, then the load distribution once applied is not uniform and it is possible to get irregular or faulty results. It is important that the size of the divided elements be as small as possible so that the total number of elements divided must be as large as possible, helping the results to be accurate. It is necessary to use the *KSCON* command.

The *KSCON* command specifies a keypoint about which an area mesh will be skewed. During meshing, elements are initially generated circumferentially about and radially away from the keypoint. It should be noted that only one concentration keypoint per unmeshed area is allowed.

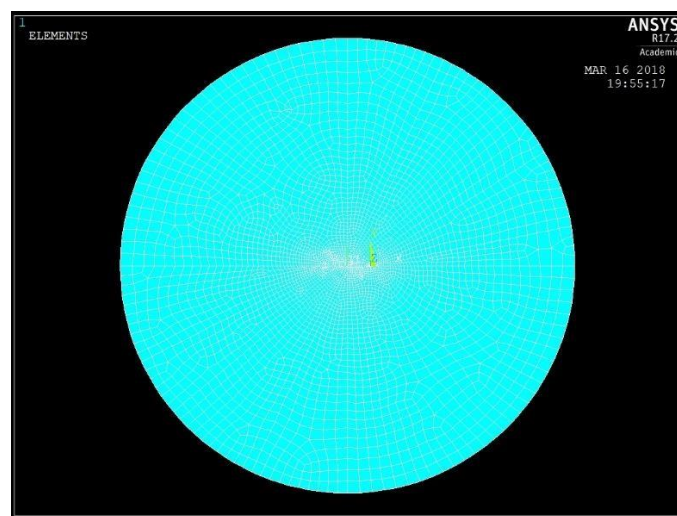


Figure 29: Meshing of the specimen.

4.6. BOUNDARY CONDITIONS

The boundary conditions are the loads and constraints that represent the effect of the surrounding environment on the model.

In this thesis, the boundary conditions that are applied to the model are the forces and the support. It will be a force applied symmetrically opposed to the support, with the aim of simulate the two symmetrical forces applied in the original test.

4.6.1. Modelling of the support

For the modelling of the support it is necessary to select the nodes where the displacements on X and Y direction will be restricted. First, it is necessary to call the solution processor of the program, in order to be able to model the boundary conditions and get the final solution of the calculation. Once the solution interface is active, it is possible to model the support.

It is necessary to write the *NSEL* command to select the nodes and specify the restriction of the displacement. Finally, the nodes and the elements drawing will be done. This is shown on the following figures.

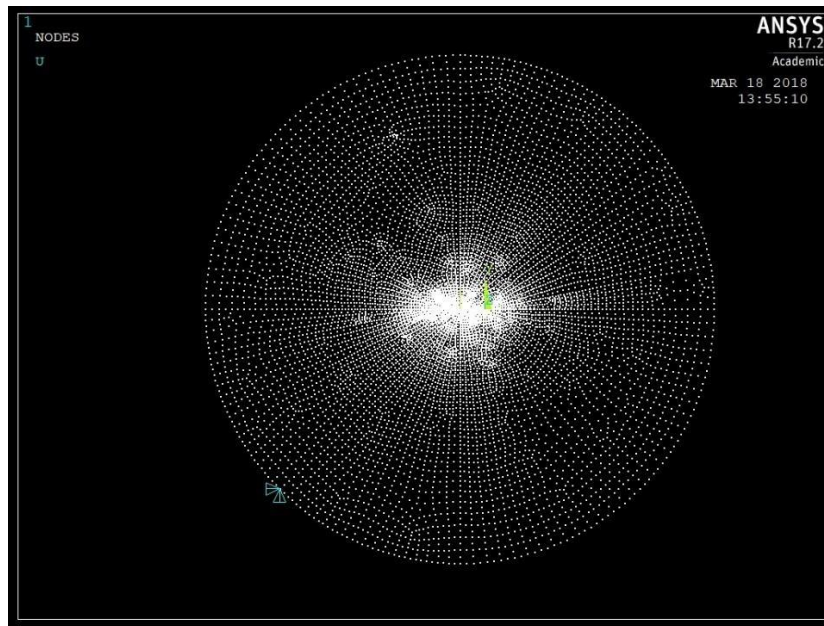


Figure 30: Boundary conditions: displacement constraints on X and Y direction.
Nodes drawing.

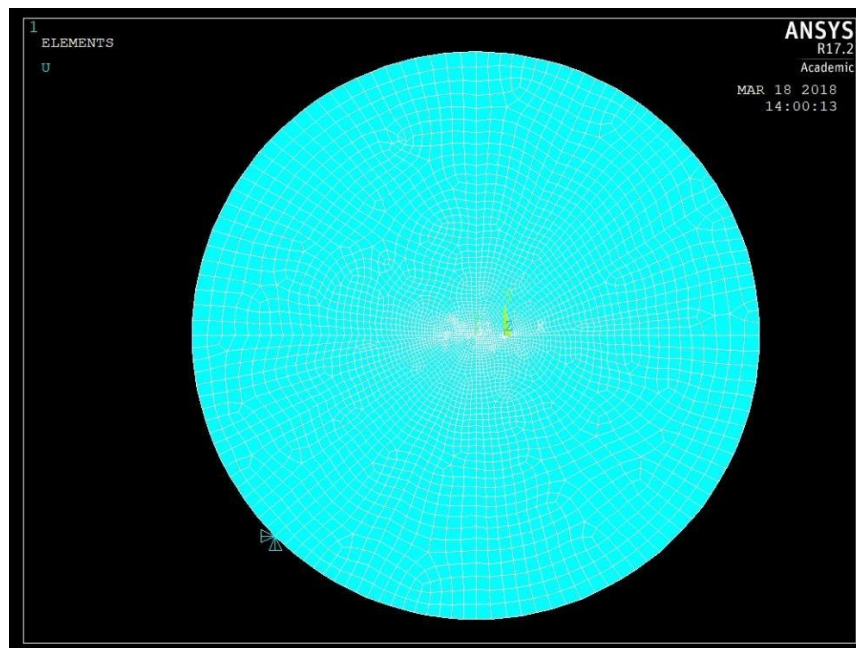


Figure 31: Boundary conditions: displacement constraints on X and Y direction.
Elements drawing.

4.6.2. MODELLING OF THE FORCES

As the force must be diametrically applied, then it will have two components, one in the X direction and the other on the Y direction. The value of the force will be 100 N. The way to model the force is the same as the support.

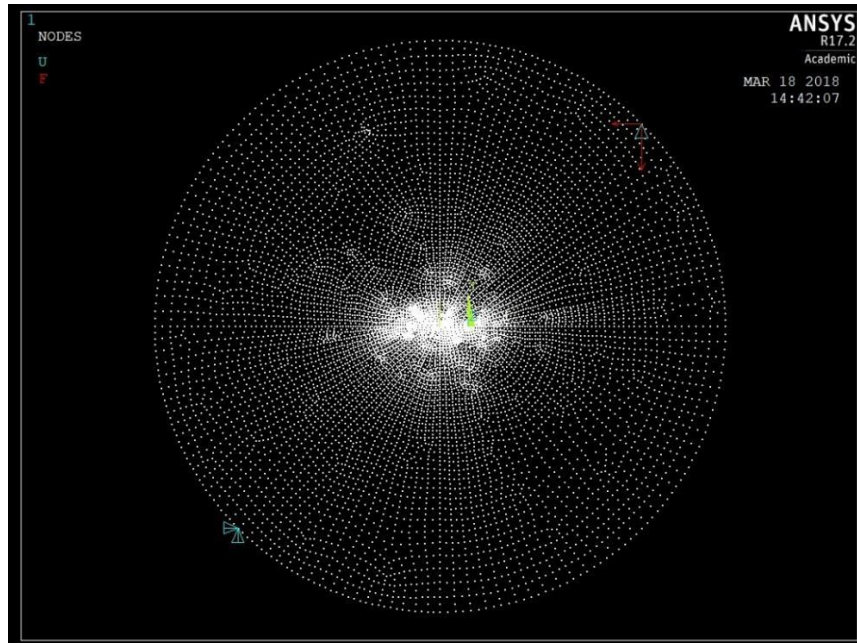


Figure 32: Boundary conditions: Forces on node for $\alpha = 45^\circ$ and $a/R = 0.1$. Nodes drawing.

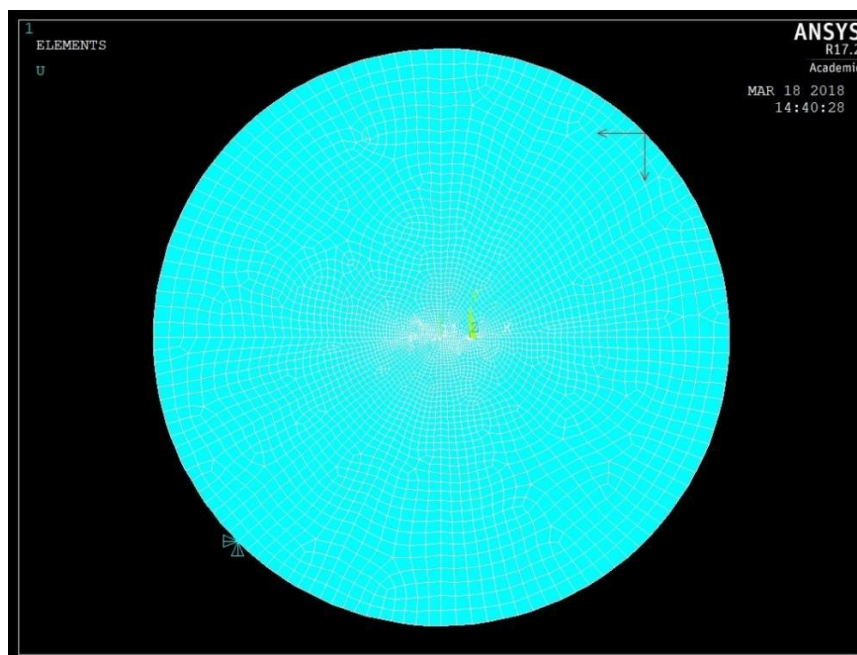


Figure 33: Boundary conditions: Forces on node for $\alpha = 45^\circ$ and $a/R = 0.1$. Elements drawing.

4.7. SOLUTION

The solution command is active and now is necessary to exit the processor interface and start the database results postprocessor.

In order to calculate SIFs of each force angle and crack length ratio, is necessary to set the path where the solution will be calculated. This path will be both sides of the crack tip, where all the stresses located on every point of the crack tip are directly proportional to the stress intensity factor. Because of that, if the SIF is known, then all the stress components of that region are also known. The path is modelled with the *LPATH* command in which it is necessary to specify the nodes that are going to be part of the path.

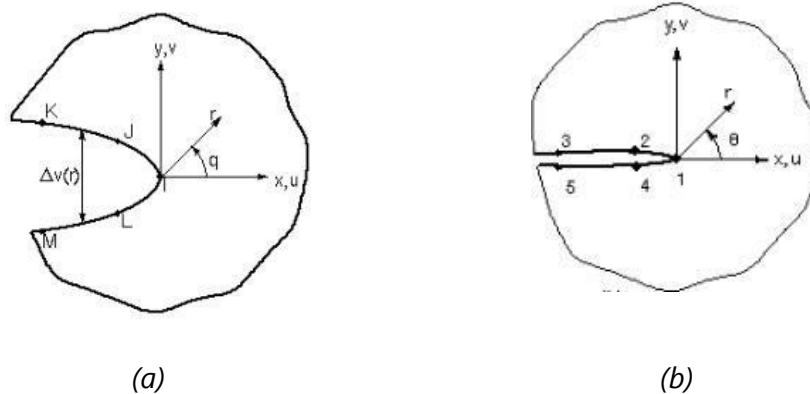


Figure 34: (a) Nodes used for the crack displacement in a full – crack model, taken from, (b) the path defined for a full – crack model. [26].

Finally, the most important part and the last step of the modelling part is the *KCALC* command which calculates the SIF results.

In this thesis, because the model has been modelled as one unique solid, it will be necessary five nodes on the path. On the same way, it has been working on plane stress condition. In my case, I will print local displacements in order to see how the crack tip has moved from its original position.

```

**** CALCULATE MIXED-MODE STRESS INTENSITY FACTORS ****

ASSUME PLANE STRESS CONDITIONS

ASSUME A FULL-CRACK MODEL (USE 5 NODES)

EXTRAPOLATION PATH IS DEFINED BY NODES:      1      128      127      126      125
WITH NODE      1 AS THE CRACK-TIP NODE

USE MATERIAL PROPERTIES FOR MATERIAL NUMBER      1
EX = 44000,      NUXY = 0.2000      AT TEMP = 0.0000

PRINT THE LOCAL CRACK-TIP DISPLACEMENTS

CRACK-TIP DISPLACEMENTS:
UXC = -0.81089E-02  UYC = 0.45965E-03  UZC = 0.78886E-30

      NODE  CRACK FACE  RADIUS      UX-UXC      UY-UYC      UZ-UZC
      ----  -
      1      TIP        0.0000      0.0000      0.0000      0.0000
      128     TOP        1.0125      0.87301E-05 -0.96919E-04  0.0000
      127     TOP        1.0500     -0.32959E-05 -0.10488E-03  0.0000
      126     BOT        1.0688     -0.73916E-05 -0.10788E-03  0.0000
      125     BOT        1.0875     -0.10965E-04 -0.11063E-03  0.0000

LIMITS AS RADIUS (R) APPROACHES 0.0 (TOP FACE) ARE:
(UX-UXC)/SQRT(R) = 0.32977E-03  (UY-UYC)/SQRT(R) = 0.66699E-04
(UZ-UZC)/SQRT(R) = 0.0000

LIMITS AS RADIUS (R) APPROACHES 0.0 (BOTTOM FACE) ARE:
(UX-UXC)/SQRT(R) = 0.18461E-03  (UY-UYC)/SQRT(R) = -0.59074E-05
(UZ-UZC)/SQRT(R) = 0.0000

**** KI = 1.0010 , KII = 2.0012 , KIII = 0.0000 ****

```

Figure 35: KCALC command for $\alpha = 45^\circ$ and $a/R = 0,1$. The same results are shown on the ANNEX II: "TABLES AND RESULTS".

5. RESULTS

5.1. SPECIMEN'S DATA

The data used to obtain the SIFs for each ratio of the crack length are shown on the following tables:

CRACK LENGHT									
	RATIO a/R								
	0.1	0.2	0.3	0.4	0.5	0.6	0.7	0.8	0.9
a [mm]	7.5	15	22.5	30	37.5	45	52.5	60	67.5
a [m]	0.0075	0.015	0.0225	0.03	0.0375	0.045	0.0525	0.06	0.0675

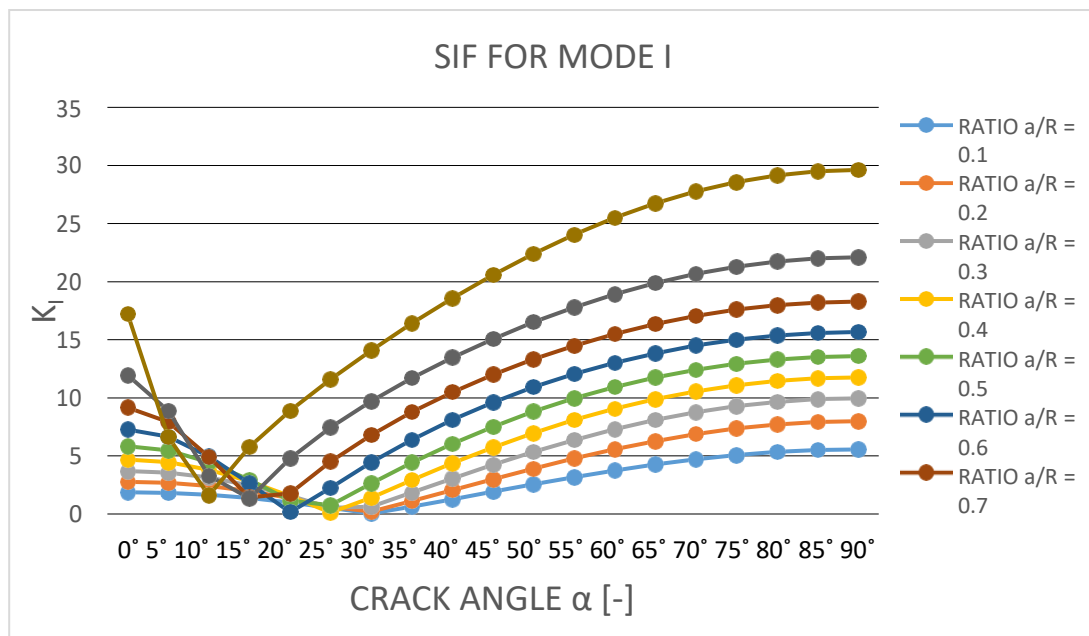
Table 5: Crack relative length for different ratio a/R .

DATA	
P [N]	100
D [mm]	150
R [mm]	75
B [mm]	1

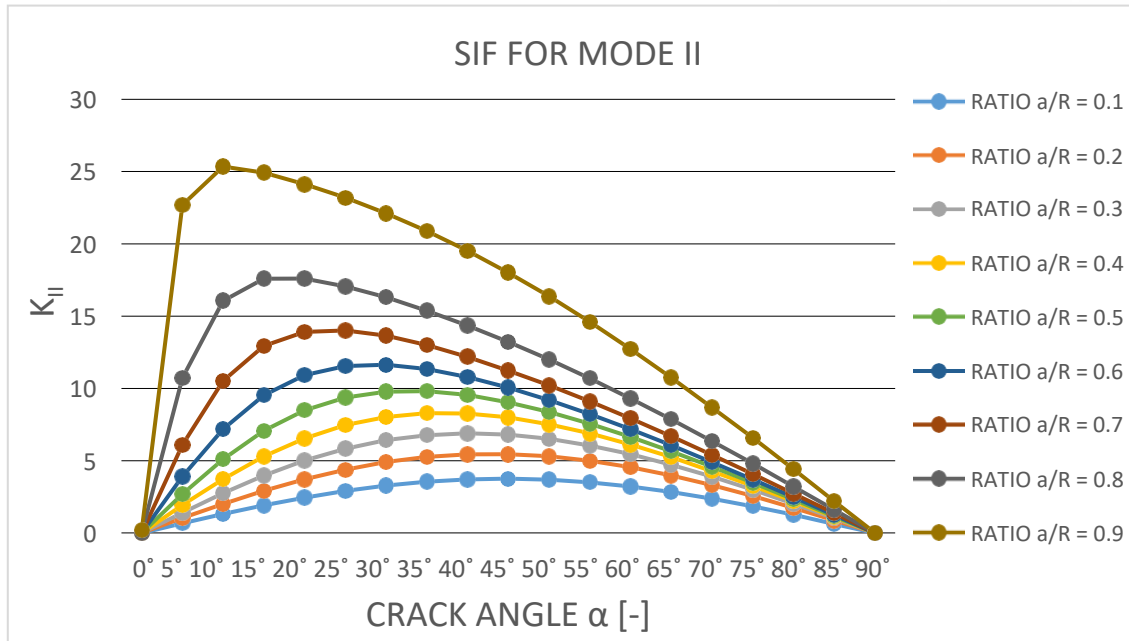
Table 6: Specimen's measures and external force.

5.2. STRESS INTENSITY FACTORS

On the following graphs it can be seen that the SIFs are dependent on the crack angle under the same force value ($P = 100$ N). These results were obtained using the FE software ANSYS with the commands explained before.



Graph 1: Stress intensity factor for mode I, versus the crack angle.



Graph 2: Stress intensity factor for mode II, versus the crack angle.

5.3. CALIBRATION CURVES

The calibration curves can be calculated from the following equations:

$$f_I(\alpha, a/R) = \frac{K_I K_B \sqrt{\pi}}{P \sqrt{a}} \sqrt{\frac{a}{R}} \quad (49)$$

$$f_{II}(\alpha, a/R) = \frac{K_{II} K_B \sqrt{\pi}}{P \sqrt{a}} \sqrt{\frac{a}{R}} \quad (50)$$

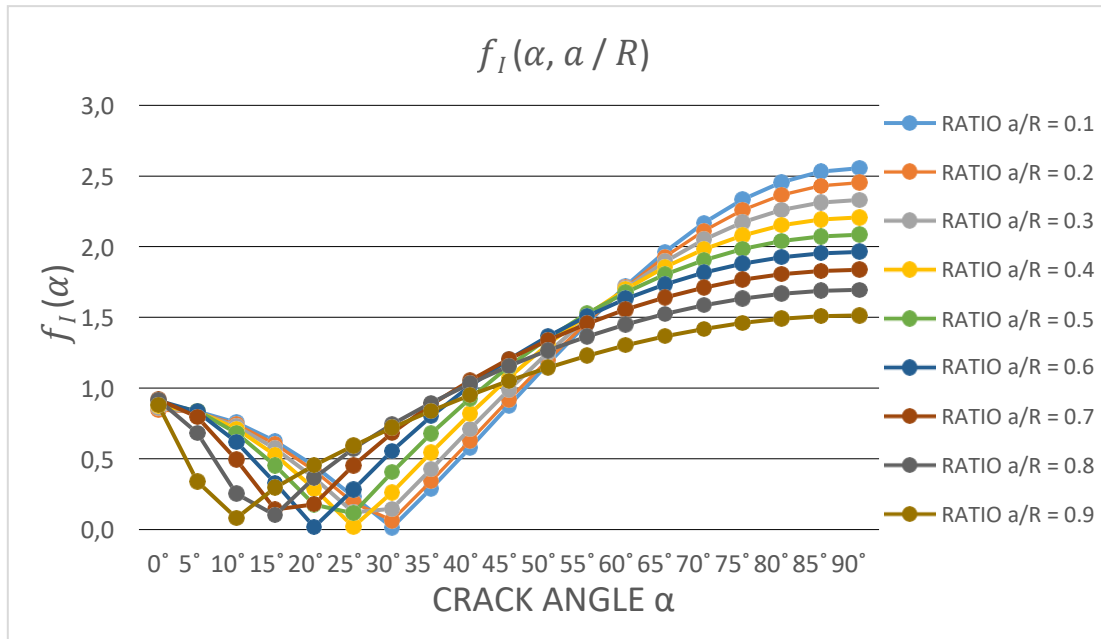
where

K_I is the stress intensity factor for Mode I, taken from ANSYS,

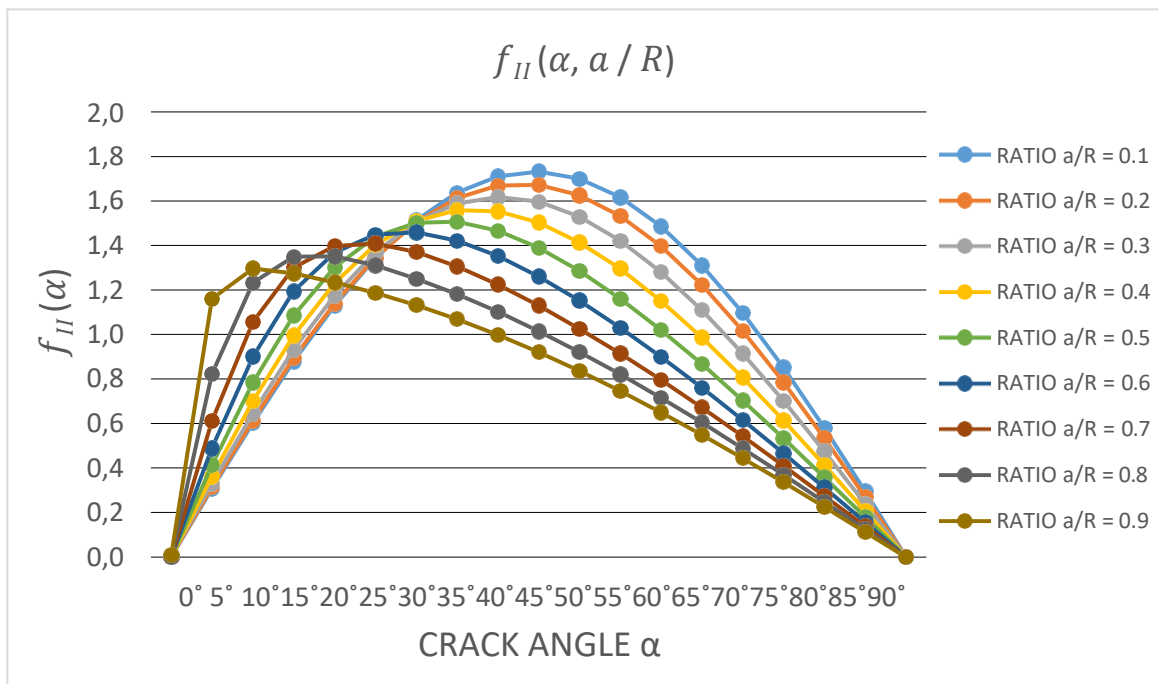
R, B, a are measured from the specimen,

P is the applied force,

By substituting the values of the SIFs taken from ANSYS and the specimen's data on the previous equations it is possible to obtain the calibration curves for different angles and ratios of the crack length, that allow to get the SIFs for several geometries. The following graphs show that relationship:



Graph 3: Calibration curve $f_I(\alpha, a/R)$ for mode I, versus the crack angle.



Graph 4: Calibration curve $f_{II}(\alpha, a/R)$ for mode II, versus the crack angle.

6. EXPERIMENTAL MEASUREMENT

The experimental results were taken by Stanislav Seitzl, Petr Miarka and Vlastimil Bílek [27].

6.1. MATERIAL

This type of material, C50/60, is a typical material used for the pre – stressed precast elements and shows very good properties such as its high compressive and tensile strength. The studied concrete contains 450 kg of CEM I 42.5 R, the water to cement ratio (c/w) is 0.40. Fine aggregate was natural sand 0/4 mm and crushed aggregates 4/8 mm and 8/16 mm from high quality granite was used along with drinking water. The concrete was mixed in a volume of 1 m³ and poured immediately into modulus. Cone was measured 540 mm according to [28].

6.2. SPECIMEN'S GEOMETRY

The experimental test was carried out on standardized specimens with the following dimensions:

- Compressive cube strength: cubes – 150 mm x 150 mm x 150 mm.
- Compressive cylindrical strength: cylinders – diameter 150 mm and height = 300 mm.
- Flexural strength: beams – 80 x 80 x 480 (400) mm.
- Young's modulus: beams – 80 x 80 x 480 (400) mm, diameter 150 mm and height = 300 mm.
- Indirect tensile strength: unnotched discs – diameter 150 mm and thickness 30 mm.
- BDC specimens were prepared from standardized cylindrical specimens used for evaluation of cylindrical compressive strength of concrete [29].

The following tables give an overview of the values measured on the experiments for two different a/R ratios for the crack relative length:

$$a/R = 0.267$$

SPECIMEN NUMBER	INCLINATION ANGLE α [°]	NOTCH LENGTH $2a$ [mm]	THICKNESS B [mm]	DIAMETER D [mm]	FRACTURE FORCE P_c [kN]
4_2_01	0	39.72	28.60	149.22	25.69
4_2_02	0	39.44	28.64	149.29	26.22
4_2_04	5	39.38	28.38	149.20	24.98
4_2_11	10	39.80	28.44	149.24	27.40
4_2_09	15	39.60	28.44	149.21	25.44
4_2_10	15	39.26	28.47	149.19	26.52
4_2_07	20	38.79	28.57	149.25	24.13

4_2_08	20	39.94	27.92	149.25	26.42
4_2_03	27.2	39.82	28.32	149.22	22.89
4_2_06	27.2	39.70	28.41	149.00	25.69

Table 7: Dimensions of BD test for $a/R = 0.267$.

$a/R=0.4$

SPECIMEN NUMBER	INCLINATION ANGLE α [°]	NOTCH LENGTH $2a$ [mm]	THICKNESS B [mm]	DIAMETER D [mm]	FRACTURE FORCE P_C [kN]
6_2_02	0	59.70	29.43	149.09	22.177
6_2_01	0	59.44	29.99	149.15	19.568
6_2_05	5	59.91	28.35	149.23	20.221
6_2_10	10	59.27	28.48	149.32	19.568
6_2_11	10	60.13	27.57	149.01	16.190
6_2_08	15	60.06	28.09	149.18	18.916
6_2_09	15	59.96	28.70	149.28	19.151
6_2_06	20	60.01	28.33	149.21	19.568
6_2_07	20	60.03	28.45	149.12	19.568
6_2_03	25.2	59.81	28.45	149.18	16.959
6_2_04	25.2	59.93	28.96	149.23	18.916

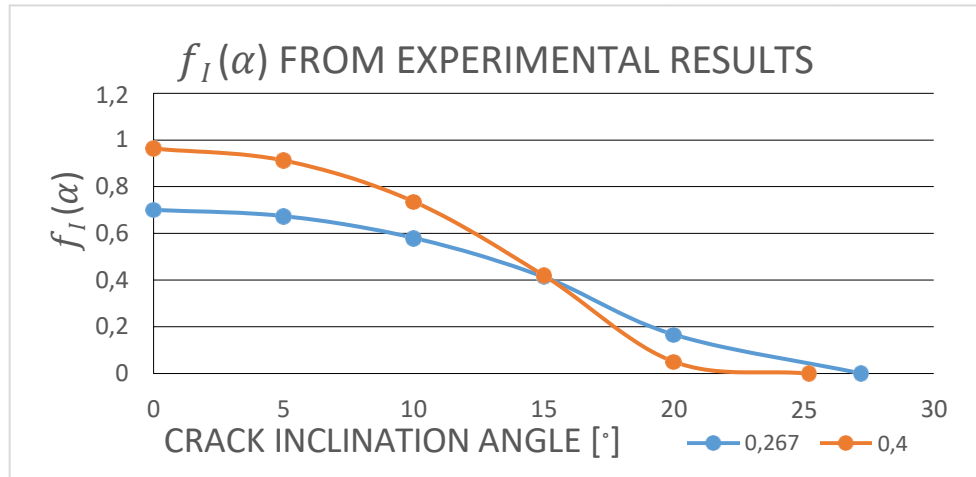
Table 8: Dimensions of BD test for $a/R = 0.4$.

6.3. EXPERIMENTAL PROCEDURE FOR BRAZILIAN DISC TEST

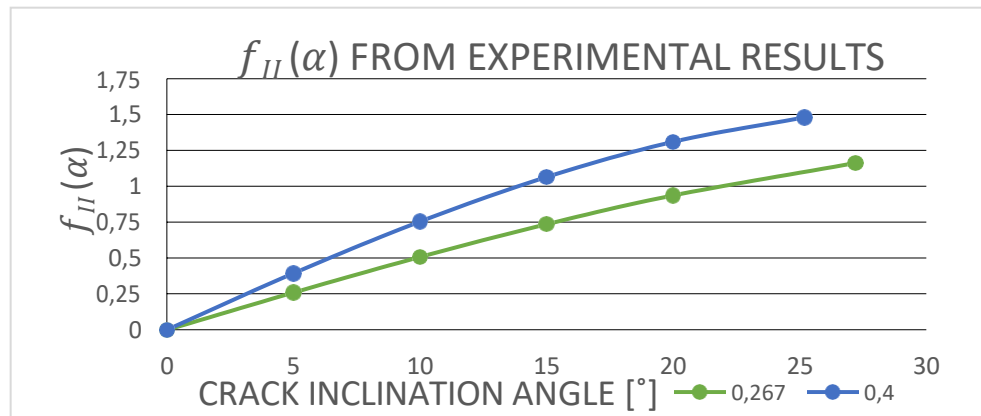
The machine used in the experimental test has maximum loading capacity of 200 kN. The speed of the induced displacement of the upper support was equal to 0.25 mm/s. BD specimens with notch lengths $a/R = 0.267$ and 0.4 were tested under the selected angles inclined against loading position, as shown on the Tables 7 and 8.

6.4. CALIBRATION CURVES FOR EXPERIMENT

From the FE software ANSYS it is obtained the SIFs values for the mode I and II. The using of the equations (49) and (50) it is possible to obtain the values for the calibration curves for both ratios of the crack relative length. These results are summarized on the following graphs:



Graph 5: Calibration curve $f_I(\alpha, a/R)$ for mode I, versus the crack inclination angle.



Graph 6: Calibration curve $f_{II}(\alpha, a/R)$ for mode II, versus the crack inclination angle.

The geometry functions, also referred to the calibration curves, for both ratios a/R are calculated with the following equations.

- For ratio $a/R = 0.267$ and for inclination angle $\alpha = [0^\circ; 27.2^\circ]$, the shape functions can be expressed as a following polynomial functions:

$$Y_I(a/R, \alpha) = + 0.7003 + 0.0009\alpha - 0.0012\alpha^2 - 9 \cdot 10^{-6}\alpha^3, \quad (51)$$

$$Y_{II}(a/R, \alpha) = - 0.0006 + 0.0529\alpha - 0.0001\alpha^2 - 1 \cdot 10^{-5}\alpha^3. \quad (52)$$

- On the other hand, for ratio $a/R = 0.4$ and for inclination angle $\alpha = [0^\circ; 25.25^\circ]$, the shape functions are:

$$Y_I(a/R, \alpha) = + 0.9634 + 0.0013\alpha - 0.0022\alpha^2 - 2 \cdot 10^{-5}\alpha^3, \quad (53)$$

$$Y_{II}(a/R, \alpha) = -0.0018 + 0.0816\alpha - 0.0004\alpha^2 - 2 \cdot 10^{-5}\alpha^3. \quad (54)$$

These equations were taken using the polynomial linear regression in Excel once the SIFs and the shape functions were calculated. These expressions allow to obtain the shape functions for every angle and then calculate the SIFs for these angles.

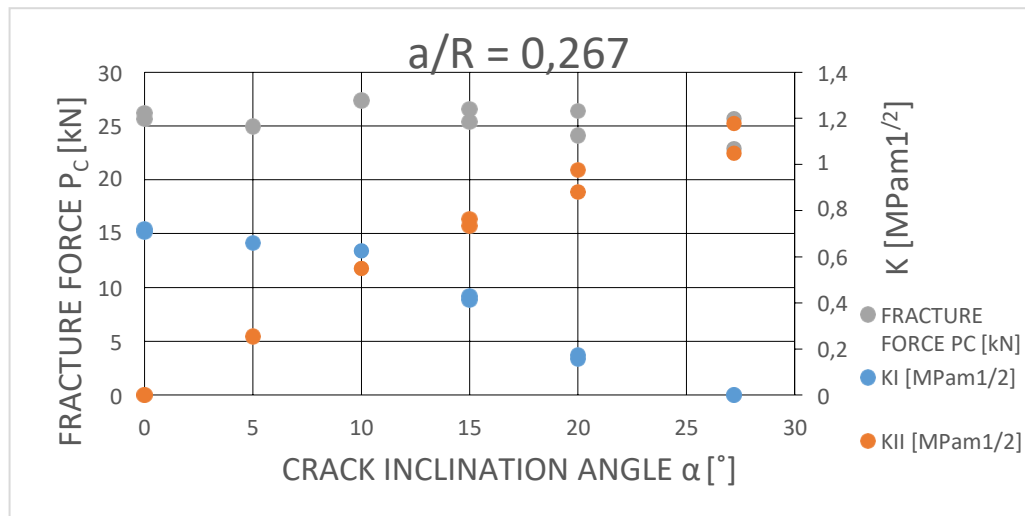
Once the calibration curves were calculated, using the following equations it is possible to evaluate the SIFs for the different specimens.

$$K_I = \frac{P\sqrt{a}}{RB\sqrt{\pi}} \frac{1}{\sqrt{1 - \frac{a}{R}}} Y_I(a/R, \alpha), \quad (55)$$

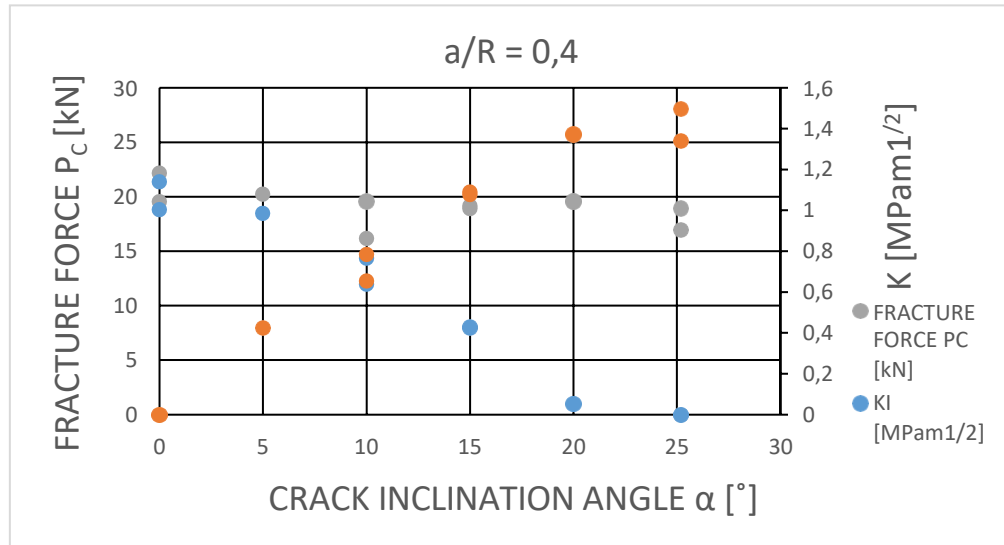
$$K_{II} = \frac{P\sqrt{a}}{RB\sqrt{\pi}} \frac{1}{\sqrt{1 - \frac{a}{R}}} Y_{II}(a/R, \alpha). \quad (56)$$

6.5. EXPERIMENTALLY OBTAIN DATA

The maximum load of Brazilian disc tests is summed up in the next graphs, together with SIFs results evaluated by Miarka et al [27]. These data could be evaluated by calibration curves calculated by Villanueva, Miarka and Ayatollahi and Aliha, and then the difference could be described like difference among mentioned calibration curves. Therefore, in next chapter, the numerical results from software ANSYS and mentioned method are compared.



Graph 7: Fracture forces and SIFs values for different angles for relative crack length $a/R = 0.267$.



Graph 8: Fracture forces and SIFs values for different angles for relative crack length $a/R = 0.4$.

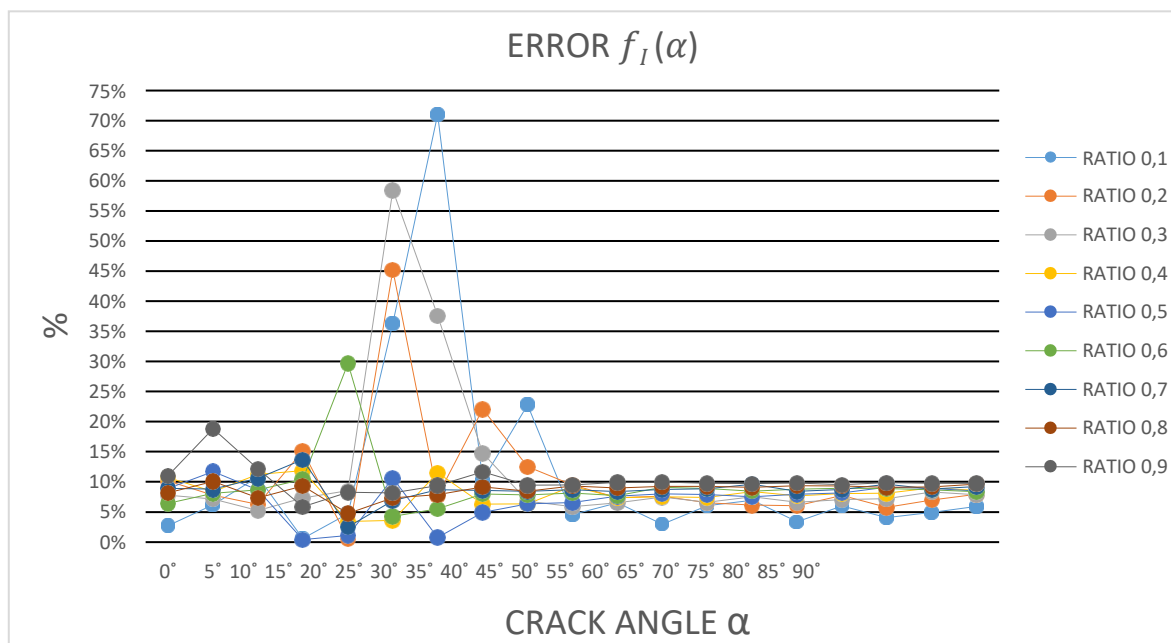
7. NUMERICAL DATA-COMPARISON

As the results I get from the FE software ANSYS can be wrong, on this part of the thesis, several comparisons will be done in order to show how different my results can be from others and what can be the reasons.

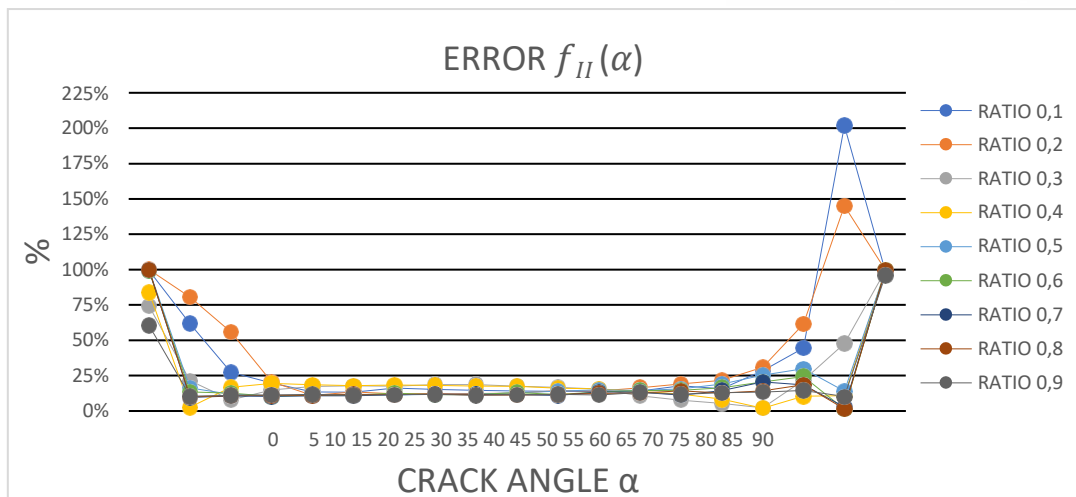
7.1. COMPARISON WITH MARIA VILLANUEVA'S THESIS

Firstly, the comparison is with the results that María Villanueva got on her thesis on the past course [30]. As me, she obtained the SIFs values from ANSYS and then the calibration curves from the same equations as me, equations (49) and (50).

The analysis of both approaches in terms of the calibration curves is shown on the following graphs:



Graph 9: Error in the calibration curves for mode I between María Villanueva's thesis and mine.



Graph 10: Error in the calibration curves for mode II between María Villanueva's thesis and mine.

It can be seen that for mode I the error that emerge is approximately constant and has an average value around the ten per cent for angles between 45° and 90°. For angles between 15° and 40° the calibration functions suffer variations that range from almost zero per cent of error to more than seventy per cent. Finally, the error for angles that oscillate from 0° to 10° is less constant that the last angles, but also with an average value around the ten per cent.

On the other hand, the mode II graph is completely different from the mode I. In this graph it is possible to observe that for angles between 15° and 65° the error value is very constant, about the fifteen per cent. Otherwise, both for angles less than 15° and for higher than 65° the error values raise very high levels, as two hundred per cent for 85° and one hundred for 0°.

These big differences of error are due to the fact that I get María's SIFs values directly from her thesis' graphs using a graph digitizer software [31] that allow me to get those values in an approximately way. Because of this, the SIFs values are no exact and therefore it is possible to see how different the calibration functions are one from the other. That is why for some angles there is so much error and however, for others there is not.

Since the calibration functions allow get the SIFs values for each specimen's geometry and angle of the crack, the problem is not the data I get or María's got but the way I obtained the SIFs values from María's thesis.

Another possible reason is the meshing. As I haven't had the MACRO document from María's thesis I couldn't see if her meshing was equal or similar as mine, so the SIFs results can change and as a result, the calibration functions.

The tables and graphs related to the SIFs values from María's thesis and the calibration functions are shown on the Annex II.

7.2. COMPARISON WITH EXPERIMENTAL RESULTS

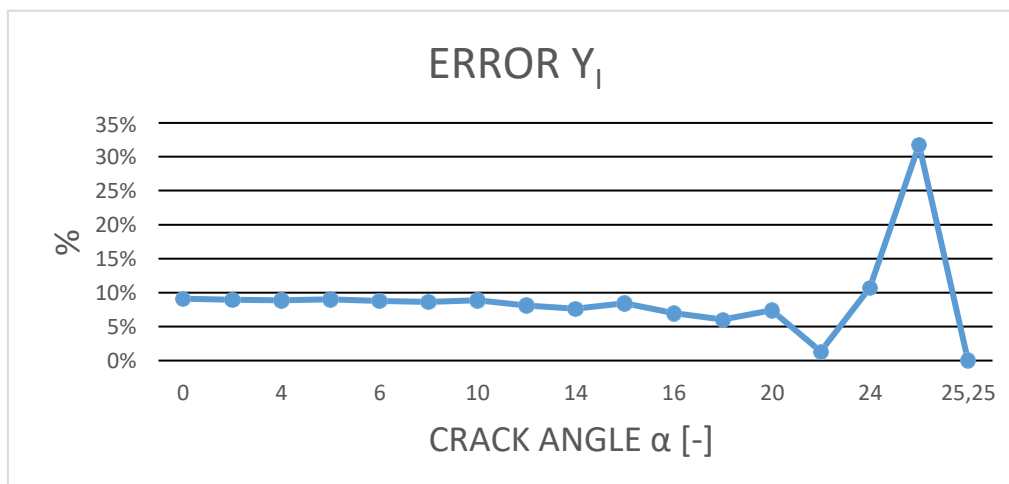
The experimental results were described on the sixth point of this thesis and now the calibration functions will be compared with mine. The experimental test was done for two relative crack lengths. $a/R = 0.267$ and $a/R = 0.4$. Inasmuch as my results do not consider the relationship $a/R = 0.267$, the comparison between both models will be only for $a/R = 0.4$.

The shape functions for angles in range $[0^\circ; 25.25^\circ]$ are shown on the Annex II. These results were given to me by Petr Miarka in order to be able to compare both models. It is also shown on the Annex the linear regression line and the equation for each mode.

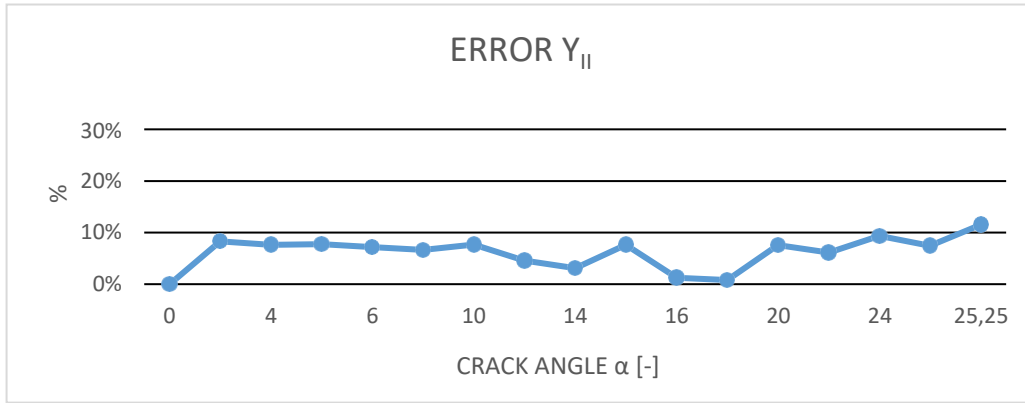
As my ANSYS results were obtained for angles in range $[0^\circ; 90^\circ]$ in an interval of 5° , it was necessary to create graphs with the calibration functions values for angles between 0° and 25° in an interval of 5° , for which I have calculated the geometry functions. Then I could get the linear regression line and the equation and be able to get the shape functions for any angle in that range and compare with Miarka's results.

These calibration curves with its respectively linear regression lines and equations are also shown on the Annex II.

As a summary, it is shown the graph where it can be noted the per cent of error that appears between both models for mode I and II. The numerical results are shown on the Annex II.



Graph 11: Error graph between both calibration curves models for mode I. Comparison with experimental test.



Graph 12: Error graph between both calibration curves models for mode II. Comparison with experimental test.

It can be seen that there is not too much difference between both models. For mode I, the error has an average value about the eight per cent until 24° . Then, for angles near 25° the difference fluctuates because in Miarka's model, at 25.25° the pure mode II is raised ($K_I = 0$) and, in my case, the pure mode II is raised at 25.51° . This value is calculated using the linear regression curve for mode I.

On the other hand, for mode II, the graph is more uniform, and the error average value is about the seven percent.

7.3. COMPARISON WITH M. R. AYATOLLAHI AND M. R. M. ALIHA RESULTS

The last comparison is with M. R. Ayatollahi and M. R. M. Aliha, from the Iran University of Technology. On their article [19], the generalized maximum tangential stress (GMTS) criterion was used for predicting the mixed – mode fracture toughness using the BD test. In it, it is given the numerical values for the shape functions Y_I and Y_{II} necessary to carry out this comparison [32].

According to them, the SIFs expressions for mode I and II a BD test specimen are written as follows:

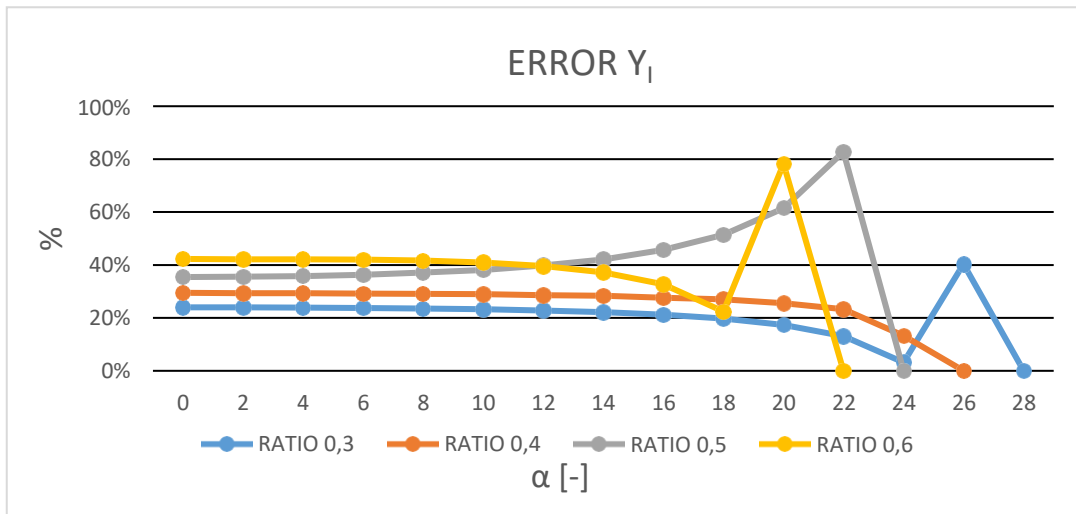
$$K_I = \frac{P}{RB} \sqrt{\frac{\pi}{\pi}} Y_I(a/R, \alpha), \quad (57)$$

$$K_{II} = \frac{P}{RB} \sqrt{\frac{\pi}{\pi}} Y_{II}(a/R, \alpha). \quad (58)$$

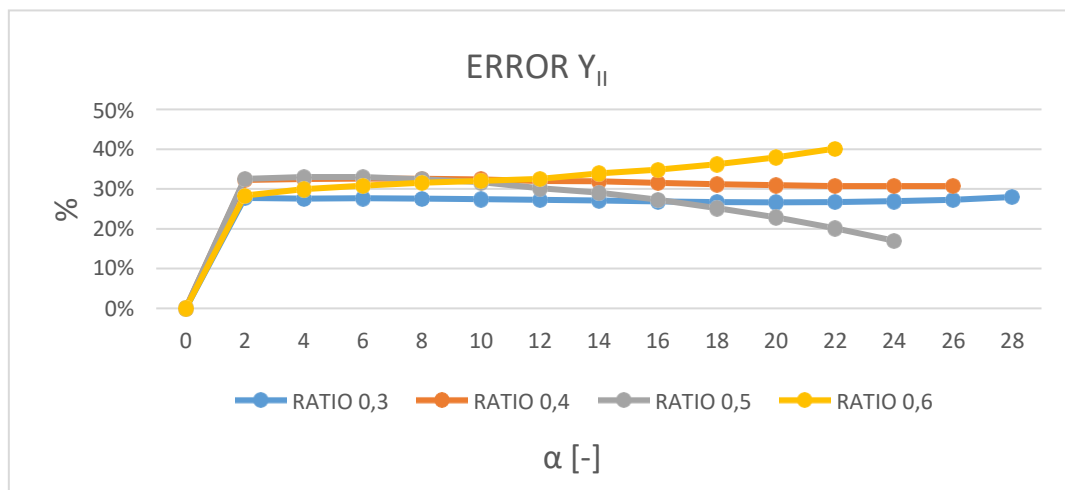
It can be proved that these equations are different from (49) and (50), used in both experimental results and in my analysis.

As in the comparison with the experimental results. it was necessary to do the different linear regression lines and equations for each ratio that will influence on the analysis. These graphs, along to the article's numerical values are exposed in the Annex II.

The error values of the calibration functions for each mode are summarized on the following graphs:



Graph 13: Error graph between both calibration curves models for mode I. Comparison with Ayatollahi and Aliha's article [19].



Graph 14: Error graph between both calibration curves models for mode II. Comparison with Ayatollahi and Aliha's article [19].

It can be seen that the error values oscillate a lot and have very high levels for both modes for the majority of the angles. There is an important reason why these values are so different from mine, apart from what was previously mentioned about meshing.

This reason is that Ayatollahi and Aliha have calculated these shape functions using a wide range of FE analysis. That means that they obtained the SIFs values from different ways and then used the equations (57) and (58) to calculate the geometry functions. The fact that it has been used different formulas to evaluate the calibration functions can explain the huge differences between approaches.

8. CONCLUSIONS

In this document, two parameters were evaluated to define the stress state on the crack tip: the stress intensity factor for Mode I and II and the calibrations functions. Then, these two variables have been compared with experimental results and data from literature.

Consequently, the following conclusions can be obtained:

- For the same crack length ratio, $a/R = 0.4$ and range of angles $[0; 25^\circ]$, the four approaches seems to be very similar.
- The difference between my results and María Villanueva's is not appreciable for angles between 40° and 70° for both modes.
- There is a clear error between María Villanueva's results and mine for the rest of angles which is probably due to the different ways of calculation.
- The results I obtained seems to be correct, at least for the crack length ratio a/R studied at the laboratory, because the error between both techniques is not very important.
- Should be necessary to do an experimental evaluation of the BD for different ratios a/R to ensure if the results I obtained are effectively right or not.
- The comparison with Ayatollahi's and Aliha's article shows the obvious difference with respect to my results due to the use of different calibration functions.
- To be able to do an accurate comparison between both models, it is recommended to use the same equations and compare the results obtained.
- It will be necessary a more in – depth analysis of different approaches and compare with both models proposed on this thesis.

Definitely, there is not a definitive conclusion to say which method is better than other to calculate the calibration curves and consequently the stress intensity factors for different angles and specimens. The three approaches are valid to calculate the stress state in the crack tip and study how the crack grow under determined applied loads.

9. ANNEXES

9.1. ANNEX I. MACRO DOCUMENT

```

!*****
!***** MACRO FOR SOLUTION OF STRESS INTENSITY FACTOR *****
!***** AUTOR: ALEJANDRO PARCERO ALONSO *****
!***** MATERIAL: CONCRETE *****
!***** PROPERTIES: E=44 GPa AND nu=0.2 *****
!***** BRAZILIAN TEST SPECIMEN. D = 150 mm. a/R = [0.1;0.9] *****
!*****
!***** ORDERS BEFORE MODELLING *****

/title,cleaning the set-up area

/replot

fini

/output,hlasky,tmp

WPCSYS,-1,0

/clear

/output

/COLOR,ELEM,BLUE

/COLOR,OUTL,WHIT

/REPLOT

/PNUM,KP,1

/PNUM,LINE,1

/PNUM,AREA,1

/filnam,BrazilianDiskSpecimen

/prep7

!*****
!***** CONDITIONS *****
!*****

pi=3.1415926535897932384626433832795

!***** SPECIMEN'S DIAMATER *****

D=150          !units mm

```

```

***** SPECIMEN'S RADIUS *****
R=D/2                      !units mm

***** RATIO a/R *****
a_R=0.1                    !the ratio a/R will vary in the range [0,1,0,9]

***** CRACK LENGTH *****
a=a_R*R                    !crack length

***** ANGLE VALUE *****
FI=45                      !the angle FI will vary in the range [0,90] in an
                           !interval of 5 degrees

*****
*****

ET,1,PLANE183

KEYOPT,1,3,2              !plane strain

*****
***** MATERIAL PROPERTIES *****
*****
MP,EX,1,44000             !Material Young modulus
MP,NUXY,1,0,2             !Material Poisson number

*****
***** MODELLING *****
*****
***** KEYPOINTS *****
***** RIGHT PART OF THE CRACK *****
k,1,0,0                   ! K1 : center of the crack tip
K,2,1,0                   ! K2 : 1 mm in X axis from the crack tip
k,3,0,1                   ! K3 : 1 mm in Y axis from the crack tip
k,4,-1,0 ! K4 : 1 mm in X axis from the crack tip K,5,-
1,0 ! K5 : same coordination as K4
K,6,0,-1                 ! K6 : bottom part of the crack

***** LEFT PART OF THE CRACK *****
K,12,2*(-a),0            ! K12
K,13,2*(-a)-1,0         ! K13

```

K,14,2*(-a)+1,0 ! K14

K,15,2*(-a)+1,0 ! K15

K,16,2*(-a),1 ! K16

K,17,2*(-a),-1 ! K17

!***** UNION OF THE TWO PARTS *****

K,7,-a,0 ! K7

K,100,-a,0 ! K100

!***** BEGINNING OF THE PERIPHERY *****

K,8,R-a,0 ! K8

K,9,-R-a,0 ! K9

!***** MODELLING OF THE PERIPHERY KEYPOINTS *****

LOCAL,11,1,-a,0,0,,,1,1 !Defines a local coordinate system

K,18,R,5 ! K18

K,19,R,10 ! K19

K,20,R,15 ! K20

K,21,R,20 ! K21

K,22,R,25 ! K22

K,23,R,30 ! K23

K,24,R,35 ! K24

K,25,R,40 ! K25

K,26,R,45 ! K26

K,27,R,50 ! K27

K,28,R,55 ! K28

K,29,R,60 ! K29

K,30,R,65 ! K30

K,31,R,70 ! K31

K,32,R,75 ! K32

K,33,R,80 ! K33

K,34,R,85 ! K34

K,35,R,90 ! K35

K,36,R,185 ! K36

K,37,R,190 ! K37

K,38,R,195 ! K38

```

K,39,R,200      ! K39
K,40,R,205      ! K40
K,41,R,210      ! K41
K,42,R,215      ! K42
K,43,R,220      ! K43
K,44,R,225      ! K44
K,45,R,230      ! K45
K,46,R,235      ! K46
K,47,R,240      ! K47
K,48,R,245      ! K48
K,49,R,250      ! K49
K,50,R,255      ! K50
K,51,R,260      ! K51
K,52,R,265      ! K52
K,53,R,270      ! K53

! *****
! ***** LINES *****
! ***** CRACK LINES *****
! ***** RIGHT PART OF THE CRACK *****

CSYS,0          ! Activates a previously defined coordinate system
L,1,2           ! L1
Larc,2,3,1,1    ! L2
Larc,3,4,1,1    ! L3
L,4,1           ! L4
L,1,3           ! L5
L,1,6           ! L6
Larc,6,5,1,1    ! L7
Larc,6,2,1,1    ! L8
L,5,1           ! L9
L,7,4           ! L10
L,100,5         ! L11

! ***** LEFT PART OF THE CRACK *****
L,12,16         ! L12

```

L,12,13 ! L13
 L,12,17 ! L14
 L,12,14 ! L15
 L,12,15 ! L16
 Larc,16,13,12,1 ! L17
 Larc,13,17,12,1 ! L18
 Larc,17,15,12,1 ! L19
 Larc,14,16,12,1 ! L20
 L,14,7 ! L21
 L,15,100 ! L22

!***** UNION OF THE END OF THE PERIPHERY *****

L,35,7 ! L23
 L,13,9 ! L24
 L,2,8 ! L25
 L,53,100 ! L26

!***** LINES OF THE PERIPHERY *****

CSYS,1

Larc,8,18,7,R ! L27
 Larc,18,19,7,R ! L28
 Larc,19,20,7,R ! L29
 Larc,20,21,7,R ! L30
 Larc,21,22,7,R ! L31
 Larc,22,23,7,R ! L32
 Larc,23,24,7,R ! L33
 Larc,24,25,7,R ! L34
 Larc,25,26,7,R ! L35
 Larc,26,27,7,R ! L36
 Larc,27,28,7,R ! L37
 Larc,28,29,7,R ! L38
 Larc,29,30,7,R ! L39
 Larc,30,31,7,R ! L40
 Larc,31,32,7,R ! L41
 Larc,32,33,7,R ! L42

Larc,33,34,7,R ! L43
 Larc,34,35,7,R ! L44
 Larc,35,9,7,R ! L45
 Larc,9,36,7,R ! L46
 Larc,36,37,7,R ! L47
 Larc,37,38,7,R ! L48
 Larc,38,39,7,R ! L49
 Larc,39,40,7,R ! L50
 Larc,40,41,7,R ! L51
 Larc,41,42,7,R ! L52
 Larc,42,43,7,R ! L53
 Larc,43,44,7,R ! L54
 Larc,44,45,7,R ! L55
 Larc,45,46,7,R ! L56
 Larc,46,47,7,R ! L57
 Larc,47,48,7,R ! L58
 Larc,48,49,7,R ! L59
 Larc,49,50,7,R ! L60
 Larc,50,51,7,R ! L61
 Larc,51,52,7,R ! L62
 Larc,52,53,7,R ! L63
 Larc,53,8,7,R ! L64

!***** LINES WITH THE PURPOSE OF DIVIDE AREAS *****

CSYS,0

L,7,30 ! L65
 L,2,19 ! L66
 L,7,25 ! L67
 L,3,23 ! L68
 L,13,37 ! L69
 L,17,40 ! L70
 L,100,43 ! L71
 L,100,48 ! L72

!*****

! ***** AREAS *****

CSYS,0

al,2,5,1	! A1
al,3,5,4	! A2
al,9,6,7	! A3
al,6,8,1	! A4
al,12,13,17	! A5
al,20,15,12	! A6
al,13,18,14	! A7
al,19,14,16	! A8
al,25,66,27,28	! A9
al,66,68,29,30,31,32,2	! A10
al,10,3,67,68,33,34	! A11
al,67,65,35,36,37,38,39	! A12
al,23,65,44,43,42,41,40	! A13
al,23,45,21,20,17,24	! A14
al,24,69,46,47	! A15
al,48,49,50,70,18,69	! A16
al,19,22,71,70,51,52,53	! A17
al,71,72,54,55,56,57,58	! A18
al,72,26,59,60,61,62,63	! A19
al,26,64,25,11,7,8	! A20

! *****

! *****

! ***** MESHING *****

! *****

Kscon,1,0,25,1,4,0,75 ! shift of node to 1/4 of L(element length)

P=0,5

Q=4

KESIZE,1,P

KESIZE,2,P

KESIZE,3,P

KESIZE,4,P

KESIZE,5,P
KESIZE,6,P
KESIZE,7,P
KESIZE,100,P
KESIZE,12,P
KESIZE,13,P
KESIZE,14,P
KESIZE,15,P
KESIZE,16,P
KESIZE,17,P
KESIZE,8,Q
KESIZE,18,Q
KESIZE,19,Q
KESIZE,20,Q
KESIZE,21,Q
KESIZE,22,Q
KESIZE,23,Q
KESIZE,24,Q
KESIZE,25,Q
KESIZE,26,Q
KESIZE,27,Q
KESIZE,28,Q
KESIZE,29,Q
KESIZE,30,Q
KESIZE,31,Q
KESIZE,32,Q
KESIZE,33,Q
KESIZE,34,Q
KESIZE,35,Q
KESIZE,9,Q
KESIZE,36,Q
KESIZE,37,Q
KESIZE,38,Q

KESIZE,39,Q

KESIZE,40,Q

KESIZE,41,Q

KESIZE,42,Q

KESIZE,43,Q

KESIZE,44,Q

KESIZE,45,Q

KESIZE,46,Q

KESIZE,47,Q

KESIZE,48,Q

KESIZE,49,Q

KESIZE,50,Q

KESIZE,51,Q

KESIZE,52,Q

KESIZE,53,Q

!Material

TYPE,1

MAT,1

AMESH,1

AMESH,2

AMESH,3

AMESH,4

AMESH,5

AMESH,6

AMESH,7

AMESH,8

AMESH,9

AMESH,10

AMESH,11

AMESH,12

AMESH,13

AMESH,14
AMESH,15
AMESH,16
AMESH,17
AMESH,18
AMESH,19
AMESH,20

FINISH

```
!*****
!***** BOUNDARY CONDITIONS *****
!*****
!*****
!***** SUPPORT *****
!*****

/sol

!***** SUPPORT FORCE UY *****

D,1767, ,0, , , ,UY, , , ,
!D,2546, ,0, , , ,UX, , , ,      !UX only for case FI = 90
degrees                          !instead of UY

ALLSEL, all

kplot
nplot
eplot

!***** SUPPORT UX - UY *****

NSEL,S,NODE,,7556                !Selection of the node

D,ALL, ,0, , , ,UX,UY, , , ,      !Define of the D,0,F of nodes

ALLSEL,all                        !Select all entitles with a single
command

nplot
eplot

!*****
!*****
!***** FORCES *****
```

```

!*****
!Constant force of 100 N
NSEL,S,NODE,,5012
F,all,Fx,-100*COS(FI*2*PI/360)    !Defines loads at nodes
F,all,FY,-100*SIN(FI*2*PI/360)
ALLSEL,all
!*****

eplot
solve
FINISH
/POST1
eplot
LPATH,1,80,79,129,128            !DEFINE PATH TO CALCULATE KI AND KII
KCALC,0,1,3,1                    !KCALC CALCULATE SIF

```

9.2. ANNEX II, TABLES AND RESULTS

9.2.1. STRESS INTENSITY FACTORS FOR MODE I AND II

On the following tables are summed up the results I obtained from FE software ANSYS under the conditions mentioned on Tables 5 and 6.

STRESS INTENSITY FACTORS FOR MODE I AND MODE II						
α	RATIO $a/R = 0.1$		RATIO $a/R = 0.2$		RATIO $a/R = 0.3$	
	K_I	K_{II}	K_I	K_{II}	K_I	K_{II}
0°	1.87190	0.00039	2.75920	0.00013	3.68120	0.00076
5°	1.81360	0.66508	2.70030	1.02100	3.53750	1.41400
10°	1.64040	1.30840	2.41990	2.00340	3.11570	2.75900
15°	1.35820	1.91000	1.96630	2.91130	2.44320	3.97400
20°	0.97638	2.45090	1.35930	3.71270	1.56160	5.00960
25°	0.50753	2.91410	0.62401	4.38170	0.52055	5.83150
30°	0.03301	3.28580	0.21021	4.89860	0.62679	6.42120
35°	0.62779	3.55500	1.11200	5.25110	1.82900	6.77430
40°	1.25820	3.71420	2.04950	5.43340	3.03970	6.89770
45°	1.90430	3.75960	2.99210	5.44630	4.21960	6.80640
50°	2.54640	3.69080	3.91100	5.29570	5.33610	6.52080
55°	3.16530	3.51100	4.78030	4.99210	6.36360	6.06370
60°	3.74260	3.22650	5.57740	4.54940	7.28280	5.45910
65°	4.26170	2.84660	6.28290	3.98410	8.07910	4.73060
70°	4.70770	2.38320	6.88100	3.31460	8.74210	3.90120
75°	5.06820	1.85020	7.35880	2.56060	9.26430	2.99290
80°	5.33290	1.26360	7.70690	1.74270	9.64050	2.02640
85°	5.49480	0.64049	7.91830	0.88189	9.86760	1.02160
90°	5.54930	0.00111	7.98930	0.00039	9.94360	0.00206

Table 9: Stress intensity factor for mode I and II for ratios $a/R = 0.1$, $a/R = 0.2$ and $a/R = 0.3$.

STRESS INTENSITY FACTORS FOR MODE I AND MODE II						
α	RATIO $a/R = 0.4$		RATIO $a/R = 0.5$		RATIO $a/R = 0.6$	
	K_I	K_{II}	K_I	K_{II}	K_I	K_{II}
0°	4.66390	0.00082	5.82800	0.00110	7.27370	0.00190
5°	4.44240	1.93220	5.46890	2.68980	6.64590	3.90730

10°	3.79980	3.73360	4.45400	5.11040	4.95110	7.18720
15°	2.80220	5.29770	2.94780	7.07030	2.64100	9.52610
20°	1.53950	6.55240	1.15110	8.48580	0.14765	10.92000
25°	0.10975	7.46510	0.75558	9.36800	2.25600	11.55300
30°	1.39660	8.03630	2.63950	9.78250	4.44650	11.63800
35°	2.90510	8.28990	4.41980	9.81550	6.39290	11.34400
40°	4.35990	8.26240	6.05370	9.54870	8.10560	10.79200
45°	5.72230	7.99410	7.52360	9.05090	9.60600	10.05800
50°	6.96710	7.52490	8.82530	8.37610	10.91500	9.19120
55°	8.07880	6.89070	9.96100	7.56500	12.04900	8.22420
60°	9.04850	6.12310	10.93500	6.64850	13.01900	7.17870
65°	9.87170	5.24900	11.75200	5.65030	13.83200	6.07080
70°	10.54600	4.29160	12.41600	4.58920	14.49500	4.91340
75°	11.07100	3.27080	12.92900	3.48060	15.00800	3.71750
80°	11.44500	2.20450	13.29500	2.33780	15.37500	2.49340
85°	11.67000	1.10860	13.51400	1.17300	15.59400	1.25060
90°	11.74500	0.00177	13.58700	0.00272	15.66800	0.00153

Table 10: Stress intensity factor for mode I and II. $a/R = 0.4$, $a/R = 0.5$ and $a/R = 0.6$.

STRESS INTENSITY FACTORS FOR MODE I AND MODE II

α	RATIO $a/R = 0.7$		RATIO $a/R = 0.8$		RATIO $a/R = 0.9$	
	K_I	K_{II}	K_I	K_{II}	K_I	K_{II}
0°	9.17420	0.00059	11.94900	0.00115	17.19500	0.18384
5°	7.92740	6.09350	8.89870	10.72600	6.63000	22.68000
10°	4.91220	10.52100	3.30120	16.06100	1.60060	25.34300
15°	1.42410	12.94600	1.34180	17.58700	5.78590	24.91100
20°	1.77590	13.90700	4.77180	17.60000	8.87600	24.12300
25°	4.50280	14.01000	7.45650	17.07000	11.57700	23.19000
30°	6.80680	13.64000	9.70730	16.29600	14.07300	22.11400
35°	8.77960	12.99800	11.68600	15.38000	16.40100	20.89000
40°	10.49600	12.18300	13.46100	14.35100	18.56900	19.52000
45°	12.00200	11.24600	15.06500	13.22200	20.57200	18.00800
50°	13.32800	10.21500	16.50700	12.00200	22.40000	16.36400
55°	14.48900	9.10410	17.79100	10.69700	24.04200	14.59700
60°	15.49300	7.92670	18.91600	9.31650	25.48900	12.72100
65°	16.34300	6.69260	19.87600	7.86940	26.73000	10.75000
70°	17.04000	5.41100	20.67000	6.36570	27.75800	8.69760

75°	17.58400	4.09130	21.29100	4.81580	28.56400	6.57950
80°	17.97300	2.74270	21.73700	3.23090	29.14500	4.41170
85°	18.20700	1.37490	22.00600	1.62240	29.49500	2.21050
90°	18.28500	0.00270	22.09600	0.00201	29.61200	0.00731

Table 11: Stress intensity factor for mode I and II. $a/R = 0.7$, $a/R = 0.8$ and $a/R = 0.9$.

9.2.2. CALIBRATION CURVES FOR MODES I AND II

The following tables summarize the calibration function values for each crack angle from the equations (49) and (50).

VALUES OF CALIBRATION CURVES FOR MODE I AND II						
α	RATIO $a/R = 0.1$		RATIO $a/R = 0.2$		RATIO $a/R = 0.3$	
	K_I	K_{II}	K_I	K_{II}	K_I	K_{II}
0°	0.86200	0.00017	0.84706	3.883E-05	0.86314	0.00017
5°	0.83515	0.30626	0.82898	0.31344	0.82945	0.33154
10°	0.75539	0.60251	0.74290	0.61503	0.73054	0.64691
15°	0.62544	0.87954	0.60365	0.89376	0.57286	0.93179
20°	0.44962	1.12863	0.41730	1.13979	0.36615	1.17461
25°	0.23371	1.34193	0.19156	1.34517	0.12205	1.36733
30°	0.01520	1.51310	0.06453	1.50386	0.14696	1.50560
35°	0.28909	1.63706	0.34138	1.61207	0.42885	1.58839
40°	0.57939	1.71037	0.62919	1.66805	0.71272	1.61732
45°	0.87692	1.73128	0.91856	1.67200	0.98938	1.59592
50°	1.17260	1.69960	1.20066	1.62576	1.25115	1.52895
55°	1.45761	1.61680	1.46754	1.53256	1.49209	1.4217
60°	1.72345	1.48579	1.71225	1.39665	1.70762	1.28001
65°	1.96250	1.31085	1.92883	1.22311	1.89433	1.10920
70°	2.16788	1.09745	2.11245	1.01757	2.04976	0.91472
75°	2.33389	0.85201	2.25913	0.78609	2.17223	0.70175
80°	2.45578	0.58188	2.36600	0.53500	2.26044	0.47513
85°	2.53033	0.29494	2.43090	0.27073	2.31369	0.23953
90°	2.55543	0.00051	2.45269	0.00012	2.33151	0.00048

Table 12: Calibration curves for mode I and II. $a/R = 0.1$, $a/R = 0.2$ and $a/R = 0.3$.

VALUES OF CALIBRATION CURVES FOR MODE I AND II						
α	RATIO $a/R = 0.4$		RATIO $a/R = 0.5$		RATIO $a/R = 0.6$	
	K_I	K_{II}	K_I	K_{II}	K_I	K_{II}

0°	0.87680	0.00015	0.89459	0.00017	0.91162	0.00024
5°	0.83516	0.36325	0.83947	0.41288	0.83294	0.48971
10°	0.71435	0.70191	0.68368	0.78444	0.62053	0.90078
15°	0.52681	0.99595	0.45248	1.08528	0.33100	1.19392
20°	0.28942	1.23183	0.17669	1.30256	0.01851	1.36862
25°	0.02063	1.40342	0.11598	1.43798	0.28275	1.44795
30°	0.26256	1.51080	0.40516	1.50160	0.55729	1.45861
35°	0.54615	1.55848	0.67843	1.50667	0.80123	1.42176
40°	0.81965	1.55331	0.92924	1.46572	1.01589	1.35258
45°	1.07578	1.50287	1.15487	1.38930	1.20393	1.26058
50°	1.30979	1.41466	1.35467	1.28572	1.36799	1.15195
55°	1.51879	1.29543	1.52900	1.16122	1.51012	1.03075
60°	1.70109	1.15113	1.67851	1.02054	1.63169	0.89972
65°	1.85585	0.98680	1.80392	0.86732	1.73358	0.76086
70°	1.98262	0.80681	1.90584	0.70444	1.81668	0.61580
75°	2.08132	0.61490	1.98459	0.53427	1.88097	0.46592
80°	2.15163	0.41444	2.04077	0.35885	1.92697	0.31250
85°	2.19393	0.20841	2.07439	0.18005	1.95442	0.15674
90°	2.20803	0.00033	2.08559	0.00042	1.96369	0.00019

Table 13: Calibration curves for mode I and II. $a/R = 0.4$, $a/R = 0.5$ and $a/R = 0.6$.

VALUES OF CALIBRATION CURVES FOR MODE I AND II

α	RATIO $a/R = 0.7$		RATIO $a/R = 0.8$		RATIO $a/R = 0.9$	
	K_I	K_{II}	K_I	K_{II}	K_I	K_{II}
0°	0.92190	5.9772E-05	0.91707	8.8201E-05	0.87980	0.00940
5°	0.79661	0.61232	0.68295	0.82321	0.3392	1.16045
10°	0.49362	1.05724	0.25336	1.23267	0.08189	1.29670
15°	0.14310	1.30092	0.10298	1.34979	0.29607	1.27460
20°	0.17845	1.39749	0.36623	1.35079	0.45415	1.23428
25°	0.45248	1.40784	0.57228	1.31011	0.59235	1.18654
30°	0.6840	1.3706	0.74503	1.25073	0.72006	1.13149
35°	0.88225	1.30615	0.89689	1.18040	0.83917	1.06886
40°	1.05472	1.22425	1.03312	1.10143	0.95010	0.99876
45°	1.20606	1.13009	1.15623	1.01478	1.05259	0.92140
50°	1.33931	1.02649	1.26690	0.92114	1.14612	0.83728
55°	1.4559	0.91485	1.36545	0.82098	1.23014	0.74687
60°	1.55687	0.79654	1.45177	0.71503	1.30417	0.65088
65°	1.64228	0.67253	1.52547	0.60397	1.36767	0.55003
70°	1.71232	0.54374	1.58641	0.48856	1.42027	0.44502

75°	1.76699	0.41112	1.63407	0.36961	1.46153	0.33668
80°	1.80608	0.27561	1.66830	0.24796	1.49124	0.22573
85°	1.82959	0.13818	1.68894	0.12451	1.50915	0.11310
90°	1.83743	0.00027	1.69585	0.00015	1.51513	0.00037

Table 14: Calibration curves for mode I and II. $a/R = 0.7$, $a/R = 0.8$ and $a/R = 0.9$.

9.2.3. STRESS INTENSITY FACTORS FOR MODE I AND II FROM MARIA'S VILLANUEVAS THESIS

The tables below show a summary of the SIFs values obtained by María on her thesis under the following conditions:

CRACK LENGHT

RATIO a/R	0.1	0.2	0.3	0.4	0.5	0.6	0.7	0.8	0.9
a [mm]	3.5	7	10.5	14	17.5	21	24.5	28	31.5
a [m]	0.0035	0.007	0.0105	0.014	0.0175	0.021	0.0245	0.028	0.0315

Table 15: Crack length according to ratio a/R .

P [N]	100
B [mm]	1
D [mm]	70
R [mm]	35

Table 16: Initial data.

It should be noted again that the SIF results are not exact because I couldn't be able to obtain from ANSYS as María did, due to I do not have her MACRO document. Therefore, as I try to get them by using a graph digitizer software, these results are approximate. as it can be seen on the tables.

STRESS INTENSITY FACTOR FOR MODE I AND II

α	RATIO $a/R = 0.1$		RATIO $a/R = 0.2$		RATIO $a/R = 0.3$	
	K_I	K_{II}	K_I	K_{II}	K_I	K_{II}
0	2.6667	0.0876	3.6667	0.1505	5.0000	0.2258
5	2.5000	0.6022	3.6667	0.8280	4.8333	1.2043
10	2.1667	1.5054	3.3333	1.8817	4.3333	3.1613
15	2.0000	2.3333	2.5000	3.5376	3.3333	4.9677
20	1.5000	3.1613	2.0000	4.8925	2.5000	6.4731
25	1.1667	3.7634	1.6667	5.6452	1.8333	7.6022
30	0.1667	4.1398	0.3333	6.3978	0.6667	8.3548

35	0.8333	4.5161	1.3333	6.8495	2.3333	8.9570
40	1.5000	4.7419	2.6667	7.0753	4.1667	9.1075
45	2.6667	4.8172	4.0000	7.0753	5.8333	8.8817
50	3.5000	4.7419	5.3333	6.7742	7.3333	8.4301
55	4.5000	4.5161	6.5000	6.3978	8.6667	7.7527
60	5.1667	4.1398	7.6667	5.7204	10.0000	6.6237
65	5.8333	3.5376	8.6667	4.8925	11.0000	5.5699
70	6.6667	3.0108	9.5000	3.9892	12.0000	4.5161
75	7.0000	2.1075	10.0000	2.8602	12.6667	3.2366
80	7.5000	1.2796	10.6667	1.5806	13.1667	1.8817
85	7.6667	0.3108	10.8333	0.5269	13.3333	0.8280
90	7.6667	0.1505	10.8333	0.2258	13.5000	0.3763

Table 17: Stress intensity factor for mode I and II. $a/R = 0.1$, $a/R = 0.2$ and $a/R = 0.3$ from María Villanueva's thesis.

STRESS INTENSITY FACTOR FOR MODE I AND II

α	RATIO $a/R = 0.4$		RATIO $a/R = 0.5$		RATIO $a/R = 0.6$	
	K_I	K_{II}	K_I	K_{II}	K_I	K_{II}
0	6.1667	0.4516	7.8333	0.5269	10.0000	0.3011
5	6.0000	1.9570	7.1667	3.3871	9.0000	5.0430
10	5.0000	4.7419	6.0000	6.6989	6.6667	9.3333
15	3.6667	7.0000	4.3333	9.3333	3.5000	12.6452
20	2.3333	8.5806	1.6667	11.2151	0.1667	14.3763
25	0.1667	9.7097	1.0000	12.2688	3.1667	15.2043
30	1.8333	10.5376	3.8333	12.8710	6.1667	15.1290
35	4.0000	10.8387	6.1667	12.8710	8.6667	14.9032
40	6.0000	10.7634	8.3333	12.4946	11.0000	14.1505
45	7.6667	10.3871	10.3333	11.7419	13.0000	13.0215
50	9.5000	9.6344	12.0000	10.7634	14.8333	12.0430
55	11.0000	8.8065	13.5000	9.6344	16.1667	10.6129
60	12.3333	7.6774	14.8333	8.5054	17.5000	9.1828
65	13.3333	6.4731	16.0000	7.1505	18.6667	7.7527
70	14.3333	5.1183	16.8333	5.6452	19.5000	6.1720
75	15.0000	3.6882	17.5000	4.0645	20.1667	4.5161
80	15.5000	2.2581	17.8333	2.6344	20.6667	2.9355
85	15.6667	1.2043	18.1667	1.5054	21.0000	1.8065
90	15.8333	0.3763	18.3333	0.3763	21.1667	0.3763

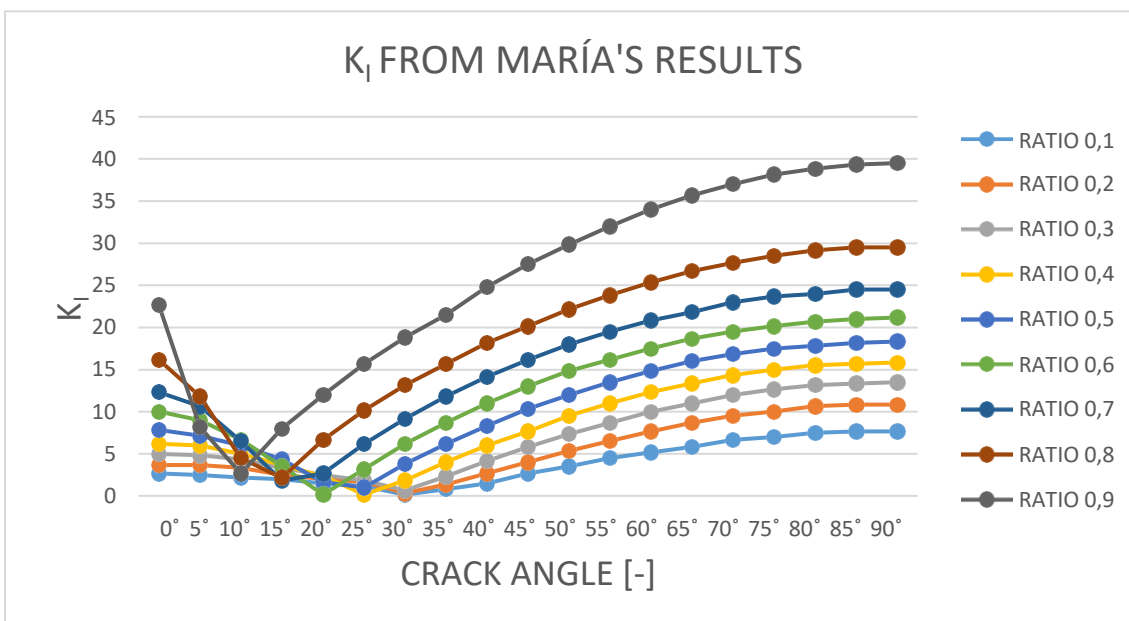
Table 18: Stress intensity factor for mode I and II. $a/R = 0.4$, $a/R = 0.5$ and $a/R = 0.6$ from María Villanueva's thesis.

STRESS INTENSITY FACTOR FOR MODE I AND II

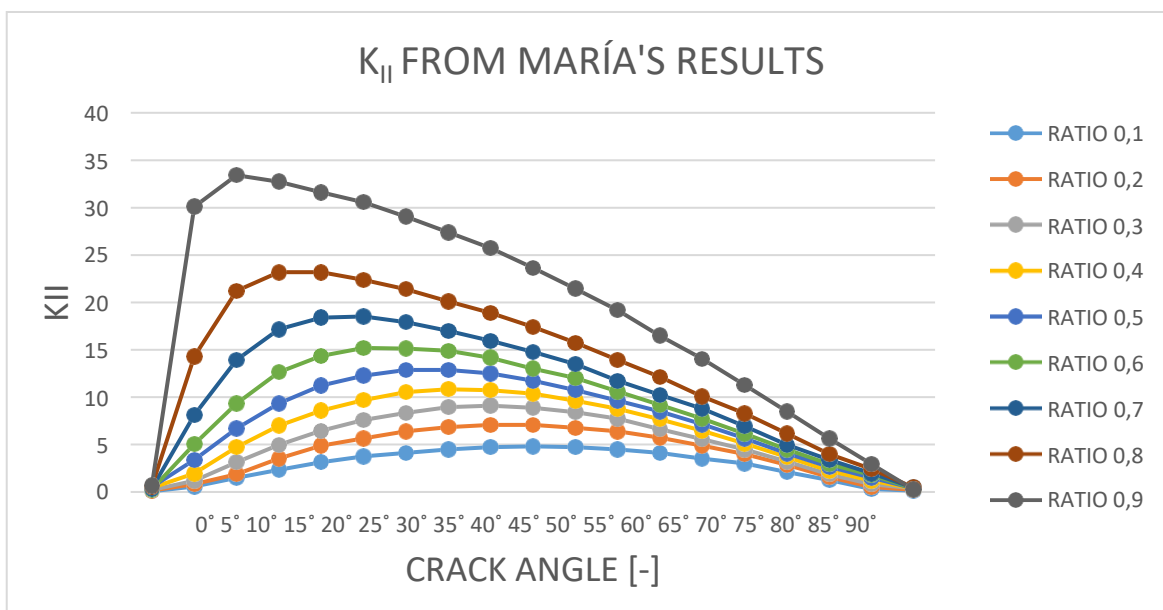
α	RATIO $a/R = 0.7$		RATIO $a/R = 0.8$		RATIO $a/R = 0.9$	
	K_I	K_{II}	K_I	K_{II}	K_I	K_{II}
0	12.3333	0.3763	16.1667	0.6022	22.6667	0.6774
5	10.6667	8.1290	11.8333	14.3011	8.1667	30.1075
10	6.5000	13.9247	4.5000	21.2258	2.6667	33.4194
15	1.8333	17.1613	2.1667	23.1828	8.0000	32.7419
20	2.6667	18.3656	6.6667	23.1828	12.0000	31.6129
25	6.1667	18.5161	10.1667	22.3548	15.6667	30.5591
30	9.1667	17.9140	13.1667	21.3763	18.8333	29.0538
35	11.8333	17.0108	15.6667	20.0968	21.5000	27.3978
40	14.1667	15.9570	18.1667	18.8925	24.8333	25.7419
45	16.1667	14.7527	20.1667	17.3871	27.5000	23.6344
50	18.0000	13.4731	22.1667	15.7312	29.8333	21.4516
55	19.5000	11.7419	23.8333	13.9247	32.0000	19.1935
60	20.8333	10.2366	25.3333	12.1183	34.0000	16.4839
65	21.8333	8.8065	26.6667	10.0860	35.6667	14.0753
70	23.0000	6.9247	27.6667	8.2796	37.0000	11.2903
75	23.6667	4.9677	28.5000	6.1720	38.1667	8.5054
80	24.0000	3.3871	29.1667	3.9892	38.8333	5.6452
85	24.5000	1.9570	29.5000	2.4086	39.3333	2.9355
90	24.5000	0.4516	29.5000	0.4516	39.5000	0.2505

Table 19: Stress intensity factor for mode I and II. $a/R = 0.7$, $a/R = 0.8$ and $a/R = 0.9$ from María Villanueva's thesis.

The following graphs show these results. These graphs seem to be similar to María's. but not equal, because María's results are exact and mine not.



Graph 15: Stress intensity factor for mode I, from María Villanueva's thesis.



Graph 16: Stress intensity factor for mode II, from María Villanueva's thesis.

9.2.4. CALIBRATION CURVES FOR MODE I AND II FROM MARIA'S VILLANUEVAS THESIS

As it has been said before. María's calibration curves are calculated from the same equations as me, (49) and (50). These results are summed up on the following tables and graphs:

VALUES OF CALIBRATION CURVES FOR MODE I AND II

α	RATIO $a/R = 0.1$		RATIO $a/R = 0.2$		RATIO $a/R = 0.3$	
	K_I	K_{II}	K_I	K_{II}	K_I	K_{II}
0°	26.52766	0.87143	24.31702	0.99835	25.32604	1.14376
5°	24.86968	5.99012	24.31702	5.49094	24.48184	6.10004
10°	21.55372	14.97529	22.10638	12.47941	21.94924	16.01260
15°	19.89575	23.21170	16.57979	23.46129	16.88403	25.16265
20°	14.92181	31.44811	13.26383	32.44647	12.66302	32.78770
25°	11.60585	37.43823	11.05319	37.43823	9.28622	38.50648
30°	1.65798	41.18205	2.21064	42.42999	3.37681	42.31900
35°	8.28989	44.92588	8.84255	45.42505	11.81882	45.36902
40°	14.92181	47.17217	17.68511	46.92258	21.10504	46.13153
45°	26.52766	47.92093	26.52766	46.92258	29.54705	44.98777
50°	34.81755	47.17217	35.37021	44.92588	37.14486	42.70025
55°	44.76543	44.92588	43.10745	42.42999	43.89848	39.26898
60°	51.39734	41.18205	50.84468	37.93741	50.65209	33.55020
65°	58.02926	35.19194	57.47660	32.44647	55.71730	28.21267
70°	66.31915	29.95058	63.00319	26.45635	60.78251	22.87514
75°	69.63511	20.96541	66.31915	18.96870	64.15931	16.39385
80°	74.60904	12.72900	70.74043	10.48270	66.69192	9.53131
85°	76.26702	3.09133	71.84575	3.49423	67.53612	4.19378
90°	76.26702	1.49753	71.84575	1.49753	68.38032	1.90626

Table 20: Calibration curves for mode I and II. $a/R = 0.1$, $a/R = 0.2$ and $a/R = 0.3$ from María Villanueva's thesis.

VALUES OF CALIBRATION CURVES FOR MODE I AND II

α	RATIO $a/R = 0.4$		RATIO $a/R = 0.5$		RATIO $a/R = 0.6$	
	K_I	K_{II}	K_I	K_{II}	K_I	K_{II}
0°	25.04408	1.83409	25.97500	1.74712	27.07468	0.81515
5°	24.36721	7.94773	23.76436	11.23147	24.36721	13.65379
10°	20.30601	19.25796	19.89575	22.21335	18.04979	25.26970
15°	14.89107	28.42841	14.36915	30.94894	9.47614	34.23637
20°	9.47614	34.84773	5.52660	37.18864	0.45124	38.92349
25°	0.67687	39.43296	3.31596	40.68288	8.57365	41.16516
30°	7.44554	42.79546	12.71117	42.67958	16.69605	40.96137
35°	16.24481	44.01819	20.44840	42.67958	23.46472	40.35001
40°	24.36721	43.71251	27.63298	41.43164	29.78215	38.31213
45°	31.13588	42.18410	34.26489	38.93576	35.19708	35.25531

50°	38.58142	39.12728	39.79149	35.69111	40.16078	32.60607
55°	44.67322	35.76478	44.76543	31.94729	43.77073	28.73410
60°	50.08816	31.17955	49.18670	28.20347	47.38069	24.86213
65°	54.14936	26.28864	53.05532	23.71088	50.53940	20.99016
70°	58.21056	20.78637	55.81862	18.71912	52.79563	16.71061
75°	60.91803	14.97841	58.02926	13.47776	54.60060	12.22727
80°	62.94863	9.17046	59.13458	8.73559	55.95434	7.94773
85°	63.62550	4.89091	60.23990	4.99176	56.85683	4.89091
90°	64.30236	1.52841	60.79255	1.24794	57.30807	1.01894

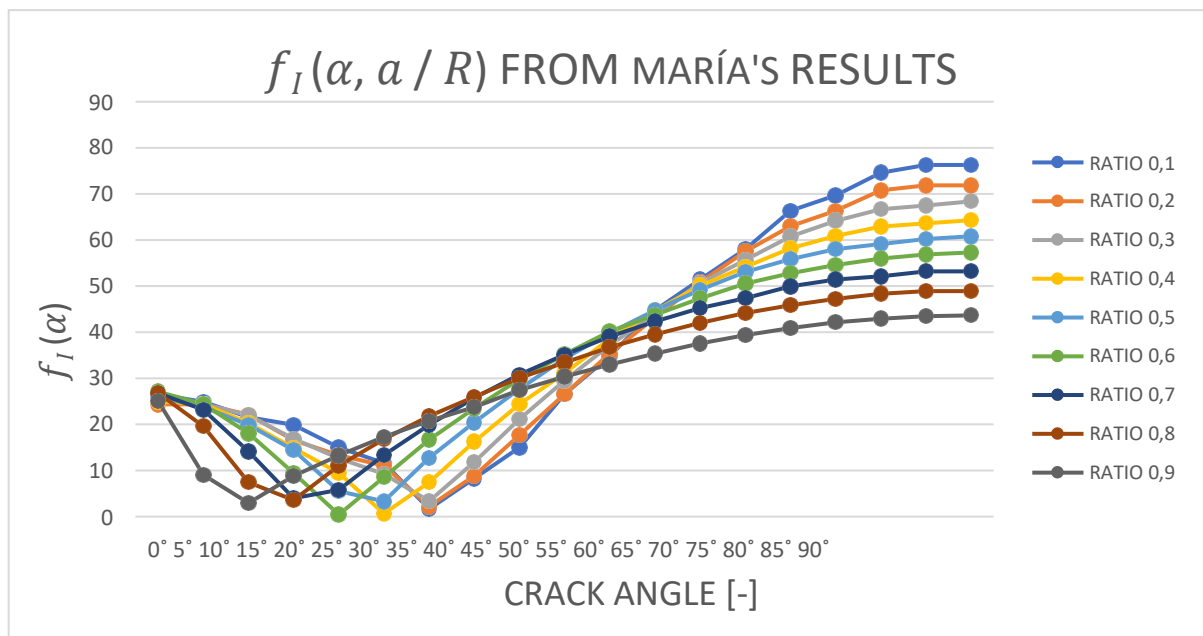
Table 21: Calibration curves for mode I and II. $a/R = 0.4$, $a/R = 0.5$ and $a/R = 0.6$ from María Villanueva's thesis.

VALUES OF CALIBRATION CURVES FOR MODE I AND II

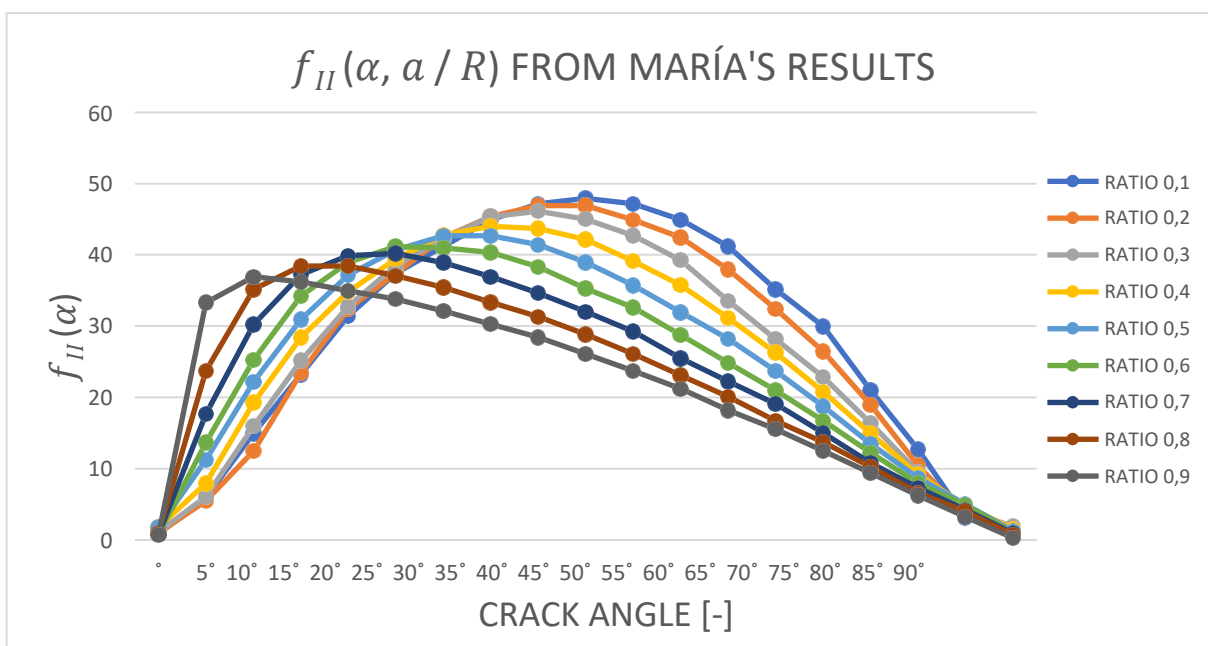
α	RATIO $a/R = 0.7$		RATIO $a/R = 0.8$		RATIO $a/R = 0.9$	
	K_I	K_{II}	K_I	K_{II}	K_I	K_{II}
0°	26.77325	0.81697	26.80399	0.99835	25.05390	0.74876
5°	23.15524	17.64653	19.61942	23.71088	9.02677	33.27843
10°	14.11022	30.22786	7.46090	35.19194	2.94752	36.93905
15°	3.97981	37.25379	3.59229	38.43658	8.84255	36.19029
20°	5.78881	39.86809	11.05319	38.43658	13.26383	34.94235
25°	13.38662	40.19488	16.85612	37.06385	17.31667	33.77760
30°	19.89903	38.88773	21.83005	35.44152	20.81684	32.11368
35°	25.68784	36.92701	25.97500	33.32002	23.76436	30.28337
40°	30.75305	34.63949	30.11995	31.32332	27.44876	28.45305
45°	35.09466	32.02519	33.43591	28.82744	30.39628	26.12357
50°	39.07447	29.24750	36.75186	26.08197	32.97536	23.71088
55°	42.33067	25.48944	39.51516	23.08691	35.37021	21.21500
60°	45.22508	22.22156	42.00213	20.09185	37.58085	18.21994
65°	47.39588	19.11708	44.21277	16.72241	39.42305	15.55766
70°	49.92849	15.03223	45.87075	13.72735	40.89681	12.47941
75°	51.37569	10.78399	47.25239	10.23312	42.18635	9.40116
80°	52.09929	7.35272	48.35771	6.61409	42.92323	6.23971
85°	53.18469	4.24824	48.91037	3.99341	43.47589	3.24465
90°	53.18469	0.98036	48.91037	0.74876	43.66011	0.27692

Table 22: Calibration curves for mode I and II. $a/R = 0.7$, $a/R = 0.8$ and $a/R = 0.9$ from María Villanueva's thesis.

The following graphs summarize the results below.



Graph 17: Calibration curves for mode I, from María Villanueva's thesis.



Graph 18: Calibration curves for mode II, from María Villanueva's thesis.

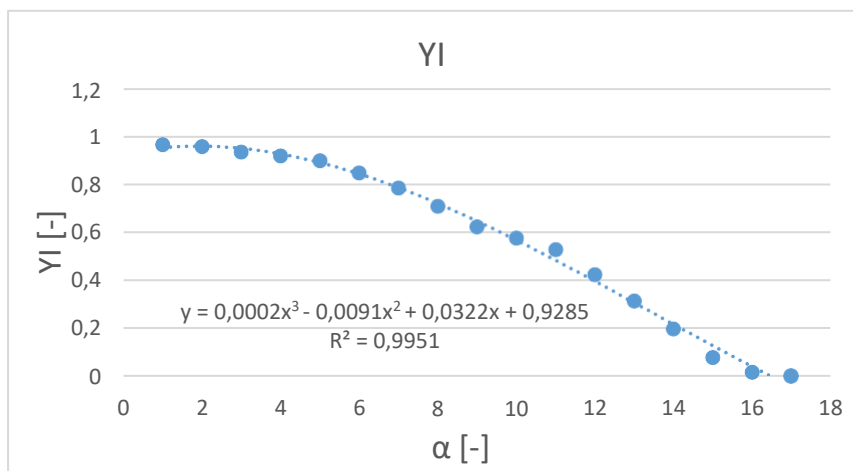
9.2.5. CALIBRATION CURVES OBTAINED EXPERIMENTALLY [27]

GEOMETRY FUNCTIONS

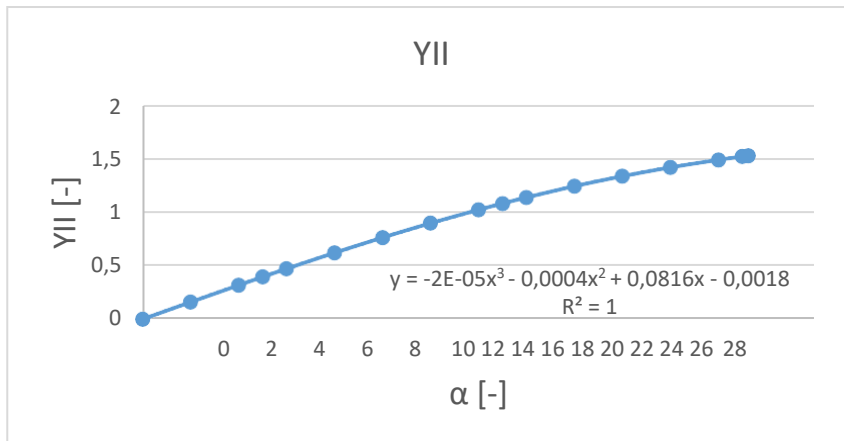
RATIO $a/R = 0.4$		
	Y_I	Y_{II}
0°	0.96443426	0
2°	0.9569435	0.15908637
4°	0.9346094	0.3163768
5°	0.91800081	0.39381705
6°	0.89783104	0.47015211
8°	0.84725311	0.61876984
10°	0.78371988	0.76075642
12°	0.70829046	0.89479176
14°	0.62216217	1.01977065
15°	0.57548312	1.07857612
16°	0.52660904	1.1348028
18°	0.42295116	1.23985752
20°	0.31257003	1.33261697
22°	0.19675503	1.41467754
24°	0.07682318	1.48533313
25°	0.01565997	1.51640133
25.25°	0	1.52375393

Table 23: Calibration curves for mode I and II obtained experimentally.

The following graphs are created from the values above. It is also shown the linear regression line and the equation.

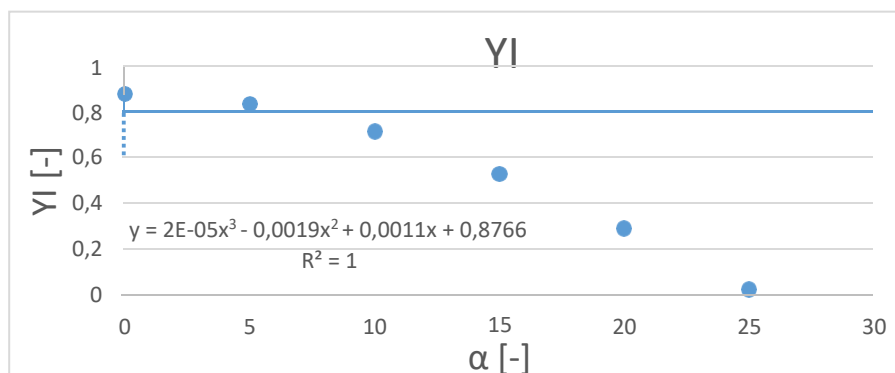


Graph 19: Calibration curve for mode I, obtained by experimental results. Linear regression equation.

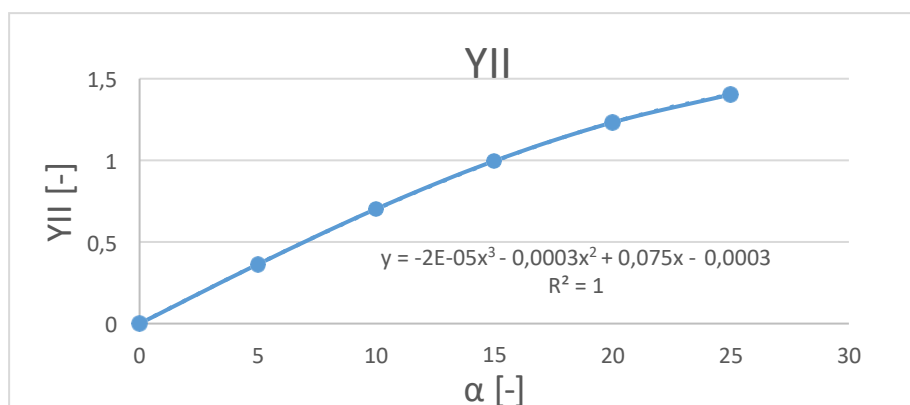


Graph 20:
Calibration curve
for mode II,
obtained by
experimental
results. Linear
regression
equation.

9.2.6. CALIBRATION CURVES OBTAINED FOR ANGLE BETWEEN 0° AND 25°



Graph 21:
Calibration
curve for mode
I, obtained by
me. Linear
regression
equation.



Graph 22:
Calibration
curve for mode
II, obtained by
me. Linear
regression
equation.

Now it is shown the comparison between Miarka's [27] model and mine, including the error for both modes.

ERROR FOR $a/R=0.4$

$\alpha [^\circ]$	Y_I MIARKA	Y_I ME	ERROR Y_I	Y_{II} MIARKA	Y_{II} ME	ERROR Y_{II}
0	0.964434256	0.876799771	9.09%	0	0	0.00%
2	0.956943504	0.87136	8.94%	0.15908637	0.1457975	8.35%
4	0.934609399	0.85188	8.85%	0.3163768	0.29219969	7.64%
5	0.918000807	0.835158409	9.02%	0.39381705	0.36324804	7.76%
6	0.897831037	0.81912	8.77%	0.47015211	0.43619991	7.22%
8	0.847253115	0.77404	8.64%	0.61876984	0.57779996	6.62%
10	0.783719876	0.714351459	8.85%	0.76075642	0.70190605	7.74%
12	0.708290464	0.65076	8.12%	0.89479176	0.85379999	4.58%
14	0.622162172	0.57448	7.66%	1.01977065	0.98819999	3.10%
15	0.575483124	0.526805531	8.46%	1.07857612	0.99595235	7.66%
16	0.526609041	0.48972	7.01%	1.1348028	1.1202	1.29%
18	0.422951162	0.39744	6.03%	1.23985752	1.2498	0.80%
20	0.312570026	0.289421567	7.41%	1.33261697	1.23183233	7.56%
22	0.196755026	0.19416	1.32%	1.41467754	1.5018	6.16%
24	0.076823183	0.08508	10.75%	1.48533313	1.6242	9.35%
25	0.015659969	0.020632684	31.75%	1.51640133	1.4034173	7.45%
25.25	0	0	0.00%	1.52375393	1.69948125	11.53%

Table 24: Error results between Petr Miarka (experimentally) [27] and me.

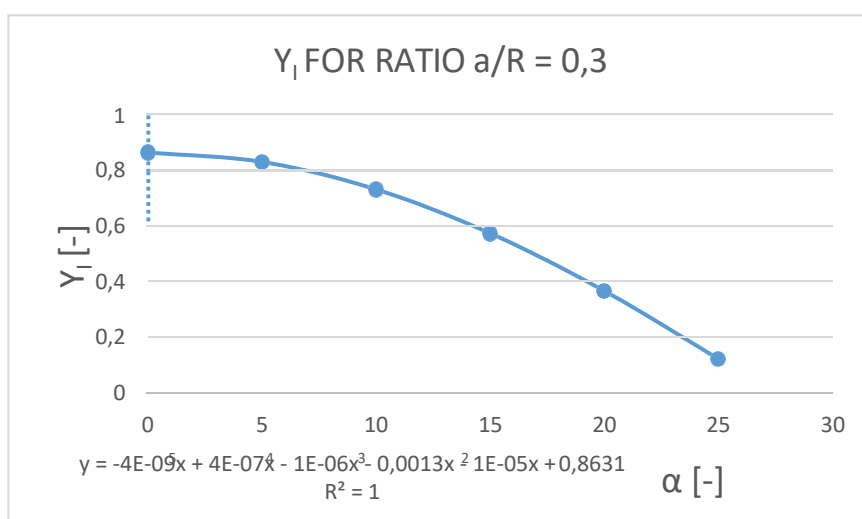
9.2.7. CALIBRATIONS CURVES OBTAINED FROM AYATOLLAHI AND ALIHA'S [19]

VALUES OF GEOMETRY FUNCTIONS [19]

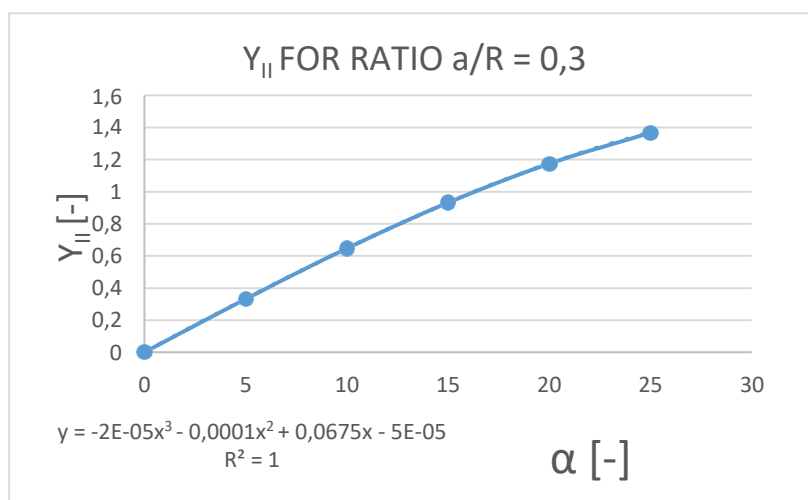
$\alpha [^\circ]$	0.3		0.4		0.5		0.6	
	Y_I	Y_{II}	Y_I	Y_{II}	Y_I	Y_{II}	Y_I	Y_{II}
0	1.135	0	1.243	0	1.387	0	1.578	0
2	1.128	0.186	1.233	0.219	1.375	0.251	1.555	0.283
4	1.107	0.369	1.204	0.435	1.339	0.5	1.488	0.566
6	1.071	0.549	1.157	0.645	1.281	0.741	1.379	0.837
8	1.022	0.723	1.091	0.846	1.202	0.968	1.234	1.093
10	0.959	0.889	1.009	1.036	1.104	1.182	1.058	1.326
12	0.884	1.046	0.911	1.209	0.991	1.371	0.86	1.535

14	0.798	1.194	0.801	1.375	0.864	1.555	0.646	1.738
16	0.701	1.33	0.677	1.521	0.727	1.712	0.429	1.903
18	0.593	1.455	0.544	1.652	0.583	1.848	0.222	2.047
20	0.477	1.568	0.401	1.767	0.433	1.964	0.013	2.161
22	0.353	1.67	0.253	1.865	0.281	2.059	0	2.253
24	0.222	1.76	0.098	1.95	0	2.132		
26	0.085	1.838	0	2.015				
28	0	1.906						

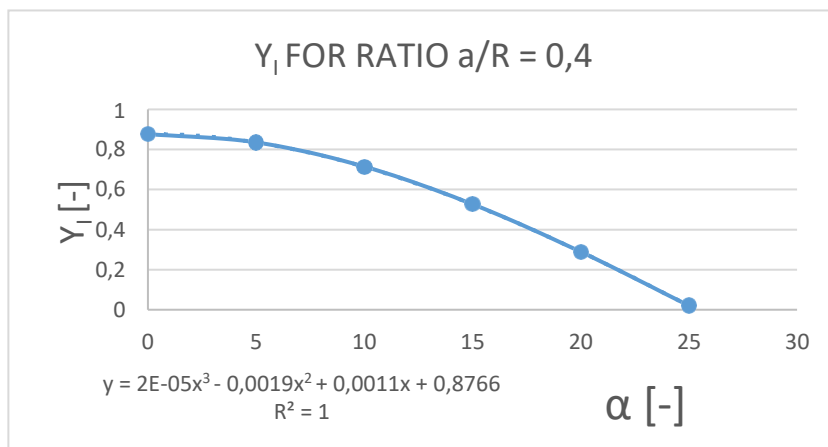
Table 25: Calibration curves for $a/R = 0.3$, $a/R = 0.4$, $a/R = 0.5$ and $a/R = 0.6$ taken from article [19].



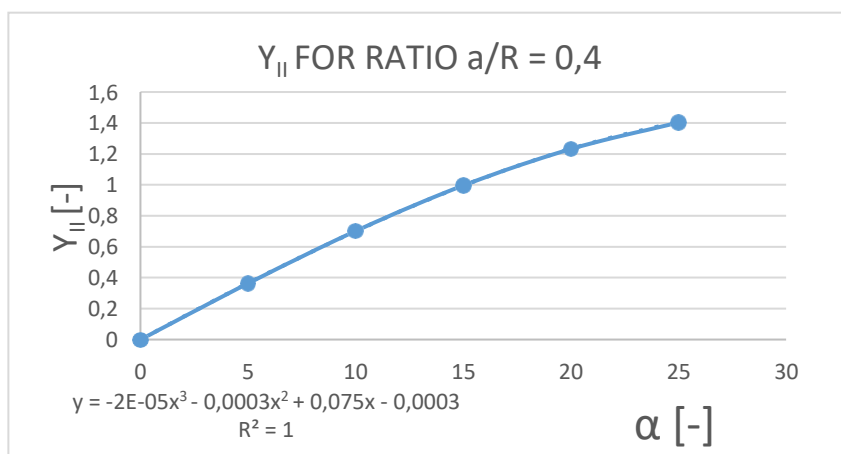
Graph 23: Calibration curve for mode I and $a/R = 0.3$, obtained by me. Linear regression equation.



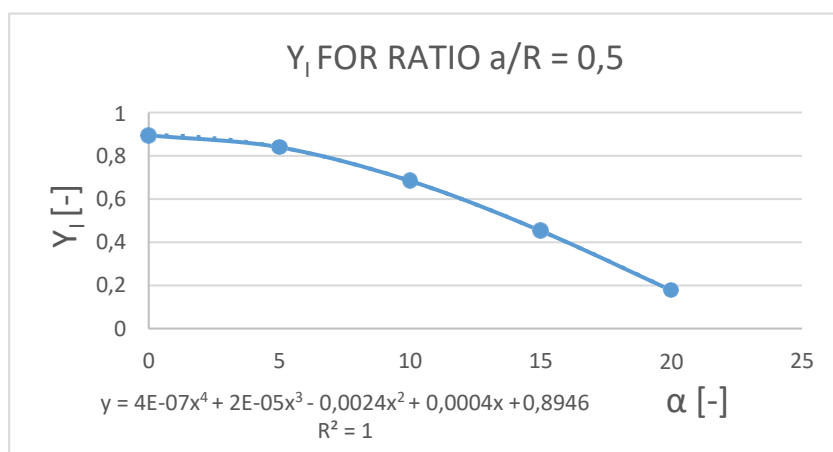
Graph 24: Calibration curve for mode II and $a/R = 0.3$, obtained by me. Linear regression equation.



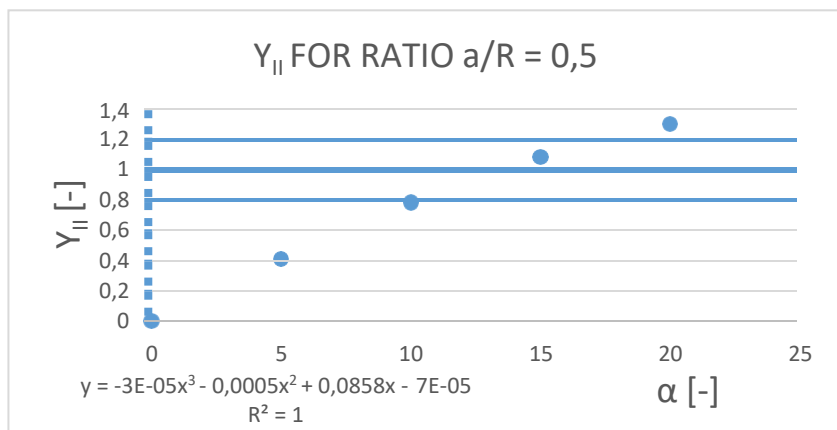
Graph 25:
Calibration
curve for
mode I and
 $a/R = 0,4$,
obtained by
me. Linear
regression
equation.



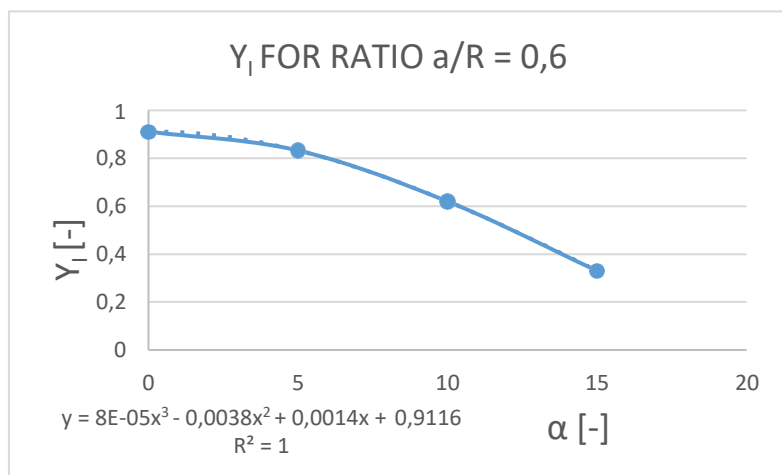
Graph 26:
Calibration
curve for
mode II and
 $a/R = 0,4$,
obtained by
me. Linear
regression
equation.



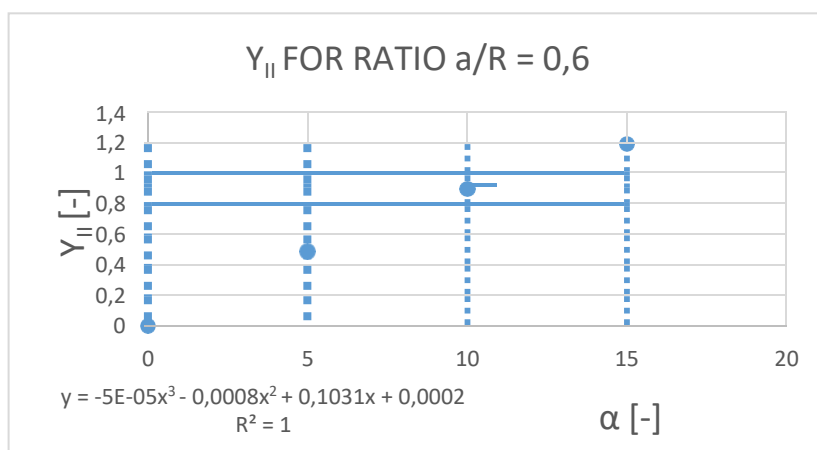
Graph 27:
Calibration
curve for
mode I and
 $a/R = 0,5$,
obtained by
me. Linear
regression
equation.



Graph 28:
Calibration
curve for mode
II and $a/R =$
0.5, obtained
by me. Linear
regression
equation.



Graph 29:
Calibration
curve for mode
I and $a/R =$
0.6, obtained
by me. Linear
regression
equation.



Graph 30:
Calibration
curve for
mode II and
 $a/R = 0.6$,
obtained by
me. Linear
regression
equation.

The following tables carry out the comparison between my results and Ayatollahi's article [19] for relative crack lengths $a/R = 0.3$, $a/R = 0.4$, $a/R = 0.5$ and $a/R = 0.6$.

CALIBRATION CURVES ERROR

α	RATIO 0.3					
	Y_I	$Y_I ME$	ERROR Y_I	Y_{II}	$Y_{II} ME$	ERROR Y_{II}
0	1.13500	0.86310	23.96%	0.00000	0.00000	0.00%
2	1.12800	0.85789	23.95%	0.18600	0.13439	27.75%
4	1.10700	0.84236	23.91%	0.36900	0.26707	27.62%
6	1.07100	0.81673	23.74%	0.54900	0.39703	27.68%
8	1.02200	0.78133	23.55%	0.72300	0.52331	27.62%
10	0.95900	0.73660	23.19%	0.88900	0.64495	27.45%
12	0.88400	0.68308	22.73%	1.04600	0.76099	27.25%
14	0.79800	0.62138	22.13%	1.19400	0.87047	27.10%
16	0.70100	0.55216	21.23%	1.33000	0.97243	26.88%
18	0.59300	0.47615	19.70%	1.45500	1.06591	26.74%
20	0.47700	0.39410	17.38%	1.56800	1.14995	26.66%
22	0.35300	0.30677	13.10%	1.67000	1.22359	26.73%
24	0.22200	0.21492	3.19%	1.76000	1.28587	26.94%
26	0.08500	0.11930	40.36%	1.83800	1.33583	27.32%
28	0.00000	0.02064	-	1.90600	1.37251	27.99%

Table 26: Calibration curve error for $a/R = 0.3$.

CALIBRATION CURVES ERROR

α	RATIO 0.4					
	Y_I	$Y_I ME$	ERROR Y_I	Y_{II}	$Y_{II} ME$	ERROR Y_{II}
0	1.24300	0.87660	29.48%	0.00000	0.00000	0.00%
2	1.23300	0.87136	29.33%	0.21900	0.14834	32.26%
4	1.20400	0.85188	29.25%	0.43500	0.29362	32.50%
6	1.15700	0.81912	29.20%	0.64500	0.43458	32.62%
8	1.09100	0.77404	29.05%	0.84600	0.57026	32.59%
10	1.00900	0.71760	28.88%	1.03600	0.69970	32.46%
12	0.91100	0.65076	28.57%	1.20900	0.82194	32.01%
14	0.80100	0.57448	28.28%	1.37500	0.93602	31.93%
16	0.67700	0.48972	27.66%	1.52100	1.04098	31.56%
18	0.54400	0.39744	26.94%	1.65200	1.13586	31.24%
20	0.40100	0.29860	25.54%	1.76700	1.21970	30.97%
22	0.25300	0.19416	23.26%	1.86500	1.29154	30.75%
24	0.09800	0.08508	13.18%	1.95000	1.35042	30.75%
26	0.00000	0.00000	0.00%	2.01500	1.39538	30.75%
28						

Table 27: Calibration curve error for $a/R = 0.4$.

CALIBRATION CURVES ERROR

α	RATIO 0.5					
	Y_I	$Y_I ME$	ERROR Y_I	Y_{II}	$Y_{II} ME$	ERROR Y_{II}
0	1.38700	0.89460	35.50%	0.00000	0.00000	0.00%
2	1.37500	0.88597	35.57%	0.25100	0.16947	32.48%
4	1.33900	0.85918	35.83%	0.50000	0.33501	33.00%
6	1.28100	0.81544	36.34%	0.74100	0.49655	32.99%
8	1.20200	0.75608	37.10%	0.96800	0.65409	32.43%
10	1.10400	0.68260	38.17%	1.18200	0.80763	31.67%
12	0.99100	0.59665	39.79%	1.37100	0.95717	30.18%
14	0.86400	0.50005	42.12%	1.55500	1.10271	29.09%
16	0.72700	0.39473	45.70%	1.71200	1.24425	27.32%
18	0.58300	0.28283	51.49%	1.84800	1.38179	25.23%
20	0.43300	0.16660	61.52%	1.96400	1.51533	22.84%
22	0.28100	0.04846	82.75%	2.05900	1.64487	20.11%
24	0.00000	0.00000	0.00%	2.13200	1.77041	16.96%
26						
28						

Table 28: Calibration curve error for $a/R = 0.5$.

CALIBRATION CURVES ERROR

α	0.6					
	Y_I	$Y_I ME$	ERROR Y_I	Y_{II}	$Y_{II} ME$	ERROR Y_{II}
0	1.57800	0.91160	42.23%	0.00000	0.00000	0.00%
2	1.55500	0.89984	42.13%	0.28300	0.20280	28.34%
4	1.48800	0.86152	42.10%	0.56600	0.39660	29.93%
6	1.37900	0.80048	41.95%	0.83700	0.57920	30.80%
8	1.23400	0.72056	41.61%	1.09300	0.74820	31.55%
10	1.05800	0.62560	40.87%	1.32600	0.90120	32.04%
12	0.86000	0.51944	39.60%	1.53500	1.03580	32.52%
14	0.64600	0.40592	37.16%	1.73800	1.14960	33.86%
16	0.42900	0.28888	32.66%	1.90300	1.24020	34.83%
18	0.22200	0.17216	22.45%	2.04700	1.30520	36.24%
20	0.01300	0.05960	78.19%	2.16100	1.34220	37.89%
22	0.00000	0.00000	0.00%	2.25300	1.34880	40.13%

24	
26	
28	

Table 29: Calibration curve error for $a/R = 0.6$.

9.3. ANNEX III. LIST OF ABBREVIATIONS

<i>GMTS</i>	<i>Generalized maximum tangential stress.</i>
<i>MTS</i>	<i>Maximum tangential stress.</i>
<i>LEFM</i>	<i>Linear elastic fracture mechanics.</i>
<i>BD</i>	<i>Brazilian disc.</i>
<i>FEA</i>	<i>Finite element analysis.</i>
<i>SIF</i>	<i>Stress intensity factor.</i>

9.4. ANNEX IV. LIST OF SYMBOLS

σ	<i>Applied stress.</i>
K_{Ic}	<i>Fracture tenacity.</i>
C	<i>Specimen's geometry constant.</i>
a	<i>Crack length.</i>
A	<i>Crack tip.</i>
σ_A	<i>Located stress at A.</i>
ρ	<i>Radius of curvature.</i>
σ_f	<i>Remote stress at failure.</i>
E	<i>Young's modulus.</i>
γ_s	<i>Surface energy per unit area.</i>
f_{ij}	<i>Dimensionless function.</i>
K	<i>Stress intensity factor.</i>
σ_{ij}	<i>Stress tensor.</i>
r, θ	<i>Polar Coordinates.</i>
K_I	<i>Stress intensity factor for Mode I.</i>
K_{II}	<i>Stress intensity factor for Mode II.</i>
K_{III}	<i>Stress intensity factor for Mode III.</i>
ν	<i>Poisson's ratio.</i>
σ_{ys}	<i>Yield strength.</i>
r_y	<i>Radius of the plastic zone.</i>
G	<i>Energy release rate.</i>
β	<i>Angle of the crack.</i>
k_I, k_{II}	<i>Local stress intensity factors at the tip of the kink.</i>
T	<i>T – stress. tangential stress.</i>
P	<i>Applied load.</i>
t	<i>Specimen's thickness or height.</i>
d	<i>Specimen's diameter.</i>
x, y	<i>Cartesian coordinates respect to the specimen's centre.</i>
a/R	<i>Relative Crack length.</i>
α	<i>Notch angle.</i>
ET	<i>Element type.</i>

9.5. ANNEX V. LIST OF FIGURES

Figure 1: Elliptical hole in a flat hole.....	11
Figure 2: Sharp microcrack at the tip of a macroscopic crack.....	12
Figure 3: Crack propagation in an ideally brittle material.....	12
Figure 4: Necessary stress to overcome atomic bonds.....	13
Figure 5: Definition of the coordinate axis and its stresses on the crack tip region	14
Figure 6: The three modes of loading that can be applied to a crack.....	14
Figure 7: Variation of σ_{yy} on the crack tip area.....	16
Figure 8: Plastic zone in the front of the crack.	17
Figure 9: Propagation of a crack not orthogonal to the applied normal stress.....	18
Figure 10: Infinitesimal kink at the crack tip and the $x - y$ coordinate system.....	19
Figure 11: Local energy release rate at the tip of a kinked crack.....	20
Figure 12: Optimum propagation angle for a crack oriented at an angle β from the stress axis.....	21
Figure 13: The specimen is loaded by compression loads along the vertical diametral plane.....	23
Figure 14: Theoretical stress distribution on horizontal and vertical axis	24
Figure 15: Stress distribution in a specimen subjected to a load applied on a curved support load plate. [23]	25
Figure 16: Scheme of geometry of a typical BD specimen with a load arbitrary position alongside crack.....	26
Figure 17: Element type PLANE183 2D 8 – node taken from [24]......	27
Figure 18: Element type PLANE183 used in ANSYS.....	27
Figure 19: Material properties in ANSYS.....	28
Figure 20: First and second keypoints. Keypoint number 2 at the coordinate (1,0) in relation with the first keypoint which is on the coordinate origin	29
Figure 21: Crack tips of the specimen.....	29
Figure 22: Crack tip left part.....	30
Figure 23: Crack tip right part.....	30
Figure 24: Periphery contour keypoints.....	30
Figure 25: Lines in the surroundings of the crack.....	31
Figure 26: Lines in the periphery contour.....	31
Figure 27: Lines dividing areas.....	32
Figure 28: Areas modelling.....	32
Figure 29: Meshing of the specimen.....	33
Figure 30: Boundary conditions: displacement constraints on X and Y direction. Nodes drawing	34
Figure 31: Boundary conditions: displacement constraints on X and Y direction. Elements drawing.....	34
Figure 32: Boundary conditions: Forces on node for $\alpha = 45^\circ$ and $a/R = 0.1$. Nodes drawing.....	35
Figure 33: Boundary conditions: Forces on node for $\alpha = 45^\circ$ and $a/R = 0.1$. Elements drawing.....	35
Figure 34: (a) Nodes used for the crack displacement in a full – crack model, taken from, (b) the path defined for a full – crack model. [26].	36

Figure 35: KCALC command for $\alpha = 45^\circ$ and $a/R = 0,1$. The same results are shown on the ANNEX II: "TABLES AND RESULTS"..... 37

9.6. ANNEX VI. LIST OF GRAPHS

Graph 1: Stress intensity factor for mode I, versus the crack angle.....	38
Graph 2: Stress intensity factor for mode II, versus the crack angle.....	39
Graph 3: Calibration curve $f_I(\alpha, a/R)$ for mode I, versus the crack angle.....	40
Graph 4: Calibration curve $f_{II}(\alpha, a/R)$ for mode II, versus the crack angle.....	40
Graph 5: Calibration curve $f_I(\alpha, a/R)$ for mode I, versus the crack inclination angle.	43
Graph 6: Calibration curve $f_{II}(\alpha, a/R)$ for mode II, versus the crack inclination angle.	43
Graph 7: Fracture forces and SIFs values for different angles for relative crack length $a/R = 0.267$	44
Graph 8: Fracture forces and SIFs values for different angles for relative crack length $a/R = 0.4$	45
Graph 9: Error in the calibration curves for mode I between María Villanueva's thesis and mine.	46
Graph 10: Error in the calibration curves for mode II between María Villanueva's thesis and mine.	47
Graph 11: Error graph between both calibration curves models for mode I. Comparison with experimental test	48
Graph 12: Error graph between both calibration curves models for mode II. Comparison with experimental test	49
Graph 13: Error graph between both calibration curves models for mode I. Comparison with Ayatollahi and Aliha's article [19].....	50
Graph 14: Error graph between both calibration curves models for mode II. Comparison with Ayatollahi and Aliha's article [19].....	50
Graph 15: Stress intensity factor for mode I, from María Villanueva's thesis.....	70
Graph 16: Stress intensity factor for mode II, from María Villanueva's thesis.	70
Graph 17: Calibration curves for mode I, from María Villanueva's thesis.....	73
Graph 18: Calibration curves for mode II, from María Villanueva's thesis.....	73
Graph 19: Calibration curve for mode I, obtained by experimental results. Linear regression equation.....	74
Graph 20: Calibration curve for mode II, obtained by experimental results. Linear regression equation.....	75
Graph 21: Calibration curve for mode I, obtained by me. Linear regression equation.	75
Graph 22: Calibration curve for mode II, obtained by me. Linear regression equation.....	75
Graph 23: Calibration curve for mode I and $a/R = 0.3$, obtained by me. Linear regression equation.....	77
Graph 24: Calibration curve for mode II and $a/R = 0.3$, obtained by me. Linear regression equation.....	77
Graph 25: Calibration curve for mode I and $a/R = 0.4$, obtained by me. Linear regression equation.....	78
Graph 26: Calibration curve for mode II and $a/R = 0.4$, obtained by me. Linear regression equation.....	78
Graph 27: Calibration curve for mode I and $a/R = 0.5$, obtained by me. Linear regression equation.....	78

Graph 28: Calibration curve for mode II and $a/R = 0.5$, obtained by me. Linear regression equation.....	79
Graph 29: Calibration curve for mode I and $a/R = 0.6$, obtained by me. Linear regression equation.....	79
Graph 30: Calibration curve for mode II and $a/R = 0.6$, obtained by me. Linear regression equation.....	79

9.7. ANNEX VII. LIST OF TABLES

Table 1: Stress Fields Ahead of a Crack Tip for Mode I and Mode II in a Linear Elastic, Isotropic Material	15
Table 2: Crack – Tip Displacement Fields for Mode I and Mode II (Linear Elastic, Isotropic Material).....	15
Table 3: Nonzero Stress and Displacement Components in Mode III (Linear Elastic, Isotropic Material).....	16
Table 4: Material Properties for concrete C50/60 used on the experiment.....	28
Table 5: Crack relative length for different ratio a/R	38
Table 6: Specimen's measures and external force.	38
Table 7: Dimensions of BD test for $a/R = 0.267$	42
Table 8: Dimensions of BD test for $a/R = 0.4$	42
Table 9: Stress intensity factor for mode I and II for ratios $a/R = 0.1$. $a/R = 0.2$ and $a/R = 0.3$	63
Table 10: Stress intensity factor for mode I and II. $a/R = 0.4$. $a/R = 0.5$ and $a/R = 0.6$	64
Table 11: Stress intensity factor for mode I and II. $a/R = 0.7$. $a/R = 0.8$ and $a/R = 0.9$	65
Table 12: Calibration curves for mode I and II. $a/R = 0.1$. $a/R = 0.2$ and $a/R = 0.3$	65
Table 13: Calibration curves for mode I and II. $a/R = 0.4$. $a/R = 0.5$ and $a/R = 0.6$	66
Table 14: Calibration curves for mode I and II. $a/R = 0.7$. $a/R = 0.8$ and $a/R = 0.9$	67
Table 15: Crack length according to ratio a/R	67
Table 16: Initial data.....	67
Table 17: Stress intensity factor for mode I and II. $a/R = 0.1$. $a/R = 0.2$ and $a/R = 0.3$ from María Villanueva's thesis.....	68
Table 18: Stress intensity factor for mode I and II. $a/R = 0.4$. $a/R = 0.5$ and $a/R = 0.6$ from María Villanueva's thesis.....	68
Table 19: Stress intensity factor for mode I and II. $a/R = 0.7$. $a/R = 0.8$ and $a/R = 0.9$ from María Villanueva's thesis.....	69
Table 20: Calibration curves for mode I and II. $a/R = 0.1$, $a/R = 0.2$ and $a/R = 0.3$ from María Villanueva's thesis.....	71
Table 21: Calibration curves for mode I and II. $a/R = 0.4$, $a/R = 0.5$ and $a/R = 0.6$ from María Villanueva's thesis.....	72
Table 22: Calibration curves for mode I and II. $a/R = 0.7$, $a/R = 0.8$ and $a/R = 0.9$ from María Villanueva's thesis.....	72
Table 23: Calibration curves for mode I and II obtained experimentally.....	74
Table 24: Error results between Petr Miarka (experimentally) [27] and me.	76
Table 25: Calibration curves for $a/R = 0.3$, $a/R = 0.4$, $a/R = 0.5$ and $a/R = 0.6$ taken from article [19].....	77
Table 26: Calibration curve error for $a/R = 0.3$	80
Table 27: Calibration curve error for $a/R = 0.4$	80
Table 28: Calibration curve error for $a/R = 0.5$	81
Table 29: Calibration curve error for $a/R = 0.6$	82

10. REFERENCES

- [1] V. P. de Freitas, J. M. P. Q. Delgado. *Durability of Building Materials and Components*. Springer Berlin Heidelberg. 2013.
- [2] F. L. Flager. *The design of building structures for improved life – cycle performance*. Doctoral dissertation. Massachusetts Institute of Technology. 2003
- [3] R. Tomek. *Advantages of Precast Concrete in Highway Infrastructure Construction*. Procedia Engineering. 196. 2017.
- [4] Belzunce Varela. F., Viña Olay J., *Cience of Materials*. University of Oviedo. AS-433992.
- [5] Belzunce Varela. J., *Technology of Materials*. University of Oviedo. 2012.
- [6] EN 12390 – 3: 2009: Testing hardened concrete - Part 3: Compressive strength of test specimens. European Committee for Standardization. 2009
- [7] EN 12390 - 3:2009: Testing hardened concrete - Part 5: Flexural strength of test specimens. European Committee for Standardization. 2009
- [8] ISO 1920 – 10: Testing of concrete in Part 10: Determination of static modulus of elastic compression. International Organization for Standardization. 2010
- [9] *Suggested methods for determining tensile strength of rock materials: International Society for Rock Mechanics*. International Journal of Rock Mechanics and Mining Sciences & Geomechanics Abstracts. 15 (1978)
- [10] <http://www6.uniovi.es/usr/fblanco/TEMAIL.2.8.MECANICAS.Ensayos.pdf>
- [11] Anderson. T. L., *Fracture Mechanics. Fundamentals and Applications*. Third Edition. 2005.
- [12] Inglis. C.E., *Stresses in a Plate Due to the Presence of Cracks and Sharp Corners*. Transactions of the Institute of Naval Architects. Vol. 55. 1913. pp. 219–241.
- [13] Gehlen. P.C. and Kanninen. M.F., *An Atomic Model for Cleavage Crack Propagation in Iron*. Inelastic Behaviour of Solids. McGraw-Hill. New York. 1970. pp. 587–603.
- [14] Hua W., Wang Q., Li. Y., Dong S. M., Li N., *T – stress for a centrally cracked Brazilian Disc under confining pressure*. Engineering Fracture Mechanics. China. 2015.
- [15] M.R. Ayatollahi. M.J. Pavier and D.J. Smith., *Determination of T-stress from finite element analysis for mode I and mixed mode I-II loading*. 1998. Department of Mechanical Engineering. University of Bristol. Bristol BS8 1TR. UK.
- [16] Gupta M. Alderliesten R.C., Benedictus R., *A review of T – stress and its effects in fracture mechanics*. Engng Fract Mech 2015; 134:218 – 8.
- [17] Fett T., *T – stresses in rectangular planes and circular discs*. Engng Fract Mech 1998;60 (5-6):631-52
- [18] Fett T. *Stress intensity factors and T – stress for internally cracked circular discs under various boundary conditions*. Engng Fract Mech 2001; 68: 1119 – 36.
- [19] Ayatollahi M.R., Aliha M.R.M., *On the use of Brazilian Disc specimen for the calculating mixed mode I/II fracture toughness of rock materials*. Iran University of Science and Technology. 2008.
- [20] Smith D.J., Ayatollahi M.R., Pavier M.J., *The role of T - stress in brittle fracture for linear elastic materials under mixed mode loading*.
- [21] Malíková L., Veselý V., *Significance of higher-order terms of the Williams expansion for plastic zone extent estimation demonstrated on a mixed-mode geometry*.

- [22] NLT – 346/90. *Diametral compression resistance of bituminous mixtures*.
- [23] Kennedy. T. W., Hudsons. W. R., *Application of the indirect tensile test to stabilized materials*. 1968.
- [24] ANSYS. Mechanical APDL command reference.
- [25] Yazdizadeh B. *Comparison of different plane models in finite element software in structural mechanics*. Yerevan State University. 2003.
- [26] Omid. O., *An explanation on Computation of Fracture Mechanics Parameters in ANSYS*. University of Tennessee Space Institute. 2014
- [27] Seitzl. S., Miarka. P., Bílek. V., *The mixed – mode Fracture resistance of C50/60 and its Suitability for use on precast elements as determined by the Brazilian disc test and three - point bending specimens*.
- [28] EN 12350 – 5: Testing fresh concrete. Part 5: Flow table test. European Committee for Standardization. 2009.
- [29] F.L. Flager. *The design of building structures for improved life – cycle performance*. Doctoral dissertation. Massachusetts Institute of Technology. 2003.
- [30] Villanueva. M., *Stress Analysis of Crack in Brazilian Disc*. Bachelor thesis. Brno University of Technology. 2017.
- [31] GetData Graph Digitizer. <http://www.getdata-graph-digitizer.com/>
- [32] Atkinson C. Smelser R. E., Sanchez J. *Combined mode fracture via the cracked Brazilian Disc test*. Int J Fract 1982;18:279-91